TRANSPORTATION RESEARCH
RECORD

No. 1481

Soils, Geology, and Foundations
Pavement Design, Management, and Performance

Environmental Moisture Effects on Transportation Facilities and Nonearth Materials' Thermal Effects on Pavements

A peer-reviewed publication of the Transportation Research Board

TRANSPORTATION RESEARCH BOARD
NATIONAL RESEARCH COUNCIL

NATIONAL ACADEMY PRESS
WASHINGTON, D.C. 1995

Transportation Research Record 1481
ISSN 0361-1981
ISBN 0-309-06119-9
Price: $23.00

Subscriber Category
IIIA soils, geology, and foundations
IIB pavement design, management, and performance

Printed in the United States of America

Sponsorship of Transportation Research Record 1481

GROUP 2—DESIGN AND CONSTRUCTION OF TRANSPORTATION FACILITIES
Chairman: Michael G. Katona, U.S. Air Force Armstrong Laboratory

Geology and Properties of Earth Materials Section
Chairman: Robert D. Holtz, University of Washington

Committee on Frost Action
Chairman: Thomas C. Kinney, University of Alaska Fairbanks
Wendy L. Allen, Richard L. Berg, George R. Cochran, Billy G. Connor, Denis E. Donnelly, Guy Dore, David C. Esch, Wilbur M. Haas, Larry K. Heinig, Karen S. Henry, Eldo Hildebrand, Ronald H. Jones, Hiroshi Kubo, Lutfi Raad, Mary Rutherford, Nelrae M. Succio, Otto J. Svec, Ted S. Vinson, Chen Xiaobai, Qiang Zhu

Committee on Environmental Factors Except Frost
Chairman: R. Gordon McKeen, University of New Mexico
Samuel H. Carpenter, Koon Meng Chua, Judith B. Corley-Lay, Delwyn G. Fredlund, Lawrence D. Johnson, Amos Komornik, Rodney W. Lentz, Robert L. Lytton, Joseph Massucco, Said Ossama Mazen, Alan Meadors, Thomas M. Petry, Miguel Picornell, Larry A. Scofield, Malcolm L. Steinberg, Gdalyah Wiseman

Transportation Research Board Staff
Robert E. Spicher, Director, Technical Activities
G. P. Jayaprakash, Engineer of Soils, Geology, and Foundations
Nancy A. Ackerman, Director, Reports and Editorial Services
Marianna Rigamer, Oversight Editor

Sponsorship is indicated by a footnote at the end of each paper. The organizational units, officers, and members are as of December 31, 1994.

Transportation Research Record 1481

Contents

Foreword

The eight papers in this volume provide information on environmental effects on transportation facilities, such as pavements, airports, and embankments. The papers are arranged into two groups. The first five papers treat the evaluation of enviromental moisture effects on the stability of transportation facilities. These papers describe methods of using soil moisture characterization in solving practical problems such as evaluation of vertical moisture barriers and the effects of moisture on resilient moduli of coarse and fine grained soils.

The three papers that follow describe the performance of transportation facilities constructed of nonearth materials for controlling frost heave. Because such applications may be cost-effective solutions to this problem, field implementations should be based on a basic understanding of the differences in the thermal properties of various nonearth and common earth materials. These papers are a source of such information.

PART 1

Environmental Moisture Effects on Transportation Facilities

Suction Measurements on Compacted Till Specimens and Indirect Filter Paper Calibration Technique

D. G. FREDLUND, JULIAN K. M. GAN, AND P. GALLEN

Standard AASHTO compacted specimens were used to provide a constant-suction environment for an indirect calibration of filter paper sensors. The suctions of the compacted till specimens were measured with tensiometers, thermal conductivity matric suction sensors; and psychrometers. The compacted specimens had essentially constant degrees of saturation at water contents greater than optimum. The matric suction of specimens compacted greater than optimum were observed to vary linearly with the water content and the void ratio (i.e., matric suction varies directly with dry density and inversely with water content). Filter paper sensors in good contact with specimens compacted greater than optimum were found to yield a more consistent calibration curve than filter paper sensors that were not in contact with the soil. Calibration curves obtained showed that the transition from where liquid flow is dominant to where vapor flow is dominant occurs at approximately 20 to 90 kPa.

The behavior of both saturated and unsaturated soils is affected by the pore-water pressures in the soil. Both positive and negative pore-water pressures have a major effect on the shear strength and volume change behavior of a soil. The effect of negative pore-water pressures on the hydraulic conductivity behavior of unsaturated soils has become increasingly important in analyzing geoenvironmental problems.

The measurement of positive pore-water pressures has become routine for engineering works such as embankments and dams. The measurement of negative pore-water pressures, however, has remained a research endeavor. The measurement of negative pore-water pressures over a wide range of values has proved to be difficult. Negative water pressures can range from 0 to 1 million kPa. The direct measurement of negative pore-water pressure is limited by the problem of cavitation. Water will cavitate when the vapor pressure is reached on an absolute pressure scale. As a result, the direct measurement of negative pore-water pressures by a tensiometer is now limited to pressures of less than 1 atm. Research at Imperial College, London, has involved the use of thin water films in a tensiometer to reduce the problem of cavitation. It is hoped that this research will provide a means of extending the range of negative pore-water pressure measurements beyond the present 1-atm constraint.

Various indirect methods of assessing the negative pore-water pressure in soils have been used for a number of years. These methods include moisture blocks, thermal conductivity sensors, blotting papers, filter papers, and psychrometers. All these methods have their own set of limitations. All methods, except the psychrometer method, rely on the absorbency properties of a sensor material and thus suffer from nonlinearity and hysteresis in the water-retention characteristics of the sensor medium. That is, the sensor materials generally display small water-content changes over large suction changes when in the high suction range.

Nevertheless, the filter paper method has some attractive features. It has been found to be applicable over a wide range of suctions. Filter paper provides an inexpensive sensor, and the methodology associated with its use is simple. The filter paper method, however, suffers from some procedural difficulties. Although the method is applicable to a wide range of suctions, the degree of accuracy is often inadequate. The filter paper method does not lend itself to automation processes, particularly in the area of data acquisition. The method is considered a destructive method in that the filter papers are not reusable.

The filter paper method is a technique that can be readily incorporated into routine site investigations. There has been considerable interest in the use of the filter paper method in several disciplines. Literature from early research (*1–5*) and from more recent research (*6–11*) into the filter paper method is listed in the References section. Recent experiences with studies related to airport pavement subgrades (*11*) and the movement of foundations of light structures (*9*) have indicated that the method deserves further consideration.

The objectives of this paper are (*a*) to determine the suction of compacted till specimens by using various suction measurement devices and (*b*) to evaluate an indirect method of calibrating filter paper sensors by using compacted soil specimens to provide constant suction environments. At present, the filter paper method has not gained wide acceptance in geotechnical engineering. The issues of whether the filter paper should be in contact with the soil or not in contact with the soil and of what suctions are measured in each case have been much debated. It is hoped that this study will assist in further resolving these questions related to the filter paper method.

PROGRAM FOR THE LABORATORY STUDY

The laboratory program involved (*a*) the measurements of suction in a set of standard AASHTO compacted till specimens and (*b*) using these compacted specimens to provide constant-suction environments for an indirect calibration of filter paper sensors.

Suction Measurement Devices

Suctions in the compacted till specimens were measured with the following suction measurement devices: jet-fill tensiometers, quick-draw tensiometers, MCS-6000 thermal conductivity matric suction sensors, and psychrometers.

Department of Civil Engineering, University of Saskatchewan, Saskatoon, Saskatchewan S7N 0W0, Canada.

Tensiometers are limited to a matric suction value of approximately 90 kPa. The MCS-6000 thermal conductivity matric suction sensors are reliable in the range from 0 to 300 kPa. Psychrometers start to become reliable at a suction near 100 kPa and measurements can be made up to 8000 kPa. Suctions of interest in geotechnical engineering generally range from 0 to 1500 kPa.

Soil Selected for the Study

The soil used in the laboratory tests program was a till from the Qu'Appelle Moraine east of the city of Regina in Saskatchewan, Canada. The grain size distributions of the till show 37 percent sand, 34 percent silt, and 29 percent clay. The till has a liquid limit of 38 percent and a plastic limit of 16 percent. Distilled water was added to the till to yield a set of samples with water contents ranging from 8 percent to 25 percent. Standard AASHTO compacted specimens were prepared from these samples for the testing. The compaction characteristics of the soil are presented in Figure 1. The till has a maximum dry density of approximately 1860 kg/m^3 and a corresponding optimum water content of approximately 15 percent.

Different suction values were obtained by compacting the till at various water contents. In other words, the suctions in the compacted specimens were not directly induced or controlled as in a pressure plate device. The matric suction or the total suction values, or both, in each specimen were measured with one or more of the following devices: jet-fill tensiometer, quick-draw tensiometer, MCS 6000 sensor, or psychrometer.

Filter Paper Selected for the Study

Schleicher Schuell No. 589 white ribbon filter paper was used in the laboratory tests. The filter papers had a diameter of 55 mm. The filter papers were pretreated by being dipped in a fungicide, drip dried, and over dried overnight. The fungicide was a mixture of 3.5 g of a technical-grade of pentachlorophenol (i.e., 86 percent by weight of pentachlorophenol) in 100 g of ethyl alcohol, which yielded a 3 percent "penta" solution.

A scanning electron micrograph of a Schleicher Schuell No. 589 white ribbon filter paper is shown in Figure 2. A scanning electron micrograph of a Whatman filter paper is also shown for comparison. The two types of filter paper appear similar in the scanning electron micrographs. The similarity of the filter papers has great implications with respect to the calibration of filter papers for suction measurements.

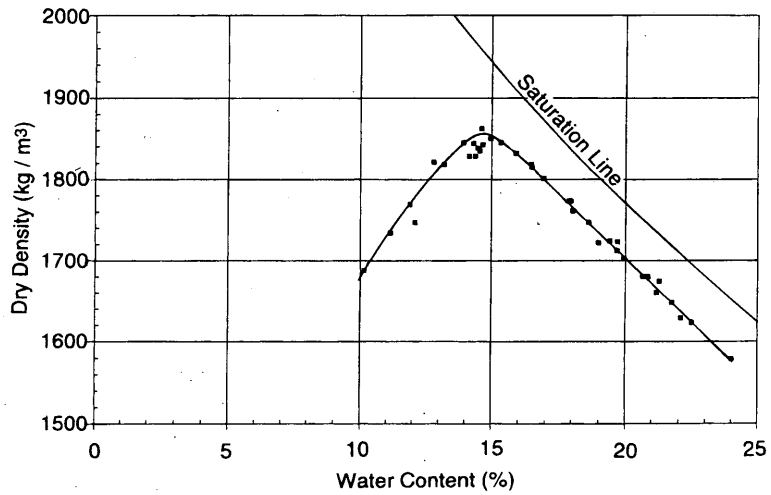

FIGURE 1 Compaction characteristics of till.

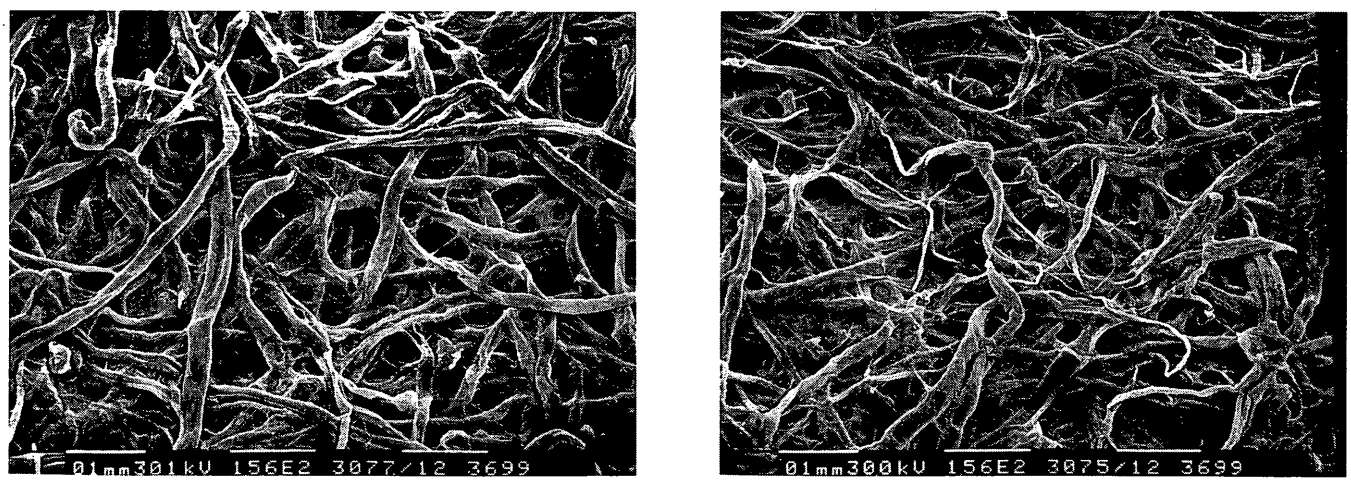

FIGURE 2 Scanning electron micrographs: *left,* Schleicher and Schuell No. 589 filter paper; *right,* Whatman filter paper.

Installation Procedures for Filter Paper Sensors

The jet-fill tensiometers, quick-draw tensiometers, or MCS-6000 thermal conductivity matric suction sensors were snugly fitted into a hole drilled into the compacted specimens (Figures 3–5). The psychrometers were installed in sets of three (Figure 6). These sensors (i.e., jet-fill tensiometers, quick-draw tensiometers, MCS-6000 sensors, and psychrometers) are subsequently referred to as reference sensors.

Installation of Good-Contact Filter Papers in Standard AASHTO Compacted Specimens

Two installation procedures were used. In the first procedure a vertical cut was made in the compacted specimen at a distance of approximately 3 cm on either side of the reference sensor (Figure 3). In the second procedure a single horizontal cut was made at a distance of approximately 2 cm below the tip of the sensor (Figure 4). The cut was made either with a bow saw equipped with a piano wire for moist specimens or a with a hacksaw blade for drier specimens.

A triple sandwich filter paper sensor was installed in each cut. The specimen was held together with masking tape, then wrapped with Saran wrap and aluminum foil followed by an outer layer of masking tape. The specimen was then placed in a styrofoam chest packed with styrofoam chips and left to equilibrate with time.

Installation of Noncontact Filter Papers in Standard AASHTO Specimens

Three vertical holes surrounding the reference sensor were drilled into one end of a compacted specimen by a 22.23-mm (⅞-in.) drill bit. A plastic hair roller was installed in each hole (Figure 5). A sin-

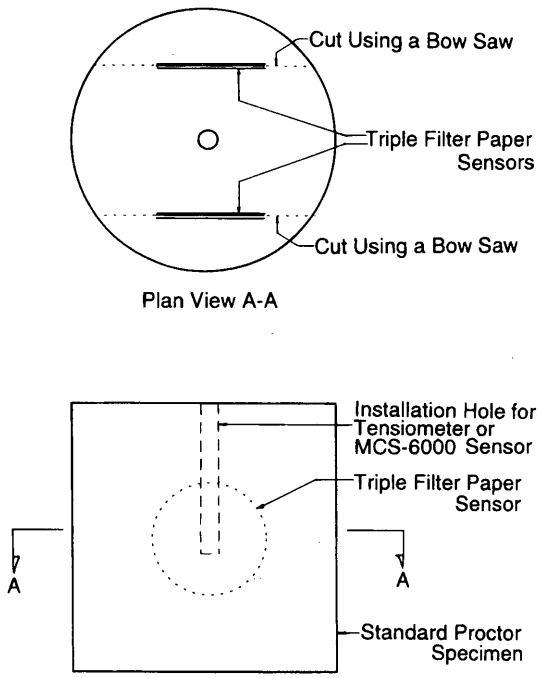

FIGURE 3 Setup 1 for calibration of good-contact filter paper sensors in standard Proctor specimens.

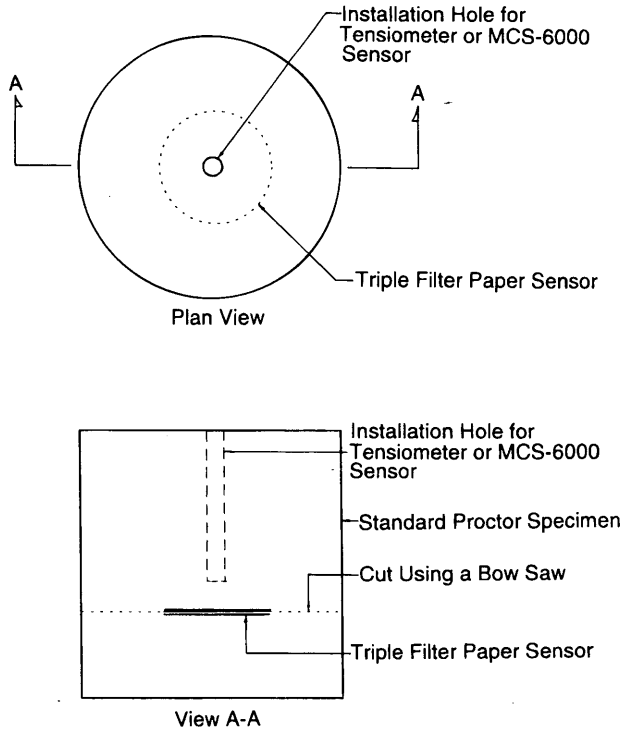

FIGURE 4 Setup 2 for calibration of good-contact filter paper sensors in standard Proctor specimens.

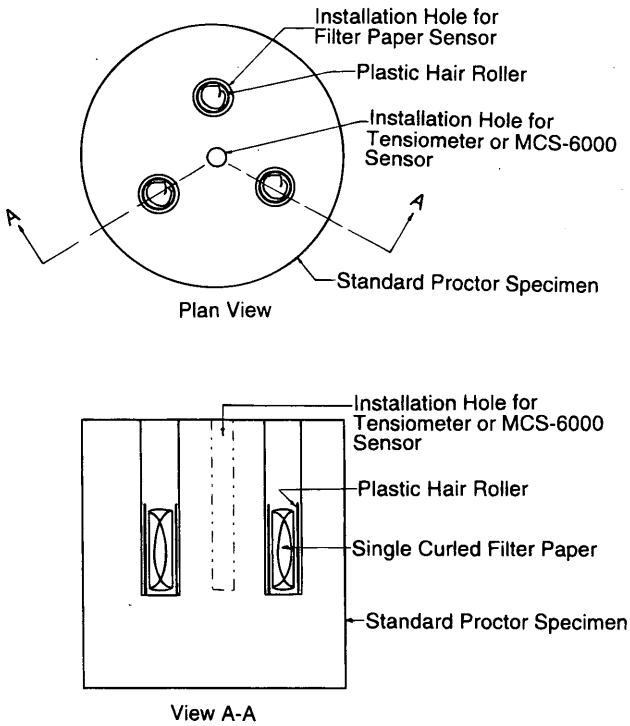

FIGURE 5 Setup for calibration of noncontact filter paper sensors in standard Proctor specimens.

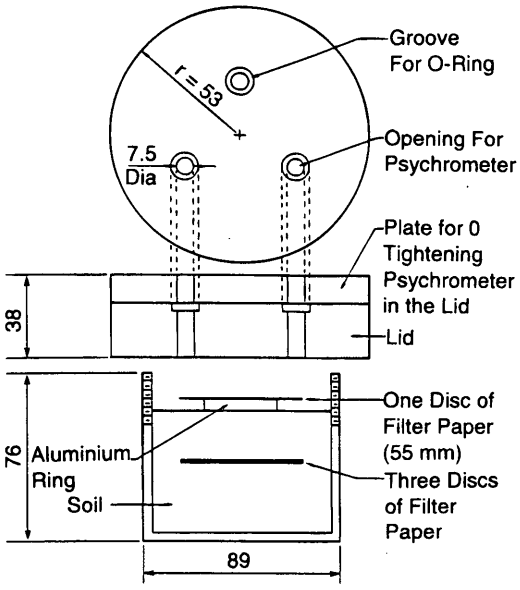

FIGURE 6 Lucite container for filter paper calibration when psychrometers are used as reference sensors.

gle filter paper sensor was curled with tweezers to fit inside each hair roller. The specimen was then wrapped in Saran wrap and aluminum foil and tightly bound with masking tape. The specimen was left to equilibrate in a styrofoam chest filled with styrofoam chips.

Installation of Good-Contact and Noncontact Filter Paper for Calibration Using Psychrometers

Two slices of soil cut from a standard AASHTO compacted specimen were trimmed to fit into a Lucite container. Each slice was approximately 3 cm thick. A triple sandwich, good-contact filter paper sensor was placed between the slices. The two slices of soil were pressed tightly together inside the Lucite container. This procedure ensured good contact between the filter paper sensor and the soil. A single noncontact filter paper sensor was also installed by placing the filter paper on an aluminum ring placed on the surface of the soil. The setup is shown in Figure 6.

The Lucite container was fitted with three psychrometers and placed in a steel beaker immersed in a water bath for equilibration (Figure 7). The temperature of the water bath was maintained at 24°C.

PRESENTATION OF RESULTS

The suction-versus-compaction water-content relationship for the standard AASHTO compacted till specimens is presented in Figure 8. The curve in Figure 8 is not a soil-water characteristic curve because the relationship was obtained from a set of nonidentical specimens. Also shown in Figure 8 are the total suction and matric suction curves obtained from another study on a similar till (*12*).

Calibration data obtained from the triple sandwich, good-contact filter paper sensors are presented in Figure 9. The water-content data for all three filter papers in each of the triple sandwich sensors were similar.

Calibration data from the noncontact single filter paper sensor are presented in Figure 10. The calibration was conducted from low suction values of less than 10 kPa to suction values of approximately 1000 kPa. In retrospect, the calibration by the sorption procedure (i.e., noncontact filter paper) would be more meaningful if it were restricted to high suction values.

DISCUSSION OF RESULTS

Results of suction measurements on the compacted till are discussed, followed by a discussion of the results of the calibration of the filter paper sensors. The filter paper calibration curves obtained from this study are compared with currently available calibration curves. The merits or demerits of the indirect calibration procedure are discussed.

Suction Measurements on the Compacted Till

The suction-versus-compaction water-content data (Figure 8) show that the suctions measured in the compacted till specimens have values comparable with those obtained from previous tests on a simi-

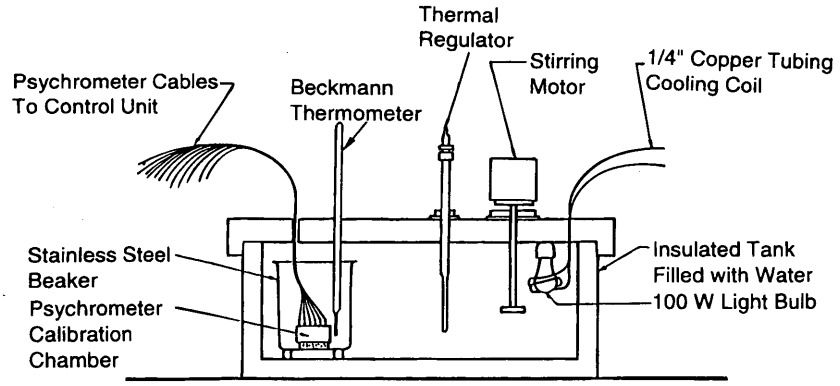

FIGURE 7 Water bath for calibration with psychrometers (*12*).

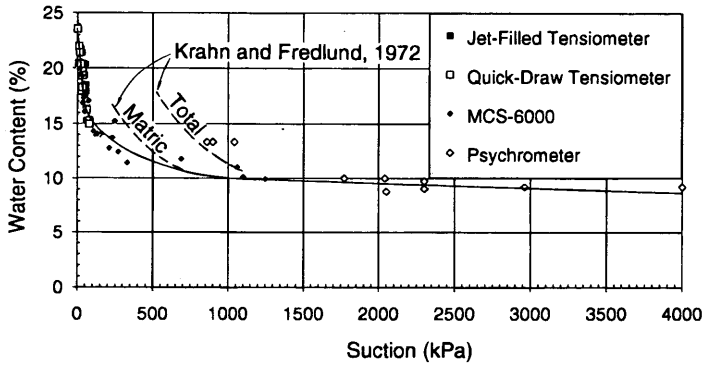

FIGURE 8 Water-content–suction relationship for compacted till.

lar till (*12*). The psychrometer readings appear to correspond well to the total suction curve from the previous study (*12*).

The suction-versus-compaction water-content data, along with the void ratio and the degree-of-saturation versus compaction water-content relationships, are shown side by side in Figure 11 for comparison. The void ratios and degree-of-saturation values were calculated from the compaction data in Figure 1.

Figures 8 and 11 show that the matric suction of the compacted specimens varied inversely linearly with compaction water content up to the optimum water content of 15 percent. At compaction water contents less than the optimum water content the matric suction values increased rapidly with a decrease in water content. The matric suction value at the optimum water content was approximately 80 kPa.

Results of Calibration for Filter Paper Sensors

The calibration curve for the good-contact filter paper sensor can be fitted by a bilinear curve (Figure 9). There appears to be significant scatter near the break in the calibration curve. The calibration data for the noncontact filter paper sensors also appear to fit a bilinear curve (Figure 10). The data from the noncontact filter paper sensors appear to be more scattered than the data for the good-contact filter paper sensor.

The water contents of the filter papers in good contact with the soil (Figure 9) were in better agreement with the suction values measured by the reference sensors than the water contents of the filter papers not in contact with the soil (Figure 10) for suction values of the compacted till below 100 kPa (i.e., above the optimum water content of the till).

It would appear that above the optimum water content of the till, there is a direct transfer of water via the liquid phase. In other words, conductive flow is more efficient and reliable in the equilibration process at water content above the optimum.

Below the optimum water content the results obtained for the noncontact filter paper sensors do not appear to be inferior to the results obtained for the good-contact filter paper sensors. Below optimum water content the water is tightly bound to the soil particles. Liquid flow is small in comparison with the vapor flow. Consequently the variations in the water content as a result of liquid flow are small. The small liquid flow may be one reason for the seemingly smaller scatter, regardless of whether the filter paper is good contact with the soil. The differences may also be exaggerated because of the use of a logarithmic scale for suctions.

The greatest scatter in the calibration data for the filter paper sensors occurs near the break in the bilinear curve. This is more obvious for the noncontact filter paper sensors (Figure 10) The scatter could be due to liquid flow being prominent in some instances and not in others at suction values near the break in the calibration curve. For the noncontact filter paper sensor it would appear to be more meaningful to restrict the calibration for suctions greater than 100 kPa.

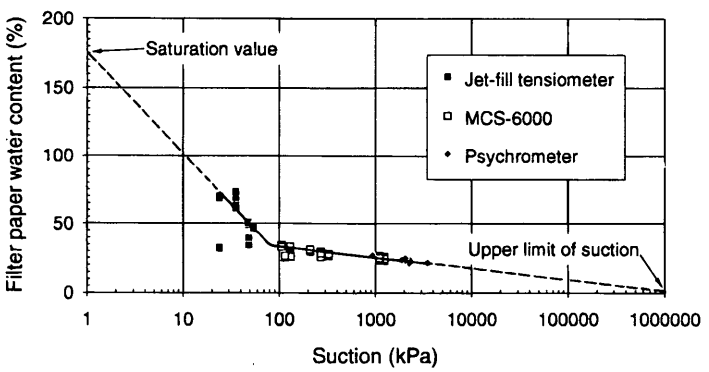

FIGURE 9 Data from calibrations of good-contact filter paper sensors, considering data from all three filter papers of each triple sandwich sensor.

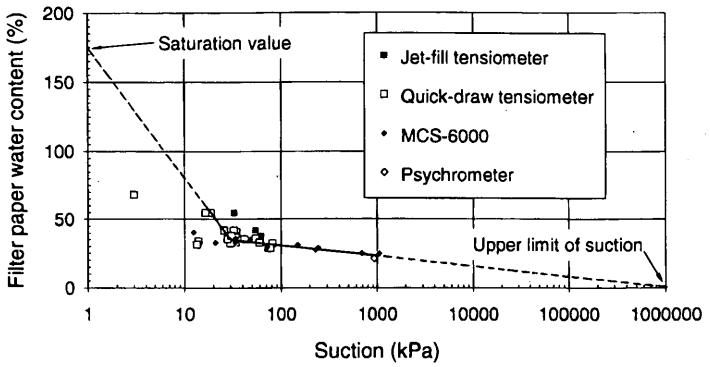

FIGURE 10 Data from calibrations of noncontact filter paper sensors.

Comparison of Filter Paper Calibration Curves

The calibration curves obtained for the good-contact filter paper sensors and the noncontact filter paper sensors are shown in Figure 12 along with some calibration curves previously obtained by others (*13,14*) for the same brand of filter paper.

There appear to be considerable variations in the calibration curves in Figure 12. There could be several reasons for the variations. First, the calibrations covered a time span from 1968 to the present. The characteristics of the Schleicher Schuell filter papers could vary over this time period. Second, the pretreatments given to the filter papers were not the same, although the same fungicide was used in each case. In the present study the treated filter papers were oven dried. The filter papers in the other calibrations (*13,14*) were air dried. The oven drying was supposed to assist in suppressing the hysteresis effects. Third, the contact of the filter paper with the soil in each case varied widely. In one case (*13*), only one calibration curve was presented, presumably applicable to both good-contact and noncontact situations. In another case (*14*) a filter paper was placed at the bottom of the soil specimen, separated from the soil by a paper towel, and a second filter paper was laid on the surface of the soil. The filter paper at the bottom of the soil was deemed to have good contact with the soil, and the filter paper laid on the soil surface was considered to be in uncertain contact with the soil.

It appears that the breaks in all the calibration curves fall between 20 and 90 kPa. This suggests that the transition from liquid flow being dominant to vapor flow being dominant occurs near 20 kPa to 90 kPa.

The low suction portion of the calibration curve for the noncontact filter paper (Figures 10 and 12) may not be meaningful, as the calibrations were obtained by a sorption process. The sorption process is more appropriate for high suction values.

Validity of the Calibration Curves from This Study

The calibration curve in Figure 9 for the good-contact filter paper sensors is applicable for assessing both matric suctions and total suctions in any soil. This is because the water contents of the good-contact filter paper in Figure 9, which correspond to matric suction values, were equated to matric suctions of the compacted till specimens.

The calibration curve for the noncontact filter paper sensors in Figure 10 is strictly valid only for the measurement of changes in

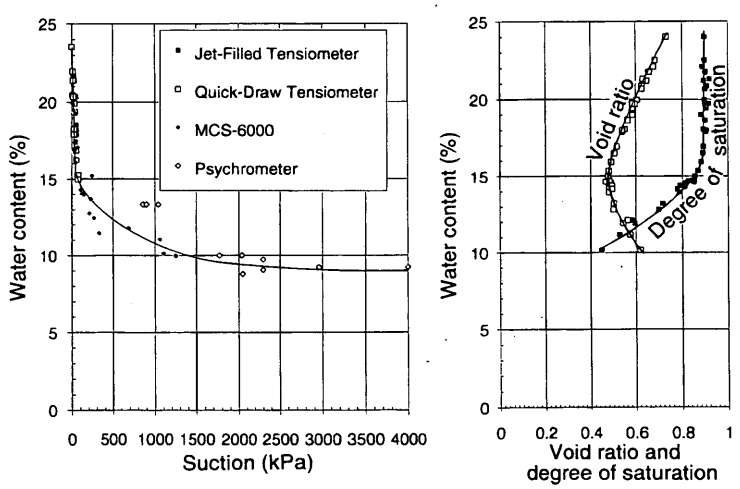

FIGURE 11 Relationship between (*left*) suction–water-content relationship and (*right*) degree of saturation (and void ratio) versus water-content relationship for compacted till.

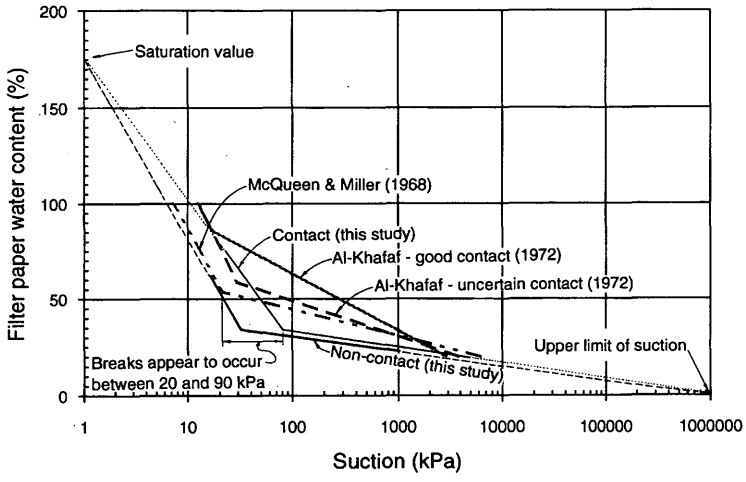

FIGURE 12 Comparison of calibration curves for Schleicher Schuell No. 589 filter paper sensors.

matric suction and preferably only in the same soil (i.e., till) that was used in the calibration. The water contents of the filter paper in Figure 10 correspond to the total suctions of the soil. The suction values in Figure 10, on the other hand, were matric suction values of the soil, which were measured with tensiometers or MCS-6000 thermal conductivity sensors. The water contents of the filter paper sensor corresponding to the total suctions of the soil were equated thus with the matric suctions of the soil. This procedure is inconsistent, and a separate evaluation of the osmotic suctions is required.

Consequently, psychrometers should be used only for the calibration of noncontact filter paper sensors. If filter paper in contact with the soil were calibrated by use of a psychrometer for assessing the suction in the soil, the water content corresponding to unknown matric suctions in the filter paper would be equated with the total suctions of the soil unless, of course, a separate evaluation of the osmotic suction were also conducted. At low water contents the extent of the contact between the soil and the filter may not be significant because the water flow will be restricted to the vapor phase.

CONCLUSIONS

The suction values were found to vary inversely linearly with compaction water contents in till specimens compacted at water contents wetter than optimum. The matric suction value at optimum water content was approximately 80 kPa for the till.

Compacted soil specimens at constant suction can be used for the calibration of filter paper sensors. The calibration, however, should be conducted in such a manner that the water contents of the filter paper sensors corresponding to matric suction values are referenced to matric suction values of the compacted soil specimens. Similarly, the water contents of the filter paper sensors corresponding to total suction values should be referenced to total suction values of the compacted soil specimens. The filter paper sensors, when calibrated appropriately, can be used for both matric suction and total suction measurement within the appropriate range of calibration values.

Calibration results for the filter paper sensors appear to have less scatter when the filter paper sensors are in good contact with the soil than when the filter papers are not in contact with the soil.

The transition from liquid flow being dominant to vapor flow being dominant in the filter paper occurs at near 20 kPa to 90 kPa.

REFERENCES

1. Fawcett, R. G., and N. Collis-George. A Filter Paper Method for Determining the Moisture Characteristics of Soil. *Australian Journal of Experimental Agriculture and Animal Husbandry,* Vol. 7, April 1967.
2. McQueen, I. S., and R. F. Miller. Calibration of a Wide-Range Gravimetric Method for Measuring Moisture Stress. *Soil Science,* Vol. 106, No. 3, 1968, pp. 225–231.
3. Al-Khafaf, S., and R. J. Hanks. Evaluation of the Filter Paper Method for Estimating Soil Water Potential. *Soil Science,* Vol. 117, No. 4, 1974, pp. 194–199.
4. Snethen, D. R. and L. D. Johnson. *Evaluation of Soil Suction from Filter Paper. Miscellaneous Paper* GL-80-4. Geotechnical Laboratory, U.S. Army Engineer Waterways Experiment Station, Vicksburg, Miss., 182 pp.
5. Hamblin, A. P. Filter-Paper Method for Routine Measurement of Field Water Potential. *Journal of Hydrology,* Vol. 53, 1981, pp. 355–360.
6. Chandler, R. J., and C. I. Gutierrez. The Filter Paper Method of Suction Measurement. *Geotechnique,* Vol. 36, 1986, pp. 265–268.
7. Sibley, J. W., G. K. Smyth, and D. J. Williams. Suction-Moisture Content Calibration of Filter Papers from Different Boxes. *Geotechnical Testing Journal,* Vol. 13, No. 3, Sept. 1990, pp. 257–262.
8. Sibley, J. W., and D. J. Williams. A New Filter Material for Measuring Soil Suction. *Geotechnical Testing Journal,* Vol. 13, No. 4, Dec. 1990, pp. 381–384.
9. Chandler, R. J., M. S. Crilly, and G. Montgomery-Smith. A Low-Cost Method of Assessing Clay Desiccation for Low-Rise Buildings. *Proceedings of the Institution of Civil Engineers, Civil Engineering,* Vol. 92, May 1992, pp. 82–89.
10. Houston, S. L., W. N. Houston, and A-M. Wagner. Laboratory Filter Paper Suction Measurements. *Geotechnical Testing Journal,* 17, 1994, pp. 185–194.
11. McKeen, R. G. *Suction Studies: Filter Paper Method. Design of Airport Pavements for Expansive Soils.* Final Report DOT/FAA/RD-81/25. FAA, U.S. Department of Transportation, 1985.
12. Krahn. J., and D. G. Fredlund. On Total, Matric and Osmotic Suction. *Journal of Soil Science,* Vol. 114, No. 5, 1972, pp. 339–348.
13. McQueen, I. S., and R. F. Miller. Calibration and Evaluation of a Wide Range Method for Measuring Moisture Stress. *Soil Science,* Vol. 106, No. 3, 1968, pp. 225–231.
14. Al-Khafaf, S. *Evaluation of the Filter Paper Method for Estimating Soil Water Potential.* M. Sc. thesis. Utah State University, Logan, 1972.

Publication of this paper sponsored by Committee on Environmental Factors Except Frost.

Monitoring of Vertical Moisture Barriers Using Troxler Sentry 200-AP Device

SANET JOOSTE AND TOM SCULLION

Vertical moisture barriers have been used in numerous locations in Texas to minimize damage associated with expansive clays. Most of the applications use an impermeable fabric 2.4 m (8 ft) deep installed in narrow trenches at the edge of the highway. If the barrier is working correctly it should stabilize the subgrade moisture content inside the barrier. Attempts to measure barrier effectiveness have frequently caused problems because of the unreliability of moisture-measuring sensors. An attempt to monitor a barrier is made with the Troxler Sentry 200-AP device. This capacitance-measuring system requires the installation of a polyvinyl chloride pipe 51 mm (2 in.) in diameter both inside and outside the barrier. The capacitance readings made inside the tubes are converted to moisture-content readings by a laboratory calibration procedure. The system is demonstrated on a major moisture barrier project on I-45 in which 90 km (56 mi) of barrier are being installed. To date the Troxler system is working well. The 2.4-m barrier appears to be effective in stabilizing the moisture content of the top 1.5 m (5 ft) of subgrade. Below that depth the moisture contents inside and outside the barrier are similar.

Expansive clays are known to cause millions of dollars' worth of damage to structures in the United States and elsewhere. Their effect on the riding quality of highways is well known. In Texas the treatment often recommended for minimizing the damage is to replace approximately 1.5 m (4.8 ft) of swelling material with a nonswelling low-plasticity-index fill material. On most projects this strategy is cost prohibitive. Therefore for the past 20 years the Texas Department of Transportation has been experimenting with various methods of minimizing damage by encapsulating clays with impermeable fabrics. Both horizontal and vertical moisture barriers have been used. References to their performance can be found in work by Steinberg (*1*) and in Picornell et al. (*2*).

To evaluate the effectiveness of these barriers, both long-term pavement performance and short-term instrumentation experiments have been conducted. The long-term studies have generally shown that these barriers have been successful in limiting the roughness induced in the highways by expansive subgrades (*1*). The short-term instrumentation studies have been less successful primarily because of the poor durability of the available moisture and suction-measuring equipment.

For a vertical moisture barrier to be working correctly it must stabilize the moisture content beneath the highway. It is the fluctuations in moisture content that are responsible for the large volume changes of swelling clays. Expansive clay damage could be minimized by limiting the infiltration of water from the edge of the highway. Therefore a quick and inexpensive method of judging the barrier effectiveness is to monitor the moisture content relative to depth both inside and outside the barrier. Once the system has reached an equilibrium condition the moisture content inside the barrier should show significantly less variation than that outside.

In the past 20 years numerous efforts have been made to monitor moisture contents with various types of devices, including psychrometers and moisture blocks. A major concern has been the durability of these systems. Several researchers have noted instrumentation problems occurring in the first couple of months after gauge installation.

Efforts have been made to use a relatively new moisture-measuring device, the Troxler Sentry 200-AP, to evaluate the effectiveness of a vertical moisture barrier being installed on a major Interstate widening project on I-45 near Dallas, Texas. This device is described in the next section of this paper, together with a description of the field installation and laboratory calibration work. This is followed by a discussion of the data collected in the first year after barrier installation.

MOISTURE MEASUREMENT WITH TROXLER SENTRY 200-AP DEVICE

Description of Device

The Sentry 200 family of products is designed for a variety of industrial and agricultural moisture-measurement applications. The Sentry 200-AP, which is the device used in this investigation, responds to changes in the dielectric constant of a material whose moisture content is to be determined. Most dry solid materials such as sand, clay, and other organic materials have a dielectric constant between 2 and 4, whereas water has a dielectric constant of 78 (*3*). The moisture content of a material is determined by measurement of changes in dielectric constant of the material.

The probe operates inside an access tube that enables it to measure moisture at any depth to which an access tube can be installed. The time and calendar record the exact time and date of the moisture measurements. The device is capable of storing up to 1000 field measurements, and the data can be stored and downloaded to a computer.

The gauge consists of a calibrated moisture probe that measures volumetric moisture content, a control unit, an access tube mount, and cable stops (Figure 1).

Installation Procedure of Access Tube

The moisture probe is lowered into an access tube from which it makes the moisture measurement. The access tube consists of a polyvinyl chloride (PVC) pipe 50 mm (2 in.) in diameter, which is installed at the depth at which a moisture measurement is to be taken. A summary of the installation procedure of the access tube follows:

Texas Transportation Institute, CE/TTI Building, Texas A&M University, College Station, Tex. 77843.

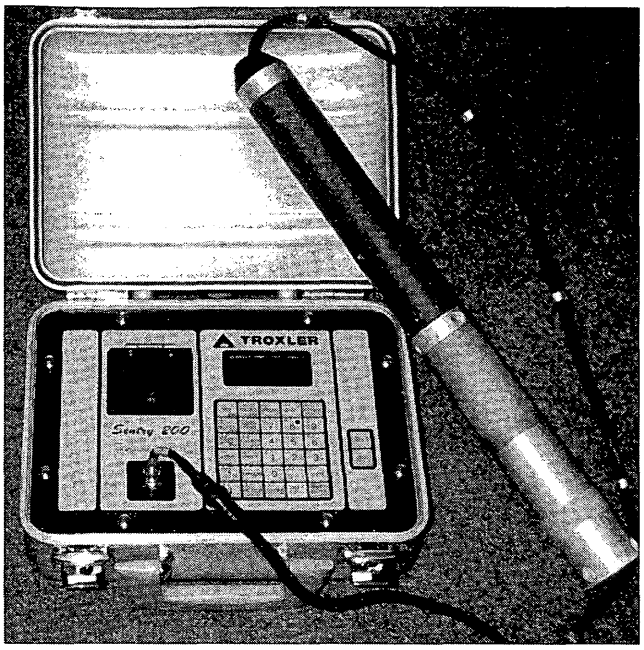

FIGURE 1 Sentry 200-AP moisture measurement device.

1. Locate the area where moisture is to be measured.
2. Determine the maximum depth of measurement.
3. Obtain a section of PVC access tube.
4. Ensure that the access tube is the correct length. The bottom of the tube must be sealed and should extend at least 150 mm (6 in.) below the lowest point at which a measurement will be made.
5. Auger a hole with the same diameter as the PVC tube into the soil to the desired depth of installation. A Shelby tube sample should also be taken to the desired depth, and the excavated soil can be saved for subsequent calibration.
6. Drive the PVC tube into the augered hole. The PVC pipe must fit tightly against the earth walls of the augered hole to prevent the formation of air voids between the access tube and the surrounding soil. The presence of air voids could lead to unreliable moisture readings.

Calibration Procedure

The calibration procedure as described by the users' manual for the Sentry 200-AP is discussed briefly in the next section. However, it was necessary to make a laboratory calibration of soil from the site where moisture measurements were to be taken because of the narrow range of moisture that the field-obtained samples had. This second calibration procedure was developed by the Texas Transportation Institute and is not included in the users' manual for the Sentry 200-AP.

Field Calibration Procedure

1. It is recommended that core samples be removed from the access tube locations. These samples will be analyzed for moisture content and the data used for performing a calibration of the Sentry 200-AP.
2. If possible obtain samples with varying moisture levels. This can be accomplished by taking samples during dry periods and also by taking samples after a heavy rain.
3. In most cases the samples can be obtained during the installation of the access tube.
4. Obtain a core sample for each measurement depth. Note: Core samples may be taken from other locations as long as the soil and moisture content are the same as those of the soil around the access tube.
5. After all the core samples have been taken it is necessary to obtain a gauge reading with the moisture probe at the exact position of each core sample. This gauge reading will correspond to the laboratory-derived moisture content of the soil samples collected from the same location.

Laboratory Calibration Procedure

It is essential that the soil from which the core samples are taken have a wide range of moisture content. If it does not, the range of moisture content over which the calibration is made will not be sufficient, and the data will not fit a regression line. This problem can lead to scattered data and inconsistent moisture measurements. If the core samples do not have at least a 15-percent variation in moisture content, it is necessary to mix samples of soils with a variety of moisture content values from the location where moisture measurements are to be taken. The procedure follows:

1. Excavate enough soil of the same type as that for which the moisture measurement is to be taken to fill at least three 20-L containers.
2. Thoroughly dry and crush the soil so it will pass through a No. 40 sieve.
3. Cut a PVC pipe long enough that the bucket can be sealed airtight, and seal off the bottom of the pipe by gluing a piece of plastic material to it or by applying an end cap. Place the PVC pipe in the center of the container.
4. Mix three or more batches of soil with different quantities of water to obtain moisture contents that vary from very dry to very wet. (The difference in moisture content between wet and dry mixes should be more than 15 percent.)
5. Carefully place the soil around the PVC pipe in the container until the bucket is half full. Compact the soil carefully so as not to disturb the PVC pipe but thoroughly enough to remove all possible large voids in the soil. There should be no gap between the PVC pipe and the soil, but if the soil is compacted too tightly against the pipe the moisture readings may be artificially high.
6. Fill the bucket and compact the soil again.
7. Save a sample of each batch with a different moisture content in a plastic bag and calculate the moisture content in the laboratory.
8. Seal all the buckets airtight and save them for subsequent calibration.
9. Gauge-derived moisture readings can be taken at this stage or later when the actual moisture content is known.

Determination of Moisture Content

Refer to the following ASTM standards for more information on determining actual moisture content: ASTM D-2216, *Laboratory Determination of Water Content of Soil, Rock, and Soil Aggregate*

Mixtures; ASTM D-4643, *Method for Determination of Water Content by Microwave Oven.*

Use the core samples obtained from the field or use the self-mixed samples from the laboratory to analyze the actual gravimetric moisture content of the soil. Then calculate the percent moisture by volume (Pv), using the following formula (*4*):

$$Pv = Pd \times Db$$

where Pd = percent moisture by dry weight and Db = bulk density (g/cm^3).

Calibration of Sentry 200-AP

1. At this stage the gauge-derived moisture readings have already been entered and saved under a suitable name.
2. Recall this calibration and enter the laboratory-obtained moisture content that corresponds to each gauge-derived reading.
3. The calibration in now completed. The Sentry 200-AP will give a fit coefficient that is an indication of how well the moisture data obtained from the laboratory fit the gauge-derived readings. A plot of the gauge readings versus the actual moisture content should result in a linear curve.

Note: In general a fit coefficient of less than 0.6 indicates a less acceptable correlation of data.

Moisture-Content Readings After Calibration

Moisture-content values can now be taken at any time simply by recalling the corresponding calibration and performing a moisture measurement. The sentry 200-AP will display the gauge reading as well as the corresponding moisture content on the screen. It is not necessary to perform a calibration for each test hole from which moisture data are to be taken. One calibration for each soil type is sufficient if the soil used for the calibration is representative of the soil type in general and if the range of moisture over which the calibration was done is wide enough.

Repeatability of Sentry 200-AP Moisture-Measuring Device

The Sentry 200-AP is equipped with a calibration factor for sandy soils only. Therefore it was necessary to obtain a standard calibration for gravel and clay soils to be able to make moisture measurements without calibrating the probe for every test location.

Repeatability tests were performed with the Sentry 200-AP on a black clay and on gravel. These tests aided in determining the reliability and accuracy of measurements made with the moisture probe and provided calibration curves for clay and gravel in general. The test procedure was as follows:

1. The soil that was used for the tests was thoroughly dried.
2. A PVC pipe 50 mm (2 in.) in diameter was sealed off with an end cap and placed in the middle of a 20-L container. The pipe was short enough that the container could be sealed airtight.
3. Three batches of soil were mixed with different amounts of moisture (from very wet to very dry) and placed in three different buckets.
4. The soil was thoroughly compacted, and the buckets were sealed.
5. A sample of each of the soil batches was taken for laboratory measurement of actual moisture-content values.
6. After these actual moisture-content values were obtained the Sentry 200-AP was calibrated with the three different soil samples as three different data points.
7. A linear curve was fitted through these points and the calibration constant entered into the sentry control unit.
8. The repeatability of the Sentry device was tested one day after calibration by repetition of the moisture measurements on the samples, using the corresponding calibration.

The results of the calculation of the actual moisture contents of the black clay and the gravel are presented in Table 1. The gauge-derived repeatability results are presented in Table 2. The results in Table 2 are graphically presented in Figures 2 and 3.

It is evident from the data in Table 2 that the repeatability of the moisture probe is very good. The difference between readings at the same moisture content was insignificantly small. A regression was performed on the moisture data obtained from the repeatability tests. For both the clay and the gravel the data can be represented by a straight-line equation. The equation constants are as follows:

	Clay	*Sand/Gravel*
Slope	22.884447	46.566363
Intercept	3403	3238

The equation is

$$y = mx + c$$

where

y = gauge reading,
x = moisture content (percent by volume),
m = slope of the curve, and
c = intercept on y axis.

TABLE 1 Laboratory-Determined Water Content

Volumetric water content of a black clay		Volumetric water content of a gravel	
Sample no.	% moisture	Sample no.	% moisture
1	44	1	8.9
2	53	2	18.9
3	67	3	19.7

TABLE 2 Gauge-Derived Moisture Content

Volumetric water content of a black clay			Volumetric water content of a gravel		
Sample no.	Gauge reading	% moisture	Sample no.	Gauge reading	% moisture
1	4424	44.6	1	3652	8.9
	4417	44.3		3655	9
	4424	44.6		3646	8.8
	4419	44.5		3651	8.8
2	4575	51.2	2	4073	17.9
	4575	51.2		4071	17.9
	4574	51.2		4070	17.9
	4570	51		4072	17.9
3	4958	69.7	3	4196	20.6
	4959	68		4196	20.6
	4955	67.8		4197	20.6
	4952	67.8		4194	20.5

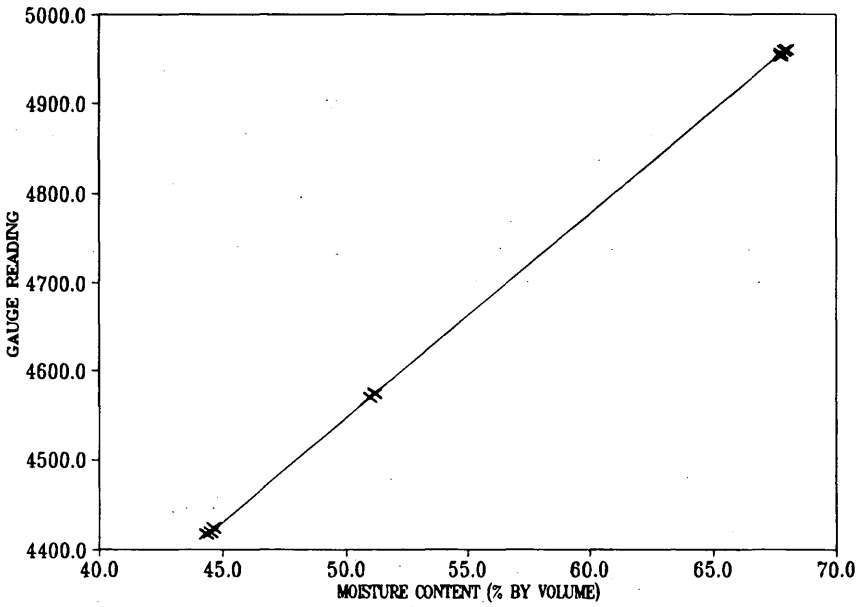

FIGURE 2 Repeatability data used for calibration of black clay soil.

CASE STUDY: FIELD DATA FROM I-45, DALLAS

Objective of Study

The objective of this study is to evaluate the moisture barrier installed on I-45. The evaluation involves stabilizing the moisture content of the soils inside the barrier and thereby minimizing the damage caused by shrinkage and swelling. To perform the evaluation the Texas Transportation Institute has placed instruments at four test locations along the highway to make moisture measurements on both sides of the barrier to a depth of 3 m (10 ft). The instrument chosen to perform the monitoring is the Troxler Sentry AP-200 device. The following section of this paper discusses moisture measurements obtained from inside and outside the moisture barrier over a period of 1 year after installation. Specific objectives for this study are to (*a*) provide moisture data from the four locations that have been instrumented in the northbound outer lanes of I-45 near Palmer, Texas, and (*b*) continue monitoring these sites for 2 years to gain the full benefit of the test program.

Description of Site

The material underlying the pavement is a grayish-brown and tan mixed clay with calcarious and limestone deposits. No seepage was encountered during drilling. This indicates that the groundwater table is below the maximum depth of drilling, which was approximately 6 m.

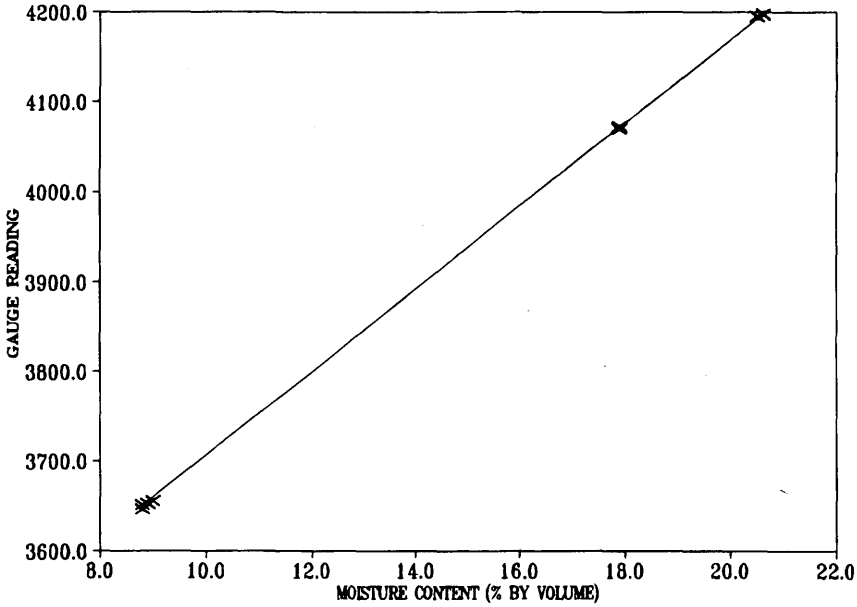

FIGURE 3 Repeatability data used for calibration on gravel.

The pavement initially consisted of 250-mm-thick concrete main lanes with an asphalt shoulder. The initial jointed concrete pavement had exhibited the roughness wavelengths typically associated with expansive clay. The pavement was scheduled for widening construction and a concrete overlay. An initial geotechnical investigation recommended replacing 1.5 m of the subgrade soil under the widened section. In lieu of this recommendation the district opted for a vertical moisture barrier, which had been reported to perform well in other districts in Texas, notably San Antonio. A moisture barrier was installed next to the new asphalt shoulder along the highway. To evaluate the effectiveness of the moisture barrier, access tubes were installed at four locations inside and outside the moisture barrier. During August 1993 a new 330-mm-thick concrete overlay was added on top of the existing concrete lanes and asphalt shoulder. Access tubes were reinstalled at the same locations along the highway. A cross section of the pavement after the new overlay was added is shown in Figure 4.

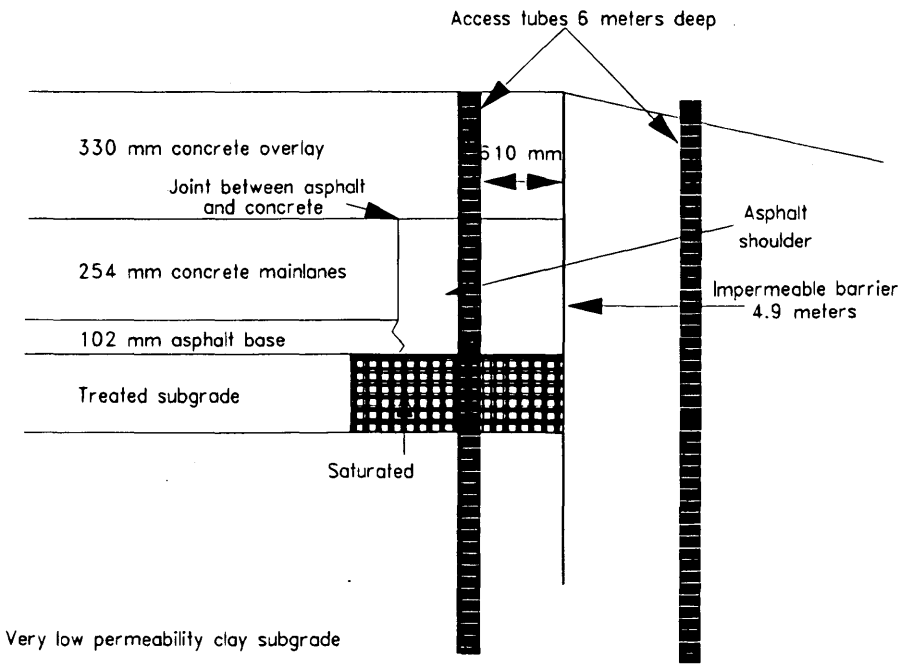

FIGURE 4 Cross section of I-45 near Palmer after concrete overlay.

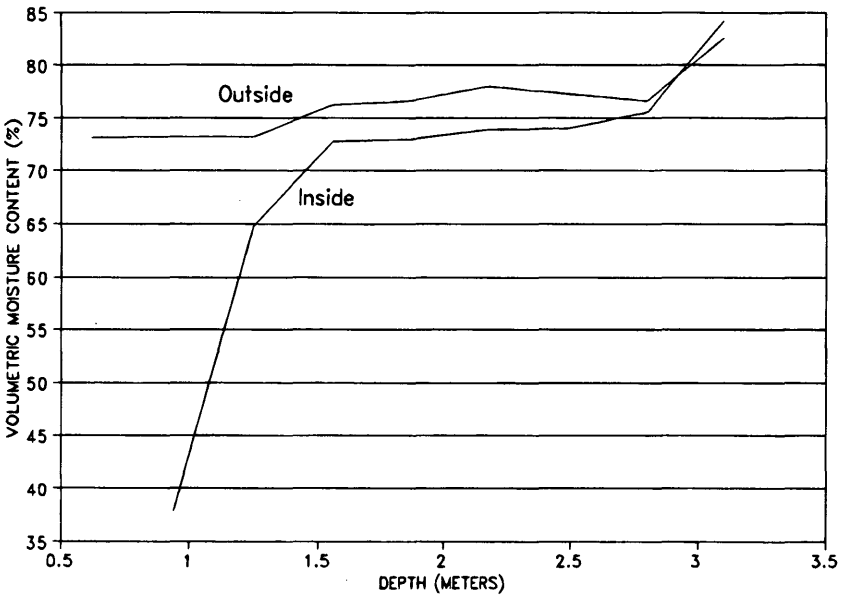

FIGURE 5 Moisture content on inside and outside of moisture barrier measured during May 1994 (Site 1).

Measurements with Sentry 200-AP Device

Moisture measurements were taken with the Sentry 200-AP device after installation of the access tubes in August 1993 and again in November 1993 and May 1994. It should be noted that all the access tubes extend to a depth of 6 m (10 ft), except at Location 2, where the depth of the hole was limited to 4.8 m (8 ft) by an impervious layer of soil. Because of distortion of some of the access tubes it was in some cases not possible to lower the moisture probe to the full depth of 6 m.

Presentation and Discussion of Results

Figures 5–8 show graphs of the measured moisture content during May 1994 inside and outside the barrier for each of the test locations. The volumetric moisture contents are reported as measured with the Sentry 200-AP with the calibration for clay soils. At each location the moisture content inside the barrier is lower than the corresponding moisture content outside the barrier for approximately the first 1.5 m (5 ft) throughout the whole period of evaluation. This is encouraging because the moisture content of the first meter below

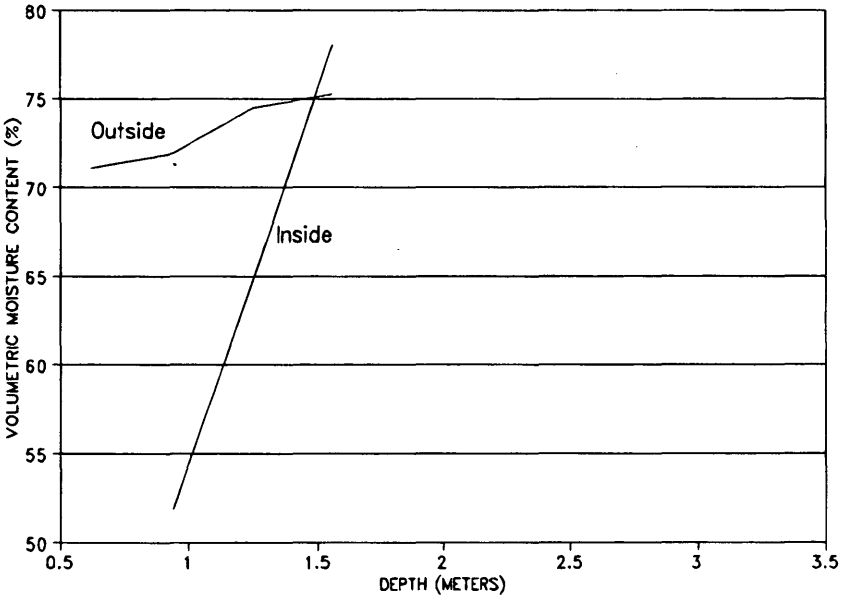

FIGURE 6 Moisture content on inside and outside of moisture barrier measured during May 1994 (Site 2).

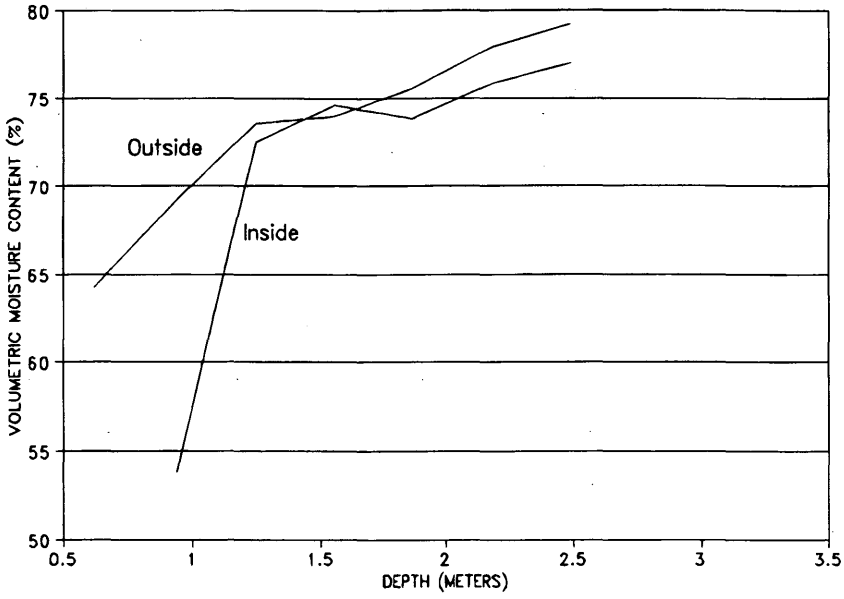

FIGURE 7 Moisture content on inside and outside of moisture barrier measured during May 1994 (Site 3).

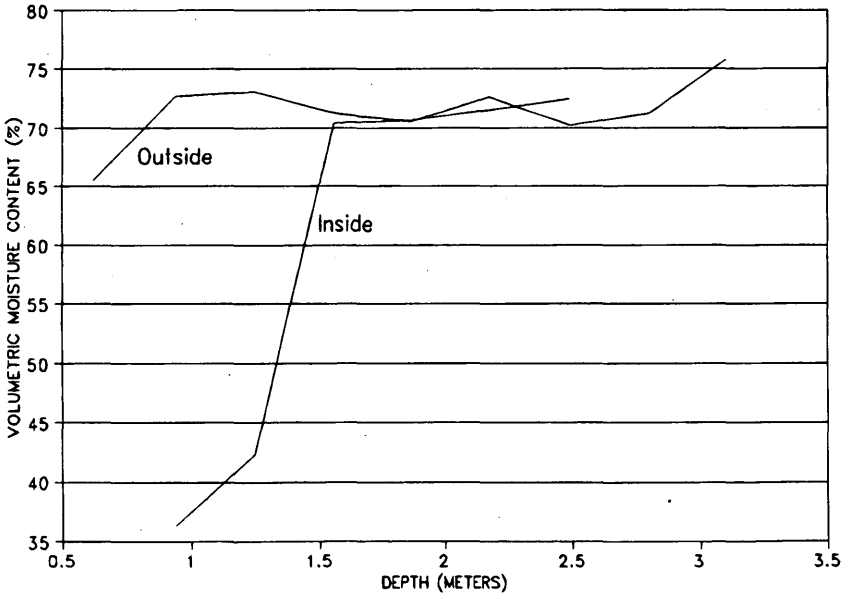

FIGURE 8 Moisture content on inside and outside of moisture barrier measured during May 1994 (Site 4).

the pavement is the most critical. Below 1.5 m the moisture content inside the moisture barrier increases gradually until it equals the moisture content on the outside at a depth of about 4.8 m (8 ft), which is at the bottom of the moisture barrier. This lends support to the conclusion that the moisture barrier operates effectively to keep water from seeping into the soil directly underlying the pavement.

However, from Figures 9–12 it is evident that the moisture content inside the barrier increases with time. It seems that the moisture outside the barrier is slowly coming into equilibrium with the moisture on the inside. This phenomenon is most probably caused by poor drainage conditions on the sides of the pavement. One proposed solution is to pave the median to prevent water from accumulating between the two lanes of pavement. Whether this would be economically feasible is questionable. Sufficient drainage on the outer lanes can be ensured by sloping earth banks at the sides of the road. Another drainage problem could be caused by the difficulty in achieving proper compaction of the backfill in the trench into which the moisture barrier is installed: high permeabilities in this area cause water to accumulate.

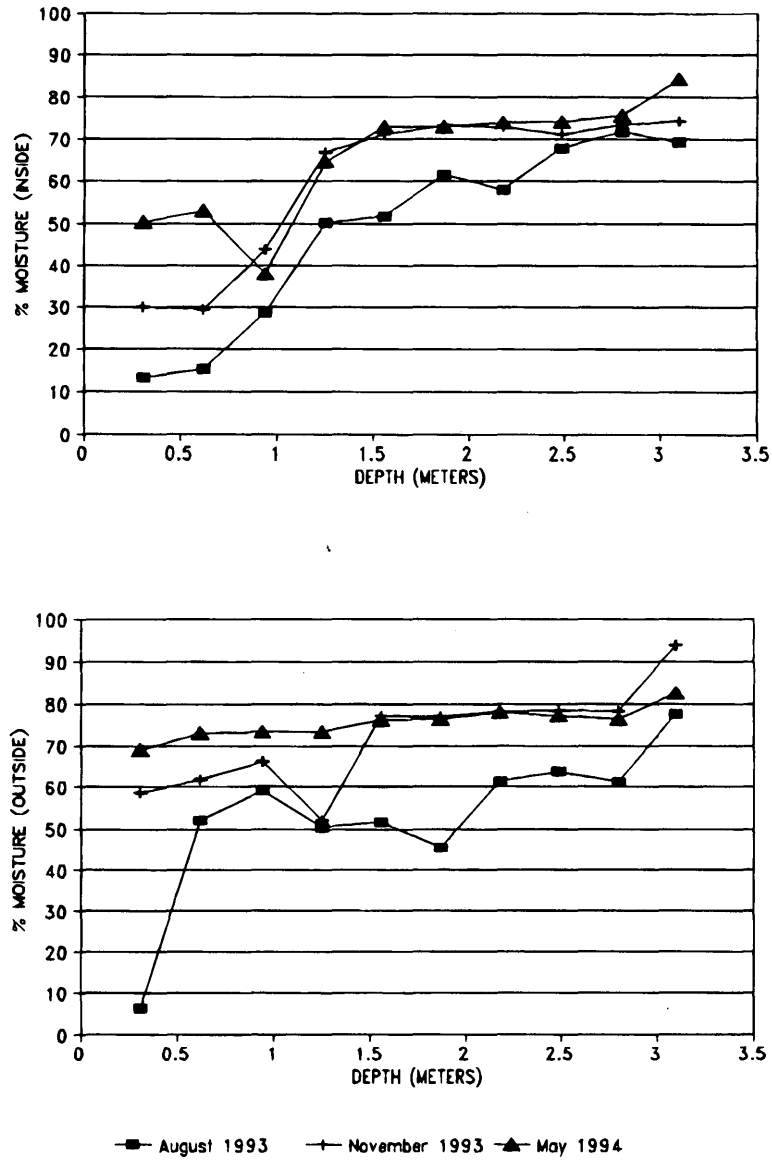

FIGURE 9 Volumetric moisture content on (top) inside and (bottom) outside of moisture barrier (Site 1).

CONCLUSIONS

From the first section of this paper it is evident that the Troxler Sentry 200-AP moisture-measuring device performs well in evaluating vertical moisture barriers. Moisture measurements taken with this device are quick and inexpensive and have been proved to be highly consistent and accurate. Laboratory calibration of the device permits moisture measurements of any soil type, and the PVC access tubes seem to be durable enough for repeated use for moisture measurements.

This device has been used for monitoring a vertical moisture barrier on a major Interstate highway near Dallas, Texas. Moisture contents inside and outside the moisture barrier have been recorded over a period of a year. The vertical moisture barrier seems to be effective in keeping the moisture content underneath the pavement from fluctuating and in keeping moisture from infiltrating from the edge of the highway. To a depth of 1.5 m the moisture content inside the moisture barrier seems to be lower than corresponding moisture contents outside the barrier. However, it is also evident that the moisture content inside the barrier increases with time as it slowly comes into equilibrium with the moisture content outside the barrier. This phenomenon could be a result of poor drainage conditions at the sides of the pavement. However, even with these poor drainage conditions the moisture activity is very slow, and the barrier is effective in keeping the moisture content from fluctuating with seasonal changes. Expansion of the subgrade clay soils is thus controlled and associated damage minimized by the use of a vertical moisture barrier.

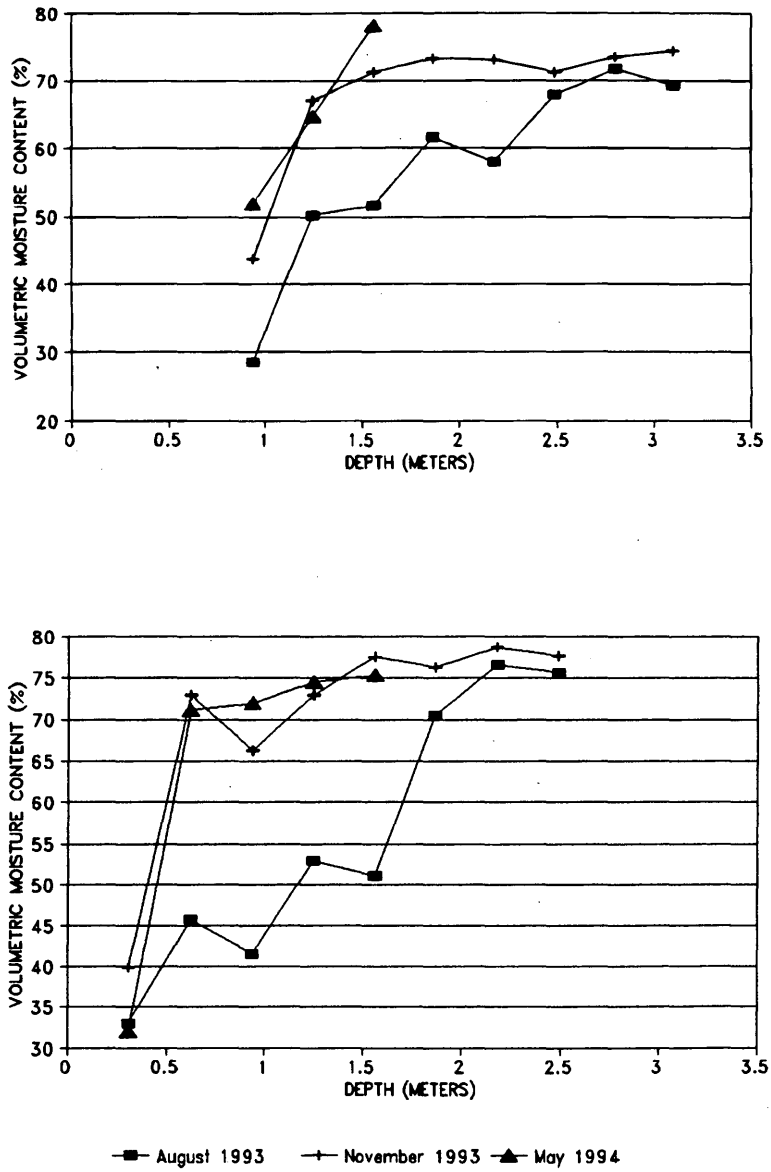

FIGURE 10 Volumetric moisture content on (top) inside and (bottom) outside of moisture barrier (Site 2).

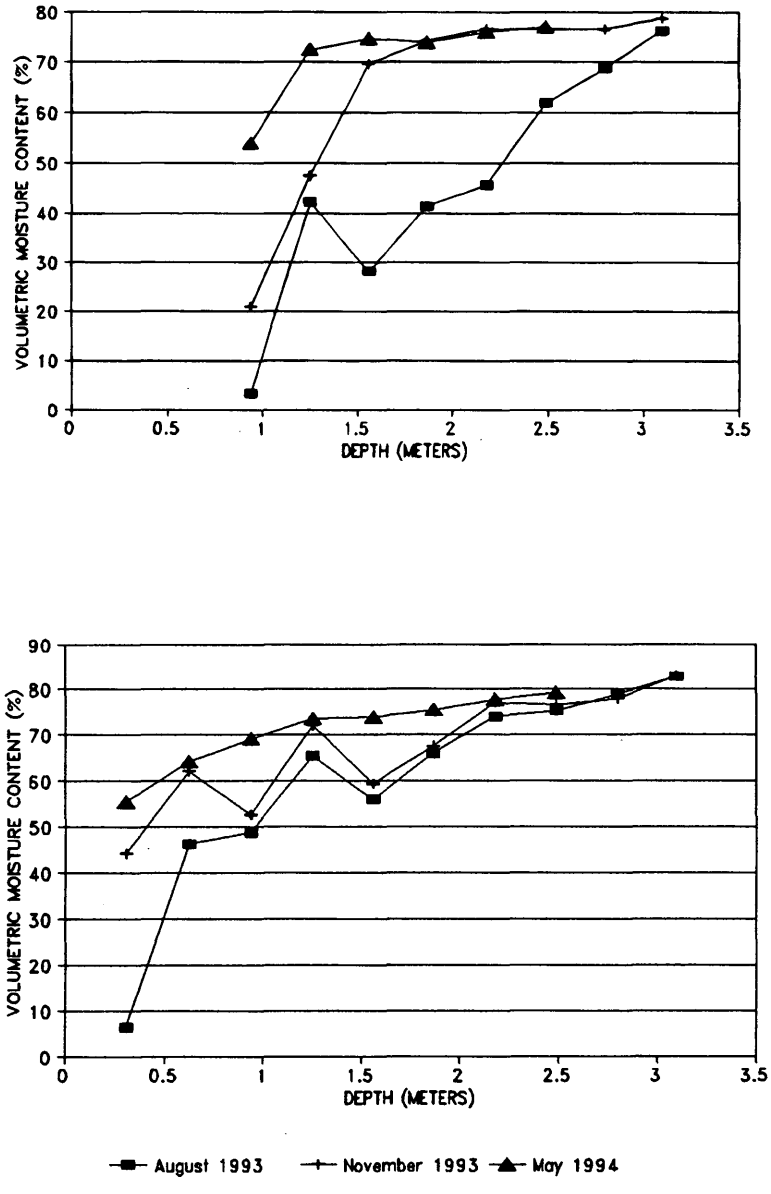

FIGURE 11 Volumetric moisture content on (top) inside and (bottom) outside of moisture barrier (Site 3).

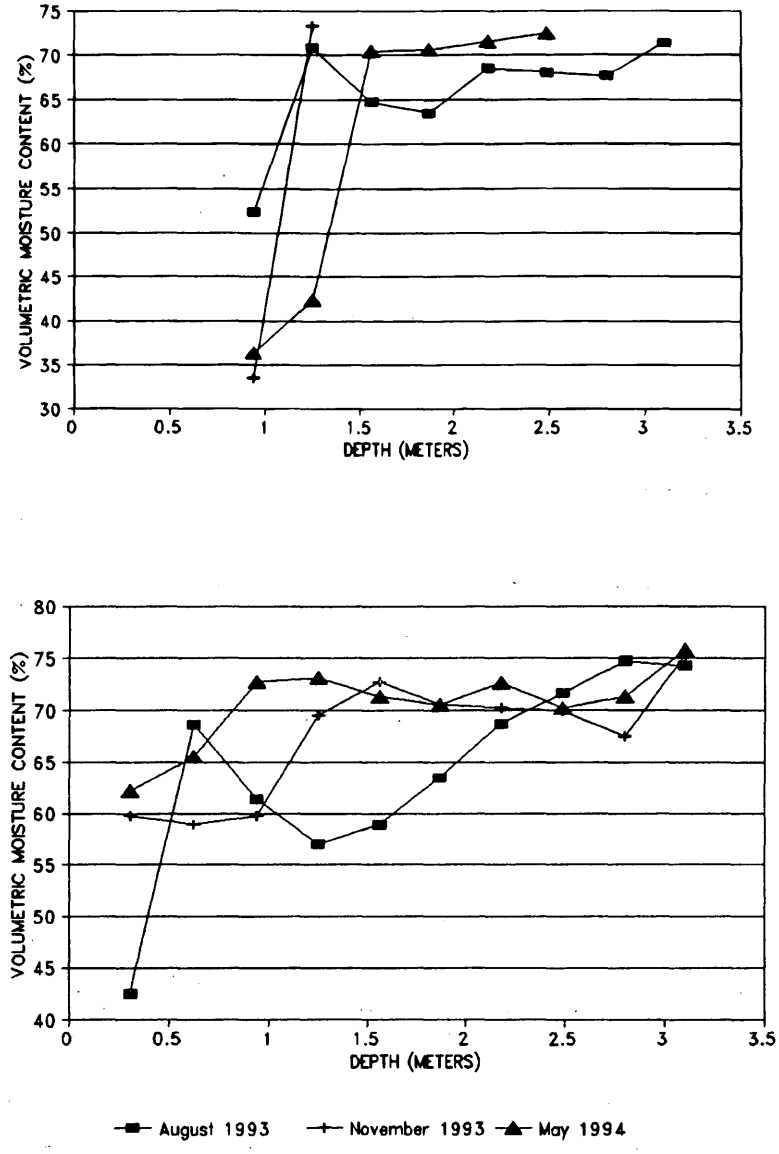

FIGURE 12 Volumetric moisture content on (top) inside and (bottom) outside of moisture barrier (Site 4).

REFERENCES

1. Steinberg, M. L. Deep Vertical Fabric Moisture Barriers in Swelling Soils. In *Transportation Research Record 790,* TRB, National Research Council, Washington, D.C., 1981, pp. 87–94.
2. Picornell, M., R. L. Lytton, and M. L. Steinberg. Matrix Suction Instrumentation of a Vertical Moisture Barrier. In *Transportation Research Record 837,* TRB, National Research Council, Washington, D.C., 1982, pp. 87–94.
3. *Sentry 200-AP User's Manual,* 2nd ed. Troxler Electronic Laboratories, Inc., March 1992.
4. Holtz, R. D., and W. D. Kovacs. *An Introduction to Geotechnical Engineering,* Prentice-Hall, Inc., Englewood Cliffs, N.J., 1981.

Publication of this paper sponsored by Committee on Environmental Factors Except Frost.

Characterization of Subgrade Soils at Simulated Field Moisture

GANESH B. THADKAMALLA AND K. P. GEORGE

It is important to assess the strength characteristics of subgrade soils at equilibrium moisture content (EMC), generally a few percentage points wet of optimum moisture content (OMC). Investigation of the effect of saturation—degree and mode—above OMC on the resilient modulus (M_R) of laboratory compacted subgrade soils is the topic of this paper. Three modes of saturating (wetting) are investigated: (*a*) capillary saturating, (*b*) vacuum saturating, and (*c*) molding wet of optimum. EMC and 96 percent saturation are the two different degrees of saturation considered. The M_R of soil samples, both coarse- and fine-grain, are evaluated for different combinations of degree of saturation and saturating mode. The test results indicate that the degree of saturation above OMC has a nominal effect (20 percent) on M_R of coarse-grain soils, whereas it has a severe effect (50 to 75 percent decrease) on the M_R of fine-grain soils. Another finding is that both degree of saturation and saturating mode affect the M_R of fine-grain soils. For interpretation of the results, particularly how M_R is affected by saturation, the four-phase concept for unsaturated soils is used.

Soils are characterized by the constants relating stress state variables or stress state variables to deformation state variables depending on the type of problem at hand. The constants relating stress state variables are cohesion and angle of internal friction for the shear strength equation, and pore pressure parameters for the pore pressure equation. Young's modulus, Poisson's ratio, bulk modulus, and so forth are the constants relating stress to strain. Sands are better characterized by bulk modulus and shear modulus than Young's modulus and Poisson's ratio, according to a work by Domaschuk and Wade (*1*). The hyperbolic equations for tangent Young's modulus and secant bulk modulus facilitating the use of generalized Hooke's law for the analysis of stresses and displacements in soil masses has been proposed (*2*). The constants for the hyperbolic tangent Young's modulus and tangent bulk modulus for a range of soils are tabulated elsewhere (*3*). All of the previously mentioned characterizations are suitable for a wide range of loading, including failure state.

The relative importance given to the behavior of soil under repeatedly applied stresses, compared with the behavior under gradual loading, can be attributed to the interest in simulating highway loading, and to developing a rational design procedure limiting the permanent deformations and deformation modulus of highway foundation for comfortable riding conditions. The characterizing parameter chosen for subgrade soil is designated as resilient modulus (M_R). M_R is the ratio of deviatoric stress to the resilient elastic axial strain.

AASHTO T274-82 encompasses the pioneering test specification proposed by AASHTO (*4*). Later, this test procedure was revised to AASHTO T292-91 I and subsequently to AASHTO T294/SHRP P46. The preceding referenced test methods are proposed for determining the dynamic elastic modulus (M_R) under conditions that reasonably represent real-world stress states of subgrade materials subjected to moving wheel loads. Application of repeated axial deviator stress of fixed magnitude, duration, and frequency to an appropriately prepared and conditioned cylindrical test specimen entails the test procedure designated in T274-82. During the test, the specimen is subjected to a static all-around stress. The resilient axial strain response of the specimen is measured and used for calculating the dynamic stress-dependent M_R. Numerous researchers have studied M_R of subgrade soils: Fredlund et al. (*5*), by molding samples at different moisture contents and densities; Edil and Motan (*6*), by preparing samples at optimum, dry and wet of optimum, and equilibrating to various soil suctions using moisture extractors; and Thompson and Robnett (*7*), by molding samples at optimum moisture content, optimum +1 percent, and optimum +2 percent and all of them at 95 and 100 percent of AASHTO T99 unit weight.

Pavement life depends on the performance and condition of its components. During the service life, subgrade undergoes moisture variations and consequently large strength fluctuations as well. To quantify the effect of the ambient conditions, AASHTO Guide (1992) proposed that an "effective modulus" be used in the design process. Effective modulus is an average modulus weighted with respect to seasonal changes. It is critical that the changes taking place in the strength characteristic of proposed subgrade soil at the expected field condition be investigated beforehand.

The subgrade is generally prepared by compacting to 95 to 100 percent of dry unit weight and at optimum moisture content (OMC), as determined by AASHTO T99. Upon sealing the ground surface, subgrade soil (with a pavement) exhibits an increase in the average water content at the shallower part of the subgrade and a decrease in fluctuations of water content over time (*8*). The moisture attained after construction is in equilibrium with the environment and is called the equilibrium moisture content (EMC). The moisture movement and moisture equilibria under covered areas have been studied by numerous researchers (*9–11*). Historically research studies of the effect of moisture on soils have coincided with a growing need to evaluate the climatic dependency of the soil parameters in highway construction projects. It has been reported (*9*) that the moisture stability beneath the greater part of the paved area is similar at every test site regardless of the climatic conditions. It was concluded (*10*) that the subgrade moisture content shows continuous small variations with seasons. Considerable work has been devoted to quantifying the factors that affect EMC. The factors known to influence EMC include the type of subgrade soil, level of water table in the vicinity, condition of the surface layer, and so forth. A moisture index designated as Thornthwaite moisture index (TMI) was developed (*12*), which relates subgrade moisture conditions to climatic indices, such as precipitation, evapotranspiration, mean monthly air temperature, and number of hours of daylight per

The University of Mississippi, Civil Engineering Department, University, Miss. 38677.

day. TMI is gaining acceptance for empirically estimating moisture conditions in pavement subgrade soils. The Corps of Engineers' study on subgrades of flexible airport pavements in Mississippi and in a few other states concludes: (*a*) the EMC in subgrade soils is often near the plastic limit and directly proportional to the liquid limit, (*b*) the degree of saturation corresponding to EMC of plastic soils exceeds 85 percent, and (*c*) the annual rainfall has no effect on EMC (*13*). Investigations of theoretical methods of estimating EMC include those of Black et al. (*14*), Russam (*15*), Coleman and Russam (*16*), and the researchers at the British Road Research Laboratory (*17*). According to a work by Chu and Humphries (*18*), the moisture content of the laboratory compacted soil sample at 0.914 m (3 ft) of water suction, applied at the top and bottom of the sample, can duplicate the field moisture content in noncoastal areas. In their work, investigations were conducted for correlating subgrade moisture with local factors such as type of subgrade soil, environmental factors, and so forth. The results, which covered 32 sites, showed that the finer the soil the greater the difference between the EMC and OMC. The maximum difference observed was approximately 8 percent at 55 percent fines content (−#200). The data trend is such that the EMC in a few soils, particularly with fines content less than 25 percent, was smaller than the OMC. Subsequently, efforts were made to develop a relatively simple procedure (capillary wetting) for conditioning soil specimens to simulate anticipated field moisture conditions.

For laboratory-compacted specimens, AASHTO T274-82/AASHTO T292-91 I test procedures suggest a backpressure saturating after molding the sample at optimum moisture content. This is a quick method of saturating when compared with the method prescribed elsewhere (*18*). AASHTO T294-92 I/SHRP protocol 46 (revised version of AASHTO T292-91 I) stipulates testing the sample at OMC and 95 percent maximum dry unit weight; however, it does not include backpressure saturating.

The objective of the study is to investigate the effect of field subgrade moisture (or EMC) on M_R and to determine the effect of saturation—degree and mode—on resilient modulus of subgrade soils. Different modes of saturating (wetting) studied include:

- Capillary saturating under 0.914 m (3 ft) of water suction (*18*). (A schematic diagram of the setup is shown in Figure 1).
- Vacuum/backpressure saturating as specified in AASHTO Designation T274-82/AASHTO T292-91 I, with slight modifications.
- Incorporating EMC or other predetermined moisture during sample preparation, and molding at a unit weight matching that attained during capillary saturating.

For interpretation of the results, particularly how M_R is affected by saturation, the four-phase concept for unsaturated soils is used (*19*).

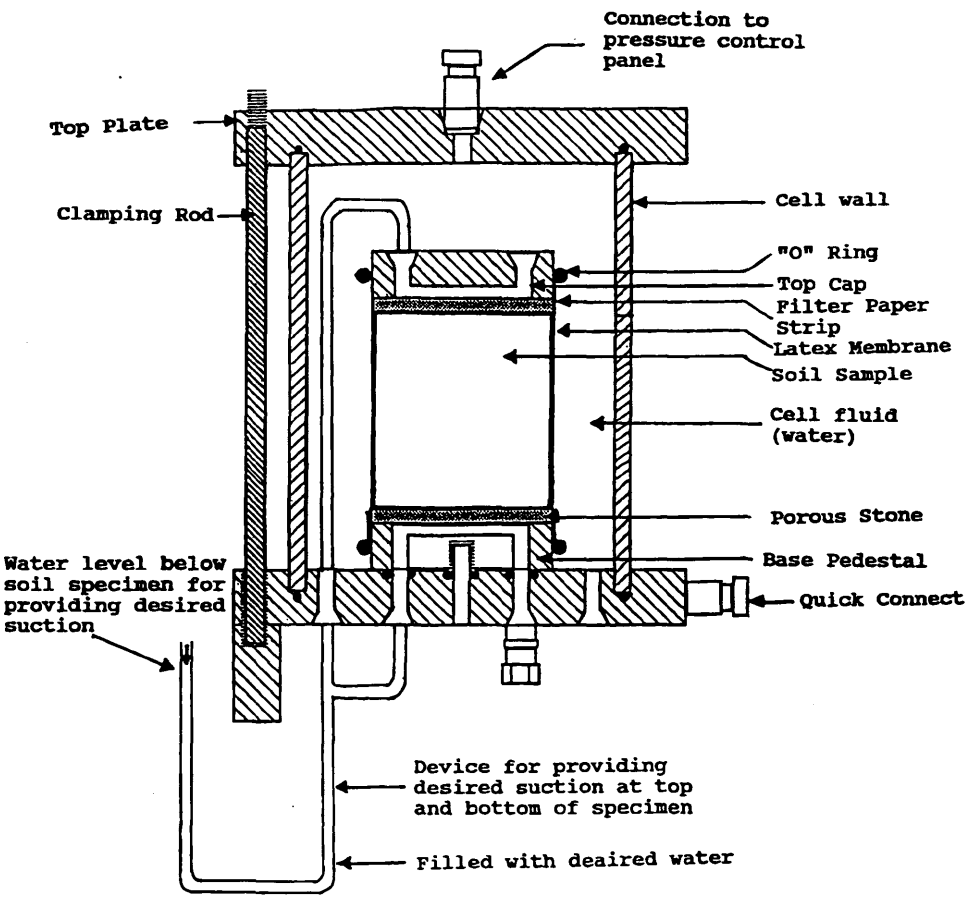

FIGURE 1 Setup for capillary saturating.

SAMPLE PREPARATION, CONDITIONING, AND TESTING

The classification and index properties of two coarse-grain and two fine-grain soils selected in this study are shown in Table 1. The soil, after mixing with a predetermined amount of water, was kept sealed in an airtight plastic bag in a humidity room for 24 hr before molding. Compaction of the specimen was in four layers by imparting 25 blows per layer. The sample, kept in the mold for 2 hr, was extruded and allowed to rebound for another 2 hr before further treatment or testing. Two conditioning procedures were followed: (*a*) capillary saturating and (*b*) vacuum or backpressure saturating. On average, capillary saturating takes 3.5 days, whereas vacuum saturating requires 1 to 3 hr. The vacuum saturating included the following steps:

1. A vacuum of 21 kPa (3 psi) was applied to the top of a specimen, which was isotropically confined by a pressure of 35 kPa (5 psi), until the air bubbles stopped coming out of the specimen.
2. The specimen was subjected to three sets of back pressures for equal amounts of time, with a differential pressure of 35 kPa (5 psi) between the bottom and top of the specimen. The confining pressure was maintained at a level 35 kPa (5 psi) greater than the highest back pressure. The set of back pressures applied at the bottom of the specimen include, 35, 69, and 103 kPa (5, 10, and 15 psi respectively).

The laboratory compacted and saturated specimens were loaded in the repeated load triaxial machine. AASHTO T274-82 (*20*) procedure was followed for M_R testing. The specimens were tested at the following conditions for each soil:

1. Molded at OMC and 97 percent AASHTO T99 unit weight;
2. Molded at OMC and 97 percent AASHTO T99 unit weight, and capillary saturated at 0.914 m (3 ft) of water suction;
3. Molded at OMC and 97 percent AASHTO T99 unit weight, and capillary saturated at 0 m of water suction;
4. Molded at OMC and 97 percent AASHTO T99 unit weight, and vacuum saturated to estimated EMC;
5. Molded at OMC and 97 percent AASHTO T99 unit weight, and vacuum saturated to maximum possible saturation (approximately 96 percent);
6. Molded at wet of optimum and corresponding unit weight, as obtained in a capillary saturated specimen at 0.914 m (3 ft) of water suction (as in test condition 2); and
7. Molded at wet of optimum and corresponding unit weight, as obtained in a capillary saturated specimen at 0 m of water suction (as in test condition 3).

The tests were repeated at each condition to obtain a triplet satisfying the Chauvenet's criteria (*21*), which states that all points should be retained within a band around the mean value, which corresponds to a probability of $1 - 1/(2N)$, where N = number of observations.

ANALYSIS OF RESULTS

The M_R test results of four soils for the various saturation conditions are shown in Table 2. Table 3 lists the OMC and EMC and the corresponding degree of saturations of all four soils. Each test value listed in Table 2 is an average of a minimum of three tests. The percentage reduction of M_R with degree of saturation, for typical coarse-grain and fine-grain soils, is shown in Figure 2. As expected, M_R decreased with saturation, resulting in the following observations:

- The M_R of coarse-grain soils is not significantly affected by the amount and manner of saturating; the reduction is approximately 20 percent.
- The M_R of fine-grain soils is drastically reduced by saturation, the reduction being 50 to 75 percent depending on the degree of saturation, and the saturating method used.
- In the case of fine-grain soils, the saturating method used has a varying effect on the M_R of the specimens tested. The M_R-value of the vacuum-saturated specimen decreases exponentially with increasing degree of saturation, whereas it decreases linearly with capillary saturating and also with specimens molded wet of optimum.
- In case of fine-grain soils, the decrease in M_R for both capillary saturated specimen and those molded wet of optimum is nearly identical.

How reasonable these results are is addressed by comparing the M_R-trend with saturation of the authors' results with those of Thompson and Robnett (*7*). Thompson's results, expressed in two equations, are sketched in Figure 3. The authors' results are plotted in the same figure. The agreement of the two sets of data validates the test results. A recent study by Li and Selig (*22*) quantified the effect of soil physical state on M_R by two path-dependent equations

TABLE 1 Soil Characteristics (*25*)

Soil No.	Location Hwy/County	Passing #200 Sieve (%)	Atterberg Limits		Proctor Test Data		Soil Classification
			LL	PI	Maximum Unit weight, (kN/m³)	Optimum Moisture, (%)	Unified/AASHTO
3	MS7/Yalobusha	26	22	4	18.87	11.2	SM-SC/A-2-4
6	US61/Coahoma	97	68	38	15.31	23.0	CH/A-7-5(45)
7	US78/Benton & Union	51	26	7	19.36	13.0	ML-CL/A-4(1)
8	US98/Forrest & Perry	23	0	NP	19.30	10.7	SM/A-2

1 kN/m³ = 6.369 lbf/cu.ft

TABLE 2 M_R Determined Using Different Saturating Procedures

Soil No.		Modulus of Resilience, kPa						
		OMC[a]	Vacuum Saturating		Capillary Saturating		Molding wet of Optimum	
			EMC	S_r = 96%	EMC[b]	S_r = 96%	EMC	S_r = 96%
Coarse Grain	#3	143,412	128,933	129,622	126,175	115,143	119,280	121,264
	#8	150,307	137,896	137,896	136,517	144,101	126,864	131,277
Fine Grain	#7	120,659	39,300	31,716	63,432	31,716	67,569	34,129
	#6	140,996	47,574	Sample Failed	81,359	31,992	112,385	77,221

[a]OMC, optimum moisture content
[b]EMC (equilibrium moisture) attained by conditioning at 0.914 m of water suction
1 kPa = 0.145 psi

relating M_R to moisture content. One equation is for the path of constant dry unit weight, and the other for the path of constant compaction effort.

To authenticate the test results, the authors tested soil No. 7, a fine-grain soil, by compacting at constant AASHTO-T99 dry unit weight and at two different moisture contents, OMC + 2 and OMC − 2. The test results show a decrease by 34 percent and an increase by 19 percent for specimens molded at wet and dry of OMC, against predicted changes of 38.5 percent decrease and 23 percent increase, respectively, using Li and Selig's constant dry unit weight equation.

Unsaturated Soil Mechanics

In saturated soils, the mechanical behavior is defined by pore water pressure as it characterizes the state of moisture and governs the only stress-state variable—effective stress. In unsaturated soils, pore air and pore water pressures govern the two stress-state variables, net normal stress and matrix suction, defining the mechanical behavior. Scrutiny of the results in Figure 2 suggests that the stress-strain characteristics of unsaturated soils is not only influenced by the degree of saturation, but also by the way moisture is imbibed into the soil. In addition, moisture imbibition influences volume change characteristics, particularly in fine-grain soils. Volume change of soil structure is governed by variations in particle orientation, pore size, and surface activity. These factors play an important role in the water retention mechanisms affecting soil water

TABLE 3 OMC, EMC, and Corresponding Saturation (Sr) Levels

Soil No.		OMC, %/Sr, %	EMC, %/Sr[a], %
Coarse Grain	3	11.2/75	13.1/86
	8	10.7/67	11.4/73
Fine Grain	6	23.0/86	26.0/90
	7	13.0/83	14.1/90

[a]Volume change in specimen while saturating is taken into account in calculating saturation level at EMC

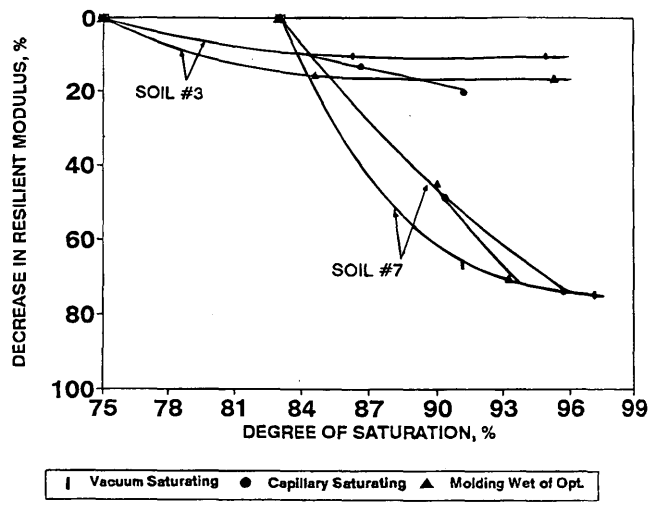

FIGURE 2 Reduction in M_R with degree of saturation for course- and fine-grain soil.

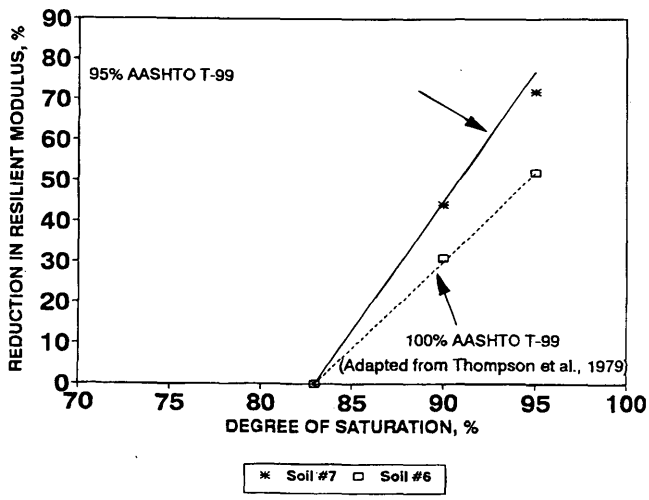

FIGURE 3 Reduction in M_R compared with those of Thompson and Robnett (7).

suction. Simply stated, water imbibition causes volume increase and simultaneous strength decrease. Although the volume changes of the conditioned specimen were measured, no attempt was made here to investigate its solo effect on M_R.

Strength and volume change characteristics can be uniquely related by applying the concepts of unsaturated soil mechanics (USM), as proposed by Fredlund and Rahardjo (*19*). According to USM concepts, unsaturated soil is made up of four phases: soil solids, water, air, and air-water interface (contractile skin). The most important property of the contractile skin is its ability to exert a tensile pull, otherwise known as surface tension, which causes the former to behave like an elastic membrane. Radius of curvature of the contractile skin is inversely related to the matrix suction. The contractile skin, when in contact with the soil solids, will apply a tensile pull between the soil solids, rendering it a major player in deciding the mechanical behavior of the soil system, apart from the soil solids. A partly saturated soil can be visualized as a mixture with two phases (soil solids and contractile skin) that come to equilibrium under applied stress gradients and the other two phases (water and air) flow under applied stress gradient. The disturbance in any of these phases will cause variation in the strength characteristic of the soil. How active the contractile skin is in the soil is dependent on the interaction of air and water phases with soil solids. At saturation levels less than 85 percent, the air phase in the soil is continuous and has interaction with soil solids (*23*). At levels greater than about 90 percent, the air phase is occluded in the water phase, leaving negligible interaction of air phase with soil solids (*24*), that is, the water suction decreases to 0. It stands to reason that when the air phase is occluded, the influence of air-water interface vanishes, as does its effect on soil strength. By process of elimination, therefore, transition of air phase from continuous state to occluded state occurs between 85 percent and 90 percent saturation levels. Figure 4 represents the soil structure constitutive surface adopted from a work by Fredlund and Rahardjo (*19*), which explains the importance of matrix suction and, indirectly, the effect of contractile skin on the strength of soil. Considering a constant plane of effective stress in Figure 4, the volumetric strain is inversely related to the matrix suction (stress-state variable attributed to contractile skin). Hence, the reduction in matrix suction increases the volumetric strain (heaving), resulting in a reduction in M_R. The specific result of decreases in M_R-values with reduction in matrix suction was experimentally shown (*6*).

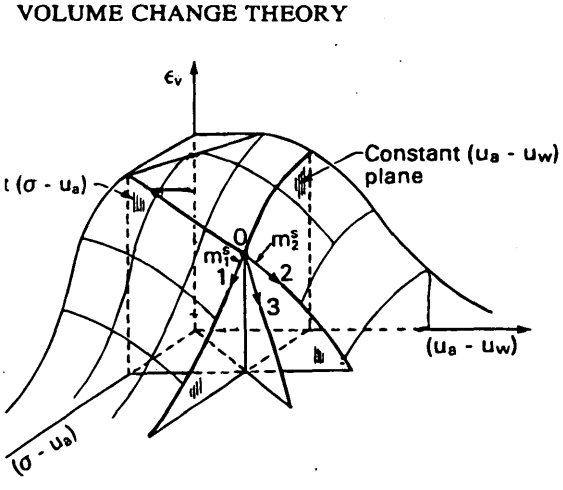

FIGURE 4 Soil structure constitutive surface (*19*).

M_R Affected by Soil Texture

From the description of the four phase system, it is clear that the contractile skin plays an important role in the strength of a soil. Therefore, alterations in the extent of contractile skin and its radius of curvature, both being a function of the particle shape and size, would result in a corresponding change in strength/M_R of an unsaturated soil. For example, a decrease in contractile skin or an increase in its radius of curvature accompanying moisture imbibition will reduce the M_R-values.

In coarse-grain soils, the surface area of the soil solids is relatively small and, hence, so is the contractile skin. Surface tension effects are relatively small in those soils compared with frictional effects in imparting strength. Insignificant strength decreases, therefore, would be realized with increases in degree of saturation. Neither the degree of saturation nor its mode of saturating has appreciable effect on M_R, as the relatively level plot of M_R versus degree of saturation indicates (Figure 2).

With very fine particles and a concomitant large surface area, fine-grain soils develop ample contractile skin at moisture levels close to optimum moisture. As the saturation is increased, the contractile skin and, therefore, soil suction, is reduced with accompanying strength loss. In other words, fine-grain soil, with extensive contractile skin, suffers large strength loss due to saturation. As the saturation is increased to high levels, such as 95 percent or so, the contractile skin loses its interaction with soil solids, that is air gets occluded in water phase. In the pores with air occlusion, surface tension disappears, and any further saturation will have a negligible effect on soil strength, as the rather constant M_R-values beyond 95 percent saturation indicate.

Effect of Saturating Mode on M_R

Not only the degree of saturation, but also the mode of saturating the specimen, has a decisive influence on strength. Examining the M_R-trend in Figure 2, it is clear that vacuum saturating has pronounced deleterious effect on soil strength compared with the other two saturating modes. These strength differences can be explained by considering the intactness of the contractile skin during moisture imbibition in each type of saturating procedure.

Capillary Saturating

The specimen is allowed to saturate under a preassigned suction to attain equilibrium between the soil water suction and the externally applied water suction. During saturation, the pore air pressure remains nearly constant, whereas the pore water pressure gradually increases from a large negative value as the external water is imbibed in the soil specimen. The reduction in capillary suction, accompanying moisture absorption, increases the radius of curvature of the contractile skin and correspondingly lowers the tensile pull on the soil solids. The result would be a gradual decrease in strength of the soil specimen, the decrease being linear until saturation reaches a particular level, perhaps characteristic of the soil, when the air phase begins to get occluded.

Vacuum Saturating

In this method of saturating, the vacuum applied to the specimen will reduce the pore air pressure, with corresponding reduction in soil water suction. Subsequently, differential back pressure is applied to both the bottom and top of the specimen, resulting in nonuniform moisture distribution [Figure 5(*a*)]. The forced-water entry under vacuum may disturb the contractile skin, promoting early occlusion of air phase. The precipitous decrease in M_R with degree of saturation corresponds to the forced-water entry phase, and the asymptotic M_R-value beyond 93 percent saturation is indicative of the air occlusion phase. Stated differently, the vacuuming of the specimen disturbs the air-water interface and in turn the contractile skin, causing substantial strength reduction.

Molding Wet of Optimum

Compaction of samples at wet of optimum (and corresponding unit weight, as obtained in a capillary saturated specimen) would result in poorly structured contractile skin, compared with that in samples molded at OMC and subsequently capillary wetted. The molding wet of optimum (MWO) samples, therefore, should yield a smaller M_R than those obtained from the latter specimens. The two procedures, however, resulted in nearly identical trend. It may be that the capillary saturated sample, by virtue of its nonuniform moisture distribution [Figure 5(*b*)], has undergone substantial strength loss with its ultimate strength equal to that of the MWO sample. Another observation worth mentioning is that the scatter of test results in MWO samples is larger than that observed in capillary saturated specimens.

The task now is to determine what mode of saturating is appropriate to simulate field moisture, referred to here as the EMC. Comparing the three methods of wetting, vacuum saturating severely affects the contractile skin with a precipitous decrease in M_R-value. The other two procedures show nearly identical M_R loss with wetting. Each method has limitations, however. Capillary saturating is time consuming and the moisture distribution is relatively nonuniform, when compared with that of MWO [Figure 5(*b*)]. Had the moisture distribution of the capillary saturated specimens been uniform, the M_R would be higher.

Capillary saturating is recommended when EMC is unknown, but long-term M_R is warranted for design purposes. MWO is appropriate when the in situ moisture content, or EMC, and the corresponding dry unit weight are known or can be estimated.

SUMMARY, CONCLUSIONS, AND RECOMMENDATIONS

Subgrade soil is susceptible to moisture variations subsequent to pavement construction. To what extent the strength characteristic of the subgrade soils is affected by moisture fluctuation is important during design and evaluation phases. Specimens of two coarse-grain and two fine-grain soils, conditioned in accordance with three different saturating (wetting) procedures, are tested for M_R. Saturating procedures tested include: (*a*) compacting at OMC and then capillary saturating at 0.914 m and 0 m (3 ft and 0 ft) of water suction, respectively, (*b*) compacting at OMC and then vacuum saturating to EMC and also to 96 percent saturation, and (*c*) compacting at EMC and at 96 percent saturation at respective reduced dry unit weights. The effect of various saturating procedures on M_R is evaluated using the four-phase system for unsaturated soils.

Observations related to decreases in M_R with the extent of saturation and saturating mode include:

1. An increase in degree of saturation above the OMC will result in decrease of M_R by approximately 20 percent and 50 to 75 percent in coarse-grain and in fine-grain soils, respectively.

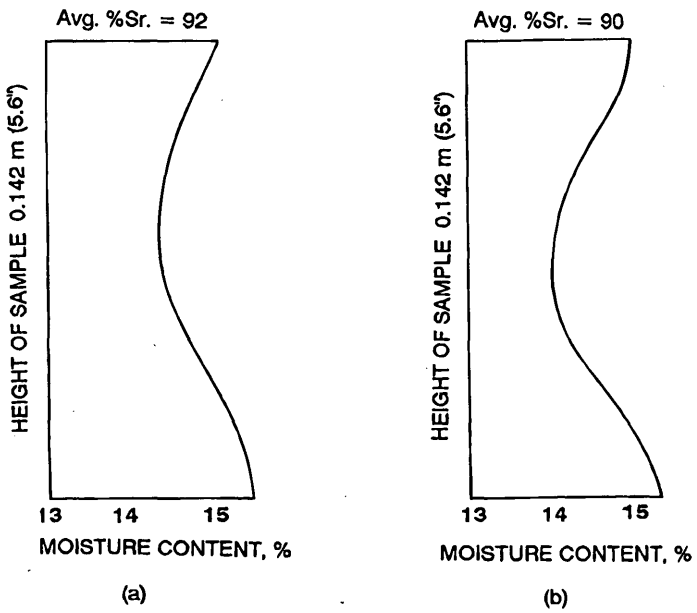

FIGURE 5 Moisture distribution in laboratory-conditioned samples after testing: (*a*) vacuum-saturated to EMC, (*b*) capillary saturated at 0.914 m (3 ft) of water suction. Sr = saturation level.

2. Besides degree of saturation, in fine-grain soils, the mode of moisture imbibition also influences the M_R.
3. Vacuum saturating causes drastic decreases in M_R-values compared with those observed with the other two methods (capillary saturating and MWO).
4. Moisture imbibition by capillarity and MWO result in a nearly identical decrease in M_R-value.

In evaluating the effect of partial saturation on strength/M_R of subgrade soils, three saturating procedures are investigated. They include:

1. Vacuum saturating as in AASHTO T 274-82,
2. Capillary saturating under 0.914 m (3 ft) of water suction, and
3. Molding samples at equilibrium or other predetermined moisture.

The following tentative recommendations for simulating field conditions are made:

1. Because vacuum saturating severely affects the air-water interface in the soil, it cannot simulate moisture imbibition akin to field conditions.
2. During the design phase, capillary saturating is recommended for evaluating the long-term M_R of the proposed subgrade soil, particularly when EMC is not known.
3. Molding at wet of optimum is recommended if the in situ moisture content and dry unit weight are known or can be estimated by empirical or approximate method.

ACKNOWLEDGMENTS

The work described in this paper was conducted with the project titled, Resilient Modulus of Soils Using Gyratory Testing Machine, sponsored by the Mississippi Department of Transportation and FHWA. The authors are grateful to Chakravarthi S. Gajula for his assistance in analyzing the results.

REFERENCES

1. Domaschuk, L., and N. H. Wade. A Study of Bulk and Shear Moduli of a Sand. *Journal of Soil Mechanics and Foundation Division,* ASCE, Vol. 95, SM2, 1969.
2. Duncan, J. M., et. al. *Strength, Stress-Strain and Bulk Modulus Parameters for Finite Element Analysis of Stresses and Movements in Soil Masses.* Report UCB/GT/80-01, College of Engineering, University of California, Berkeley, 1980.
3. Boscardin, M. D., E. T. Selig, R-S. Lin, and G-R. Yang. Hyperbolic Parameters for Compacted Soils. *Journal of Geotechnical Engineering,* ASCE, Vol. 116, No. 1, 1990.
4. *Revised Guide for Design of Pavement Structures.* AASHTO, Washington, D.C., 1986.
5. Fredlund, D. G., A. T. Bergan, and P. K. Wong. Relation Between Resilient Modulus and Stress Condition for Cohesive Subgrade Soils. In *Transportation Research Record 642,* TRB, National Research Council, Washington, D.C., 1977.
6. Edil, T. B., and S. E. Motan. Soil Water Potential and Resilient Behavior of Subgrade Soils. In *Transportation Research Record 705,* TRB, National Research Council, Washington, D.C., 1979.
7. Thompson, M. R., and Q. L. Robnett. Resilient Properties of Subgrade Soils. *Journal of Transportation Engineering,* ASCE, Vol. 105, TE1, 1979.
8. Hardcastle, J. H. *Subgrade Resilient Modulus for Idaho Pavements.* Report RP110-D. FHWA, Department of Civil Engineering, University of Idaho, Moscow, 1992.
9. Atchison, G. D., and B. G. Richards. A Broad Scale Study of Moisture Condition in Pavement Systems throughout Australia. *Moisture Equilibria and Moisture Changes in Soils Beneath Covered Areas,* Butterworth, Australia, 1965.
10. Low, P. F., and C. W. Lovell Jr. The Factor of Moisture in Frost Action. In *Highway Research Bulletin 225,* HRB, National Research Council, Washington, D.C., 1959.
11. Dempsey, B. J., and A. Elzeftawy. *Moisture Movement and Moisture Equilibrium in Pavement Systems.* Interim Report UILU-ENG-76-2012. Department of Civil Engineering, University of Illinois, Urbana, Champaign, 1976.
12. Thornthwaite, L. W. An Approach Toward a Rational Classification of Climate. *The Geological Review,* Vol. 38, No. 1, 1948.
13. *Field Moisture Content Investigation.* Report No. 2, Technical Memorandum 3401. Corps of Engineers Waterways Experiment Station, Vicksburg, Miss., 1955.
14. Black, W. P. M., D. Croney, and J. C. Jacobs. Field Studies of the Movement of Soil Moisture. Technical Paper 41, *Road Research Laboratory,* England, 1958.
15. Russam, K. The Distribution of Moisture in Soils at Overseas Airfields. Technical Paper 58, *Road Research Laboratory,* England, 1962.
16. Coleman, J. D., and K. Russam. The Effect of Climatic Factors on Subgrade Moisture Conditions. *Geotechnique,* the Institute of Civil Engineers, Vol. 11, London, England, 1964.
17. *Estimation of Subgrade Moisture Content.* Leaflet L.F. 98, Road Research Laboratory, Crowthorne, England, 1967.
18. Chu, T. Y., and W. K. Humphries. *Investigation of Subgrade Moisture Conditions in Connection with the Design of Flexible Pavement Structures.* Final Report. College of Engineering, University of South Carolina, Columbia, 1972.
19. Fredlund, D. G., and H. Rahardjo. *Soil Mechanics for Unsaturated Soils.* John Wiley and Sons, Inc., New York, 1993, pp. 14–29, 38–49, 117, 178–188, 346–373.
20. *Standard Method of Test for Resilient Modulus of Subgrade Soils.* AASHTO Designation T274-82, Washington D.C., 1982.
21. Coleman, H. W., and W. G. Steele, Jr. *Experimentation and Uncertainty Analysis for Engineers.* John Wiley and Sons, Inc., New York, 1989, pp. 17–37.
22. Li, D., and E. T. Selig. Resilient Modulus for Fine-Grained Subgrade Soils. *Journal of Geotechnical Engineering,* ASCE, Vol. 120, No. 6, 1994.
23. Corey, A. T. Measurement of Water and Air Permeability in Unsaturated Soil. *Proceedings, Soil Science Society of America,* Vol. 21, No. 1, 1957.
24. Matyas, E. L. Air and Water Permeability of Compacted Soils. *Permeability and Capillary of Soils,* ASTM, STP 417, 1967.
25. George, K. P. *Resilient Modulus of Subgrade Soils using Gyratory Testing Machine.* Final Report MSHD-RD-92-096. Department of Civil Engineering, University of Mississippi, 1992.

Publication of this paper sponsored by Committee on Environmental Factors Except Frost.

Suction Study on Compacted Clay Using Three Measurement Methods

CHE-HUNG TSAI AND THOMAS M. PETRY

An investigation was conducted to determine the effects of water contents and dry unit weights on measured suction pressures. The soil mixture used was a highly plastic clay with high shrink–swell potential. Four different configurations of soil specimen were compacted at two different water contents by using both standard and modified Proctor energies. The suction methods investigated in this study were pressure plate, filter paper, and thermocouple psychrometer. Matric and total suction parameters were compared, and their relationships to water content and dry unit weight were explored. The effectiveness of the filter paper method was recognized. The relationships of suction to moisture levels were confirmed and strengthened. The results indicate that effects of variations in dry unit weight on soil suction measurements may be neglected for disturbed samples in the field.

The concept of soil suction has been used by soil scientists and geotechnical engineers for many years. Soil suction can be described as a measure of a soil's need for water. Generally, the drier the soil, the greater its suction. The definitions of soil suction, its components, and the different potentials that make up the total potential of soil water have been given by the International Society of Soil Science (*1*). Soil suction may result from the attractive and repulsive forces between charged clay particles and polar water molecules, surface tension forces of water, solution potentials caused by dissolved ions, and gravity potential (*2*). In engineering problems, total suction is considered to be composed of matric suction and osmotic suction. Matric suction is believed to be caused by the clay and associated ions, and osmotic suction is a result of unbalanced ion concentrations in the pore water.

Devices generally used to measure soil suction include pressure plate apparatuses, tensiometers, heat dissipation sensors, pressure membrane apparatuses, gypsum blocks, centrifuges, fiberglass moisture cells, filter paper (the noncontact test), thermocouple psychrometers, and vacuum desiccators. The three last-named devices are used to measure total suction, whereas the first seven devices can be used to evaluate matric suction.

The relationship between dry unit weight and soil suction has been investigated and reported. In a work by Chu and Mou (*3*) matric suction was used to evaluate the swelling potential of clay soils. Their results showed that an increase in the dry unit weight with similar initial water contents resulted in an increase in soil suction. In other words, matric suction of compacted soils with the same water content increases as compaction energy increases. Croney et al. (*4*) indicated that matric suction is affected by the dry unit weight of an incompressible material. However, for a compressible compacted clay they found that matric suction was not affected by a change in dry unit weight.

C. H. Tsai, Patton, Burke & Thompson, Engineering Consultants, 10555 Newkirk St., Dallas, Tex. 75220. T. M. Petry, The University of Texas at Arlington, P.O. Box 19308, Arlington, Tex. 76019–0308.

Campbell and Gardner (*5*) investigated the effect of bulk density on soil water potential, using thermocouple psychrometers. Their results showed there is apparently little change of water potential with bulk density except in a swelling clay subsoil. In 1972 Krahn and Fredlund (*6*) concluded that, for remolded compacted soils, the matric and total suction are dependent on the water content but are essentially independent of dry unit weight.

Based on a review of the literature, the relationship between soil suction and dry unit weight appears to be uncertain. However, it is clear that soil suction increases as water content decreases. To investigate further the correlations between initial conditions of soil samples and suction pressures, a testing program was designed and performed during this study.

MATERIAL

The soil chosen for testing was a highly active clay soil consisting of a mixture of 75 percent materials weathered from the Eagle Ford geologic formation and 25 percent bentonite clay. The Eagle Ford is a locally available material in the Dallas–Fort Worth area, and the bentonite was that commonly used for drilling fluids. The mixture was dark gray. It was passed through a No. 4 sieve and air dried. The results of clay mineralogy tests, x-ray diffraction, and differential thermal analysis indicated that the predominant mineral was montmorillonite.

According to the grain size distribution for the soil tested, 80 percent of the soil by dry weight was able to pass through a No. 200 sieve, and 20 percent was finer than 0.002 mm. The specific gravity was 2.72, and the average Atterberg limits included a liquid limit of 100 percent, a plastic limit of 24 percent, and a plasticity index of 76 percent. The average linear shrinkage was 19 percent. The standard Proctor maximum dry unit weight for this soil was found to be 14.9 KN/m^3 (94.5 pcf) at an optimum water content of 21 percent. The modified Proctor compaction parameters were 17.5 KN/m^3 (111.3 pcf) maximum dry unit weight and 15 percent optimum water content.

TESTING PROGRAM

Four configurations of compacted soil were prepared and used in this study. These four configurations are referred to in this paper as Soils I, II, III, and IV. Soils I and II were compacted using standard Proctor energy levels. Soils III and IV were produced using modified Proctor compaction. Soils I and III, compacted at a water content of approximately 17 percent, had dry unit weights of approximately 14.5 KN/m^3 (92 pcf) and 17.4 KN/m^3 (111 pcf), respectively. Soils II and IV, molded at a water content near 22 per-

cent, had dry unit weights of about 14.6 KN/m^3 (93 pcf) and 16.3 KN/m^3 (104 pcf), respectively. Soil III had the highest dry unit weight among the four configurations of compacted sample. Soils I and II had similar values of dry unit weight. A summary of the initial conditions of compacted soils is given in Table 1.

Swelling pressures obtained by the constant-volume swell pressure test on compacted samples ranged from 206 kPa (2.15 tsf) to 731 kPa (7.63 tsf). Volumetric swell, under free swell conditions, ranged from 13.0 to 21.2 percent. According to these results Soil III displayed the highest potential to undergo volume change and had the largest swell pressure. Soil II showed less potential to swell and had smallest swell pressure. Summaries of the physical properties of the test soils are given in Table 2.

Three devices, a pressure plate, filter paper, and a thermocouple psychrometer, were used to measure the soil suction. The thermocouple psychrometer and the filter paper were used to measure total suction of the soil. Matric suction was determined directly by the pressure plate method.

Pressure Plate Method

The apparatus used in the pressure plate method included 5- and 15-bar pressure plate extractors from Soil Moisture Equipment Corp., California. Four suction–water characteristic curves for Soils I, II, III, and IV were established with air pressures of 0.5, 1.0, 1.5, 2.0, 4.0, 6.0, 8.0, and 10.0 bars.

Filter Paper Method

The filter paper used in this study was Baxter grade 381 filter paper 55.0 mm (2.17 in.) in diameter. Filter papers were calibrated with NaCl solutions of various concentrations. A way to prepare the calibrating solutions of NaCl can be found elsewhere (*7*). The water potentials of NaCl solutions at different concentrations were provided in a work by Lang (*8*). In addition, information from a work by Frazer et al. (*9*) about vapor pressures of salt solutions can be used to evaluate the water potentials of NaCl solutions at various concentrations.

Figure 1 shows the calibration curve, $R^2 = 0.99$, for Baxter 381 S/P filter paper. NaCl solutions at 12 different concentrations were used to establish this curve. At each concentration there were at least three tests, and the average of those results was used to draw the calibration line.

Four suction–water characteristic curves for Soils I, II, III, and IV were obtained by the filter paper method. The soil specimens used were 25.4 mm (1 in.) high and 63.5 mm (2.5 in.) in diameter. To produce different water contents for each soil configuration, the soil specimens were wetted with varying amounts of distilled demineralized water or dried at room temperature for varying lengths of time. For Soils In and III the maximum amount of water added to the specimens was 45 mL (1.52 oz) and the maximum time used to dry the specimens was 24 hr. For Soils II and IV the maximum amount of water added was 30 mL (1.01 oz) and the maximum dry time was 72 hr. To ensure uniform water contents, the wet specimens were wrapped with plastic, sealed, and cured in a polystyrene thermal box for at least 2 days before suction testing.

TABLE 1 Initial Conditions of Compacted Soils

	Soil Configuration			
Initial Conditions	I*	II*	III+	IV+
Water Content (%)	17	22	17	22
Dry Unit Weight (KN/m^3)	14.5	14.6	17.4	16.3

* Standard Proctor + Modified Proctor

TABLE 2 Physical Properties of Test Soils

Property	Soil Mixture
Liquid Limit (%)	100
Plastic Limit (%)	24
Plasticity Index (%)	76
Linear Shrinkage (%)	19
Specific Gravity	2.72
Silt and Clay < 0.074 mm (%)	80
Clay Fraction < 0.002 mm (%)	20

	Soil Configuration			
Property	I	II	III	IV
Swell Pressure (kPa)	213	206	731	243
Free Swell (%)	15.2	13.0	21.2	18.4

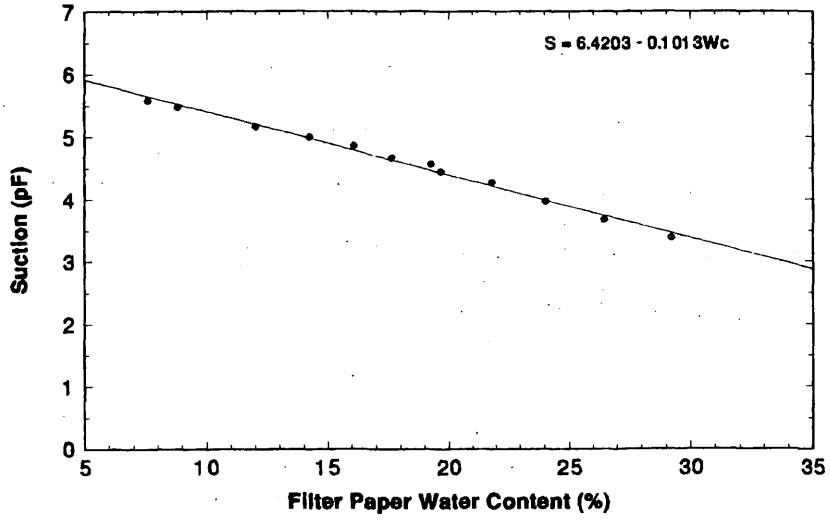

FIGURE 1 Calibration line for Baxter 381 S/P filter paper.

Thermocouple Psychrometer Method

A WESCOR HR-33T Dewpoint microvoltmeter with a PS-10 psychrometer switch box was used during this investigation. The thermocouple psychrometers used were Wescor PCT-55 with a SUREFAST connector in which a chromel-constantan junction is enclosed in a ceramic cup. The HR-33T permits water potential to be determined with a variety of sensors in either the dew point or the psychrometric mode. Generally, the two modes should give similar readings in a controlled-temperature environment in the laboratory. The advantage of the dew point mode may be that the voltage is more sensitive to water potential and less sensitive to temperature. According to a work by Briscoe (*10*), because the dew point mode provides a continuous output instead of the falling plateau given by the psychrometric mode accurate measurements may be easier to obtain. However, the accuracy of the instrument depends on the correct setting of the cooling coefficient (*11*).

In this research all readings from thermocouple psychrometer method were taken at both dew point and psychrometric modes. The suction pressure reported was an average of the values obtained from these two modes. Solutions of NaCl at seven different concentrations were used to establish the calibration curves of used thermocouple psychrometers. Each psychrometer had its own calibration curve. Typical calibration curves of a thermocouple psychrometer from the two different output modes, psychrometric and dew point, are shown in Figure 2.

The way in which soil specimens of each soil configuration were prepared at different water contents was the same in this case as for the filter paper method; however, the maximum amounts of water and drying time were different from those of the filter paper method. Because of the lower capacity of the thermocouple psychrometers used, this suction method was unable to work well with samples that were too dry or too wet. In other words, thermocouple psychrometers do not work well for soils with very low or very high suction pressures. In this method the maximum amount of water used was 25 mL (0.85 oz) for Soils I and III and 20 mL (0.68 oz) for Soils II and IV. The maximum drying time for samples was 2 hr for Soils I and III and 36 hr for Soils II and IV.

RESULTS AND ANALYSIS

Twelve suction–water characteristic curves for the four configurations of compacted soil were determined with three suction measurement methods. For each soil configuration a total of three suction–water characteristic curves were established.

Thermocouple Psychrometer

Thirteen psychrometers were used, and at least two psychrometers were used to establish a suction–water characteristic curve for each soil configuration. A comparison of suction–water characteristic curves for the four configurations of soil is shown in Figure 3. These results consist of 102 points, and every point was the average of the two suction values obtained by the psychrometric and dew point modes. The logarithmic unit pF is used because the water contents can be linearly related to suction values in pF units and because of the wide range of values usually measured. A pF unit is the logarithm of the negative water pressure (in centimeters). The range of water content covered by the thermocouple psychrometer method was approximately 15.5 to 40 percent, and suction pressures ranged from 3.3 to 4.7 pF. The results showed that soil samples with water contents ranging from 17 to 30 percent were generally able to provide positive and reliable readings with psychrometers during the study.

From the results shown in Figure 3 it was found that suction increases with a decrease in soil moisture content. In addition, it appears that total suction pressure is not significantly affected by a change in dry unit weight of remolded soils. According to the analysis of the *t*-statistic for the equality of intercepts and slopes, there is no evidence that the four regression lines shown in Figure 3 differ at a 0.05 level of significance.

Filter Paper Method

To measure total suction, the filter papers used were suspended above the soil specimen in a container for a minimum of 7 days.

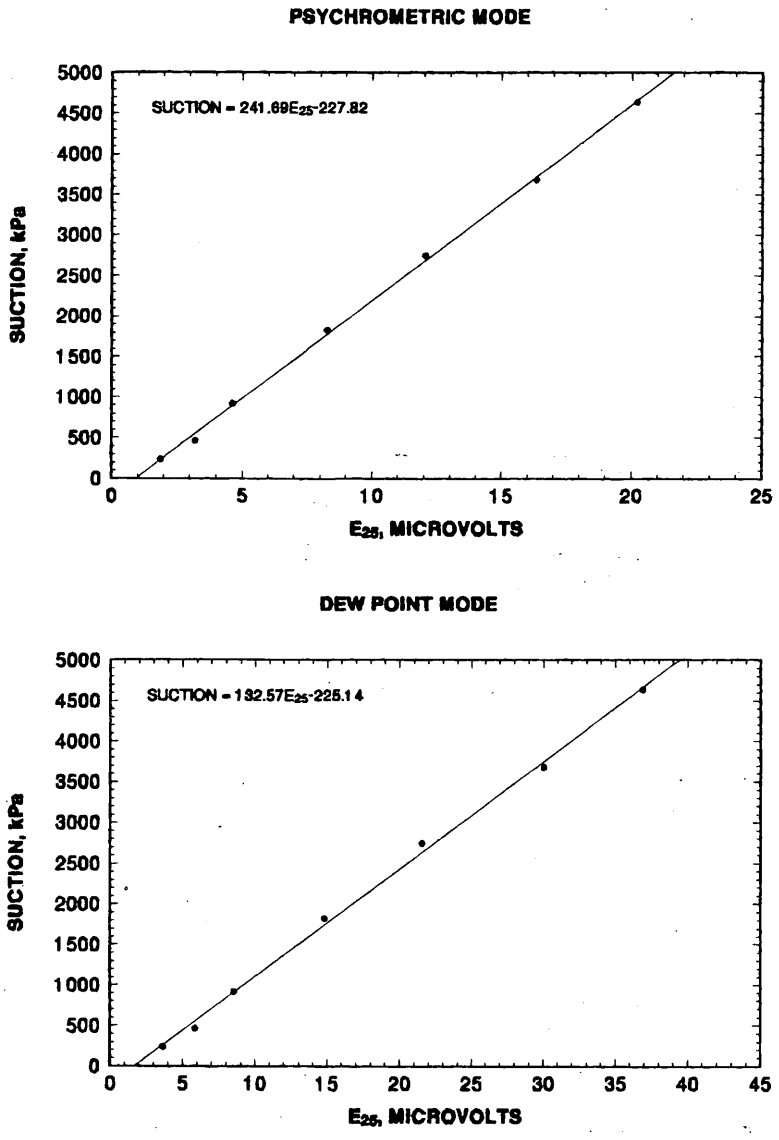

FIGURE 2 Typical calibration lines of psychrometer from two different output modes.

Theoretically, the equilibrium water content of the filter paper corresponds to the total suction of the soil when the filter paper is not in contact with the soil.

It was found that there were no good linear correlations between suction and water content for samples having water contents higher than 33 percent. Results showed considerable variability and unreliable outputs at these low suction values. It should be pointed out that great care must be taken when doing this test, especially for wet samples.

The suction–water characteristic curves of Soils I, II, III, and IV are shown in Figure 4. The results include 147 points with suction pressures ranging from 3.3 to 5.3 pF and water contents ranging from 13 to approximately 41 percent. The four linear regression lines appear to have similar slope and have an average R^2 value of 0.82. It was found that total suction was not significantly influenced by a variation in dry unit weight of soil specimens tested by the filter paper method. From the analysis of the *t*-statistic using a 0.05 level of significance, there is insufficient evidence to reject the null hypotheses about the equality of intercepts and slopes of the regression lines shown in Figure 4.

A comparison between the average values of the four total suction curves (in kilopascals) from the thermocouple psychrometer and filter paper methods is illustrated in Figure 5. The results show that these methods gave nearly the same values for samples that had similar water potentials. It also appears that suction increased rapidly as the water contents of samples became lower than 22 percent. On the other hand, soils showed little change in suction when their moisture contents were higher than certain values, in this case approximately 30 percent.

From this study it was found that the filter paper method has three distinct advantages with respect to the thermocouple psychrometer method. These advantages are that (*a*) it is relatively simple, (*b*) it

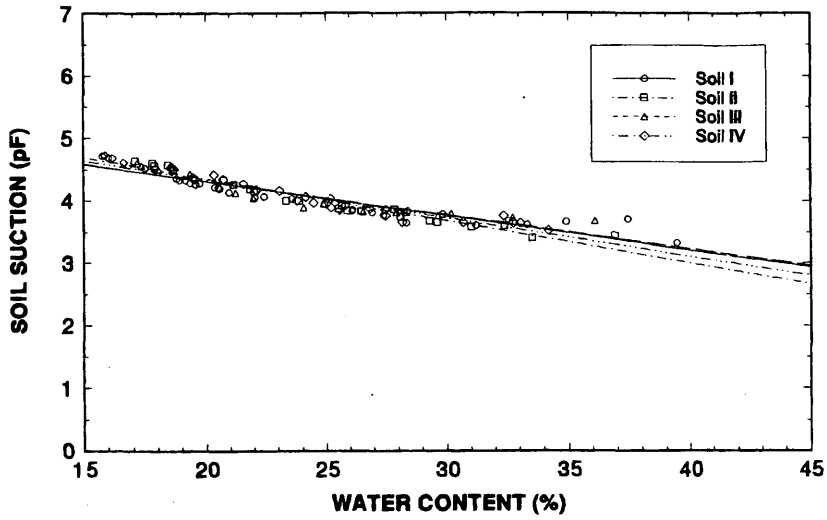

FIGURE 3 Relationships between suction and water content for four configurations of soil determined by thermocouple psychrometer.

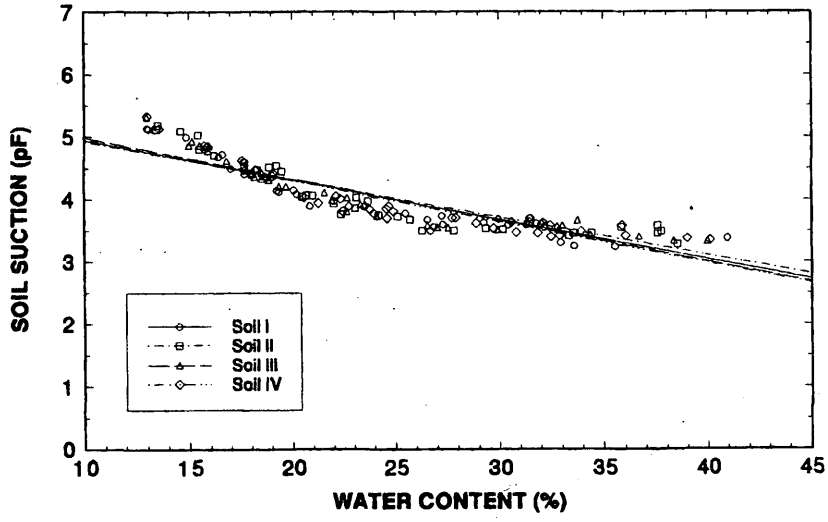

FIGURE 4 Relationships between suction and water content for four configurations of soil determined by filter paper method.

is an inexpensive test method to determine total suctions of soil samples, and (*c*) it has a wider range of measurable suction than the psychrometer method. However, compared with those of the psychrometer method, the results from the filter paper method generally exhibit more scatter. Therefore, to achieve best results using the filter paper method it is necessary to prepare more tests for every soil sample.

Pressure Plate Method

A comparison of soil–water characteristic curves of the four configurations of soil is shown in Figure 6. It appears that a variation in dry unit weight has no effect on the matric suction of compacted soils. From the results of the *t*-statistic at a 0.05 level of significance there is no evidence to suggest that the slopes and intercepts of these regression lines are different. Because of limitations on its capacity, the pressure plate was unable to determine soil–water characteristic curves for high suction pressures. However, it worked well for low suction pressures. The results of this test show that the highest water content obtained during testing was 42 percent and the lowest water content was approximately 23 percent, with the respective matric suctions ranging from 2.71 to 4.01 pF.

Curves showing average total suction, matric suction, and the difference between total and matric suctions for Eagle Ford clay including 25 percent bentonite appear in Figure 7. The results indicate that the shapes of the total suction and the matric suction curves are similar. The total suction curves shown in Figure 7 were obtained by taking the average of suction values (in kilopascals) of the psychrometer and filter paper methods for all soil configura-

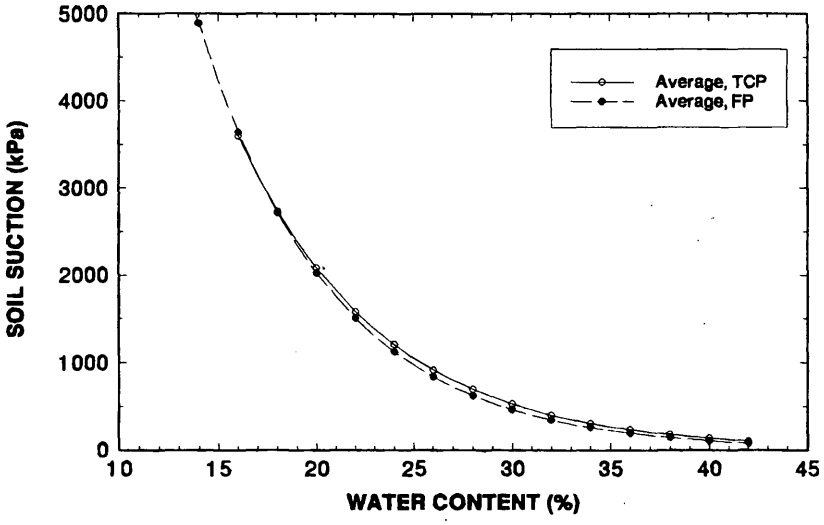

FIGURE 5 Comparison of average total suction from filter paper (FP) and thermocouple psychrometer (TCP) methods.

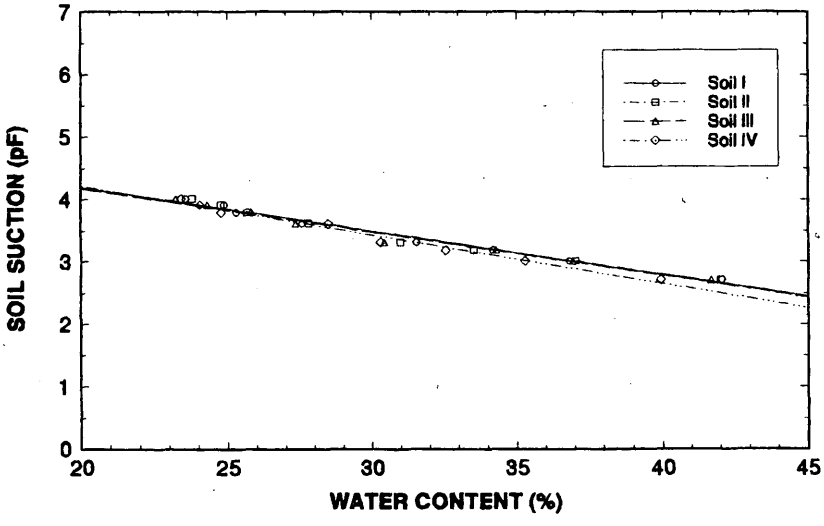

FIGURE 6 Relationships between suction and water content for four configurations of soil determined by pressure plate method.

tions. It appears that the difference between the total suction and the matric suction curves increases as water content decreases. In other words, osmotic suction increases with a decrease in water content. It also appears that the values of osmotic suction were lower than those of matric suction at high suction levels but became similar or higher for the wet samples.

CONCLUSIONS

Discussions and analyses for test results during this study were presented. The soil mixture used was a highly plastic clay with high shrink–swell potential. According to analyses of clay mineralogy tests, the predominant mineral appeared to be montmorillonite. Four configurations of compacted soil were prepared and used in this study. For each soil configuration suction–water characteristic curves were determined with a specific filter paper, with thermocouple psychrometers, and with a pressure plate apparatus.

On the basis of the results and discussions presented, the following conclusions are drawn:

1. From suction–water characteristic curves of the four configurations of soil tested it appears that suction pressure decreases with increasing soil water content and increases rapidly in dry soils with little decrease in water content.
2. Both matric suction and total suction are not significantly affected by a change in the dry unit weight of compacted soils used in this study. In other words, effects of variations in dry unit weight

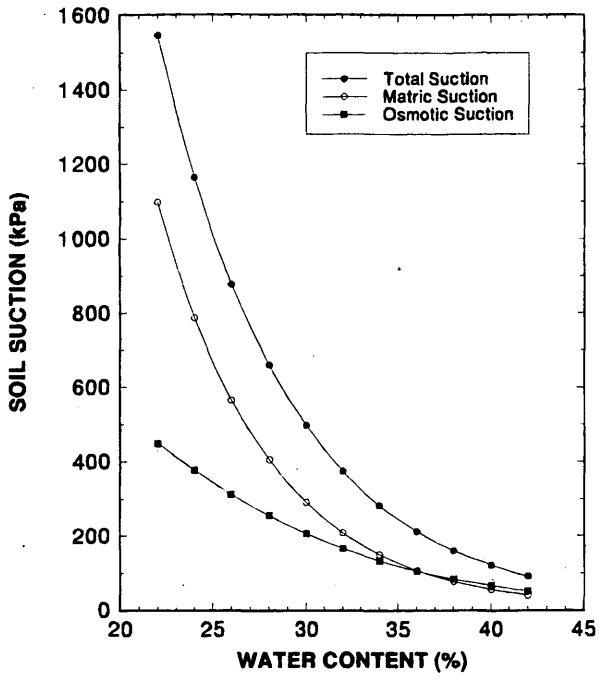

FIGURE 7 Average total, matric, and osmotic suction pressures for Eagle Ford clay including 25 percent bentonite.

on soil suction measurements may be neglected for remolded soil samples.

3. The advantages of the filter paper method in measuring total suction of soil samples are that (*a*) it is relatively simple, (*b*) it is an inexpensive test method, and (*c*) it is capable of measuring a wide range of suction potential. However, compared with those of the thermocouple psychrometer method, the results of the filter paper method generally exhibit more scatter. Inasmuch as a small difference in handling test samples may produce a large difference in results, special care must be taken during the filter paper test. Regardless of the high and low suction levels, the psychrometer method is generally able to provide very positive and reliable results for daily suction readings in the laboratory and for field applications.

4. Because of the capacity of the pressure plate apparatus used, including 15- and 5-bar extractors, it was not possible to provide the measurement of matric suction in the range of high pressures. However, the pressure plate apparatus can provide a very good and reliable matric suction measurement for moister soil conditions. The problems of conducting tests on clay soils with the pressure plate apparatus can include the following: (a) the initial conditions of soil specimen can be changed over a long period for equilibrium, (b) the sample size may be too small and thus unrepresentative for undisturbed soils, and (c) this method cannot be used practically in the field.

5. The difference between total suction and matric suction, as the osmotic suction, increases with decreasing soil water content. Osmotic suction is lower than matric suction at high suction levels but becomes similar or higher for wet samples. At high water contents the values of both matric and osmotic suctions are usually small. Practically speaking, the moisture effects of clay are much more important at low moisture levels and are believed to contribute the most to swell potential.

REFERENCES

1. Engineering Concepts of Moisture Equilibria and Moisture Changes in Soils. *Proc. Moisture Equilibria and Moisture Changes in Soils Beneath Covered Areas,* Statement of the Review Panel, Butterworth, Australia, 1965, pp. 7–21.
2. McKeen, R. G. *Design of Airport Pavements for Expansive Soils.* Report DOT/FAA/RD-81/25. New Mexico Engineering Research Institute, University of New Mexico, 1981.
3. Chu, T. Y., and C. H. Mou. Soil-Suction Approach for Evaluation of Swelling Potential. In *Transportation Research Board Record 790,* TRB, National Research Council, Washington, D.C., 1981, pp. 54–60.
4. Croney, D., J. D. Coleman, and W. P. M. Black. Studies of the Movement and Distribution of Water in Soil in Relation to Highway Design and Performance. Presented at 37th Annual Meeting of the Highway Research Board, National Research Council, 1958.
5. Campbell, G. S., and W. H. Gardner. Psychrometric Measurement of Soil Water Potential: Temperature and Bulk Density Effects, *Soil Science Society of America,* Vol. 35, 1971, pp. 8–12.
6. Krahn, J., and D. G. Fredlund. On Total, Matric and Osmotic Suction, *Soil Science,* Vol. 114, 1972, pp. 339–348.
7. Wiebe, H. H., G. S. Campbell, W. H. Gardner, S. L. Rawlins, J. W. Cary, and R. W. Brown. *Measurement of Plant and Soil Water Status.* Bulletin 484. Utah Agricultural Experiment Station, Utah State University, 1971.
8. Lang, A. R. G. Osmotic Coefficients and Water Potentials of Sodium Chloride Solutions from 0 to 40°C, *Australian Journal of Chemistry,* No. 20, 1967, pp. 2017–2023.
9. Frazer, J. C. W., R. K. Taylor, and A. Grollman. Two-Phase Liquid-Vapor Isothermal Systems, Vapor-Pressure Lowering, *International Critical Tables,* Vol. 3, 1928, pp. 292–298.
10. Briscoe, R. D. *Thermocouple Psychrometers for Water Potential Measurements.* Wescor, Inc., Logan, Utah, 1984.
11. Savage, M. J., A. Cass, and J. M. de Jager. Measurement of Water Potential Using Thermocouple Hygrometers, *South African Journal of Science,* Vol. 77, 1981, pp. 24–27.

Publication of this paper sponsored by Committee on Environmental Factors Except Frost.

Moisture and Strength Variability in Some Arizona Subgrades

SANDRA L. HOUSTON, WILLIAM N. HOUSTON, AND TIMOTHY W. ANDERSON

A series of cone penetrometer tests was performed on subgrade materials at 18 sites along Arizona highways. At each site, water content and cone penetration data were obtained at two locations, 10 m apart, along the right-wheel path of the right lane and at a third location along the adjacent shoulder. The cone penetration and water-content data indicate pronounced variations in subgrade properties over distances of only a few meters horizontally. Variations in subgrade properties were also significant over small vertical distances. Soil profiles at the 18 test sites contained a wide range of soil types; however, most upper subgrade materials were classified as silts or sands with silty fines. Relationships among soil water content, soil suction, and shear strength are explored, and the effect of highly variable subgrade properties on pavement design is discussed.

Variations in subgrade materials can lead to variable performance of pavement systems over a fairly short length of highway section. Pavement and subgrade properties vary because of differences in material type but may also vary with seasonal moisture fluctuations (*1*). Often subgrade variabilities that occur over short segments of highway go undetected because it is prohibitively expensive to perform highly detailed geotechnical investigations for the long stretches of roadway typical of most transportation projects. In addition, many projects involve upgrading and maintaining existing sections of highway, and it is generally not considered practical to perform the destructive testing that would normally be done to produce detailed information on subgrade variability. Therefore, a reliance on nondestructive testing (NDT) has become very common for most pavement upgrading and maintenance projects. In some cases there is an attempt to capture seasonal variations by conducting nondestructive tests at different times of the year.

The focus of this study is to evaluate the typical subgrade property variation for several Arizona highway sections. The investigation of subsurface profiles and spatial variability involved soil testing to determine basic characteristics and classifications. Water-content and cone penetrometer profiles were obtained at three closely spaced locations at each of the test sites. Although direct field suction measurements were not obtained, at some locations soil suction was qualitatively assessed by using typical soil-water characteristics curves and relating suction to water content. Variations in NDT deflection basins were available at each of the test locations. The details of the NDT studies are not given in this paper but have been reported elsewhere (*2*).

SITE CHARACTERISTICS

The test sites are located on in-service Interstate systems, U.S. highways, and state routes. Twelve of the eighteen sites are on the Interstate system. A wide range in subgrade material was encountered, including clayey, silty, and sandy soils as well as gravelly material. A summary of the upper subgrade characteristics, showing Unified Soil Classification, is given in Table 1. Most of the upper subgrade materials were classified as sands with silty fines or silts, but materials ranged from gravel to clay.

Complete boring logs were obtained at each site to a depth of approximately 9 m or refusal (*3*). The geologic settings of the test sites are summarized in Table 1. During the site-selection process geographical distribution was an important concern for ensuring that the entire range of geological and climatic conditions was included in the data base to be developed in the study. Previous work by the Arizona Department of Transportation identified nine climatic zones in the state of Arizona. On consideration of all selection criteria, eight of the state's nine climatic zones were represented in the test sites. Thus, there was an attempt to remove data bias based on geological setting or climatic conditions.

CONE-PENETRATION DATA

Cone-penetration testing (CPT) was performed at three locations at each test site. In general, these locations corresponded to (*a*) Station 1, located on the right-wheel path of the right lane, (*b*) Station 4, located approximately 10 m from Station 1 and on the right-wheel path of the right lane, and (*c*) Station 1S, located on the shoulder adjacent to Station 1. The CPT consisted of advancing an electric friction cone penetrometer attached to a truck-mounted CME 55 drill rig unit. The CPT was performed according to ASTM procedure D3441-86. The cone data were obtained to depth of 9 m or at refusal. In some cases (if the boring logs indicated feasibility) when refusal was met at relatively shallow depth, the cone penetrometer was removed, the hole was augered down to softer material, and then the cone was readvanced in the softer material beneath the hard layer.

Normal output from the CPT consists of a digital readout of the friction sleeve resistance and cone tip resistance. These values are displayed every 10 cm and represent an average over a 10-cm zone. Although sleeve resistance was obtained, cone tip resistance only will be reported here because it is the cone tip resistance for which most correlations with soil shear strength and modulus have been successfully made (*4,5*). In addition, the sleeve resistance values are somewhat temperature sensitive. Moisture-content data were obtained from disturbed samples taken from the boring log holes drilled at the sites. The moisture-content data were obtained very near the time of the CPT testing because water content profiles vary seasonally.

A summary of the cone penetrometer tip resistance, q_c, and the water content, w, profiles for each site is given in Table 2. In most

S. L. Houston and W. N. Houston, Department of Civil Engineering, Arizona State University, Tempe, Ariz. 85287–5306. T. W. Anderson, Foree and Vann, Inc., 9013 North 24th Avenue, Phoenix, Ariz. 85021-2851.

TABLE 1 Summary of Upper Subgrade Characteristics Showing Unified Soil Classification

Site	Subgrade Characteristics Depth Below T.O.P.	USCS	Geologic Setting
1	0.75 m	SM & SC	Quaternary & Tertiary Alluvium, very thick and coarse grained
2	1.4 m	ML & SM	Quaternary Alluvium, fine grained and thick
3	1.4 m	CL	Thin Quaternary Alluvium (derived from the Chinle Formation) overlying early Triassic Moenkopi Sandstone
4	1.0 m	CL	Same as for Site 3
5	1.0 m	SM	Thin Quaternary Alluvium overlying the Bidahochi Formation (sedimentary in nature, most likely sandstone)
6	0.75 m	ROCK	Permian age Kaibab Limestone
7	0.6 m	SM	Recent Alluvium overlying the Bidahochi Formation
8	0.75 m	SM	Same as for Site 7
9	1.25 m	CL-CH	Thin Alluvium (detritally weathered) overlying Tertiary Basalt
10	1.0 m	CH	Same as for Site 9
11	1.0 m	GC-CL	Quaternary Alluvium (fine grained) overlying Granite of early Proterozoic age
12	0.75 m	SM & SC	Same as for Site 1
13	0.30 m	SC	Thin Alluvium (detritally weathered) overlying Kaibab Limestone of Paleozoic age
14	0.30 m	SC-CH	Thin Alluvium (detritally weathered) overlying Kaibab Limestone and the Toroweap Formation (sandstone)
15	0.6 m	SM	Very thick Quaternary Alluvium, predominantly comprised of coarse grained sands and gravels
16	0.30 m	SM-ML	Very thick Quaternary Alluvium, predominantly fine grained sands and clays
17	0.15 m	ML	Thin Alluvium (detritally weathered) overlying the Naco Group (sedimentary rocks of Permian & Pennsylvanian age)
18	0.75 m	SM & GM	Thin Quaternary Alluvium overlying Tertiary aged Conglomerate
19	0.6 m	SC-CL	Thin Alluvium overlying Quaternary and Tertiary Basalt
20	1.0 m	GM & GP	Thick to very thick Quaternary Alluvium

Notes: T.O.P. - Top of Pavement
USCS - Unified Soil Classification System

cases data were obtained at Stations 1 and 4, located 10 m apart. However, as indicated in Table 2, occasionally the cone data were obtained at 20-m (Stations 1 and 7) or 12-m (Stations 1 and 5) spacings. The cone penetrometer data demonstrate the great variations in material properties that are possible, vertically and laterally. As an example, Site 1 exhibits a very hard layer in the 1- to 2.5-m depth range at Station 1, whereas the material in the 1 to 2.5-m depth range at Station 4, 10 m away, exhibits a much lower cone resistance, indicating a less stiff layer. It can also be noted that, because of natural vertical and lateral profile variations, cone penetrometer data along the shoulder of the road may not accurately represent subgrade properties and layering for material beneath the pavement. In general, it is difficult and expensive to capture vertical and lateral variations by using field or laboratory tests on relatively small sample volumes.

The vertical and lateral variations of cone resistance and water content are more clearly seen in Figures 1, 2, and 3 top, showing profiles of q_c and water content for three typical sites. The layering

TABLE 2 Summary of Cone Data and Water Content

Site	Depth(m)	Station 1		Station 1S		Station 4/7	
	(m)	qc(MPa)	w(%)	qc(MPa)	w(%)	qc(MPa)	w(%)
1	0.8	2.9	4.5	7.0	6.9	2.1	4.3
	1.2	11.2	8.5	7.4	6.8	8.9	3.0
	1.8	13.9	7.3	22.7	8.3	7.5	7.0
	2.4	22.3	7.5	9.9	5.9	3.2	10.9
	3.0	4.4	10.7	10.6	7.3	28.5	11.1
	3.7	7.7	9.4	23.4	7.3	N/A	13.9
	4.3	9.7	15.1	N/A	9.5	N/A	11.1
2*	0.8	19.6	5.9	8.6	8.6	34.8	6.0
	1.2	16.0	7.1	11.2	5.6	N/A	8.0
	1.8	1.9	6.4	8.2	5.8	2.5	8.2
	2.5	15.5	5.4	N/A	5.2	3.4	5.0
	3.0	N/A	4.8	N/A	5.1	7.3	6.4
	3.7	N/A	5.1	N/A	5.3	10.0	4.9
	4.3	18.7	3.5	N/A	4.6	22.0	3.1
	4.9	25.1	2.4	N/A	4.8	28.2	1.9
3*	0.8	N/A	11.8	4.5	12.6	N/A	11.6
	1.2	15.4	9.0	8.5	12.2	16.8	9.7
	1.8	2.5	17.1	2.5	17.6	2.8	18.5
	2.4	2.2	14.3	1.5	20.4	2.7	13.4
	3.0	2.4	17.2	3.0	17.8	2.6	17.4
	3.7	4.6	10.7	2.4	9.7	3.0	10.5
	4.3	2.7	9.0	3.7	9.7	3.7	12.7
	4.9	5.3	6.3	4.3	7.7	6.4	11.7
	5.5	4.6	9.8	2.3	7.7	5.1	10.0
	6.1	3.2	10.6	4.6	7.6	2.9	7.5
	6.7	3.2	15.4	2.0	8.0	3.7	7.5
	7.3	2.1	23.1	3.0	19.2	6.8	7.5
	7.9	3.6	23.1	6.9	23.1	10.1	7.5
4	0.8	6.0	22.8	1.4	19.6	19.4	9.8
	1.2	0.9	20.5	0.8	23.4	3.4	12.8
	1.9	0.7	27.1	0.6	25.4	0.5	27.5
	2.4	0.8	26.5	1.1	25.2	0.8	23.9
	3.0	1.3	25.1	1.3	26.2	1.2	27.8
	3.7	1.7	sat'd	3.4	sat'd	8.1	sat'd
	4.3	4.0	sat'd	5.1	sat'd	7.5	sat'd
	4.9	8.6	sat'd	9.0	sat'd	6.3	sat'd
	5.5	6.8	sat'd	7.6	sat'd	4.0	sat'd
	6.1	11.4	sat'd	1.0	sat'd	2.3	sat'd
	6.7	5.6	sat'd	7.1	sat'd	1.3	sat'd
	7.3	3.1	sat'd	7.4	sat'd	2.2	sat'd
	7.9	3.6	sat'd	11.0	sat'd	7.0	sat'd
5	0.8	9.6	12.0	8.7	10.0	12.8	11.6
	1.2	10.8	10.8	6.3	9.9	14.5	7.7
	1.8	37.3	6.4	7.4	15.1	12.2	7.0
	2.4	N/A	15.8	7.9	20.6	N/A	9.1
	3.0	N/A	19.3	6.1	20.0	N/A	16.1

NOTES: N/A - Not Available
* - Data under Station 4/7 applies to Station 7
sat'd - saturated, no water content samples taken

(continued on next page)

is significantly different at the three locations at Site 12 (Figure 1), indicating high lateral variation in properties. On the other hand, Site 3 profiles, Stations 1 and 7 (Figure 2), show consistent cone resistance profiles, demonstrating that pavement subgrades can be uniform in properties at some locations. Figure 3, Site 15, demonstrates the potential for significant vertical soil layering over short distances as well as lateral variability.

CORRELATIONS OF WATER CONTENT AND CONE RESISTANCE

The observed water-content variations are often indicative of material-type variations because some soils, such as clays, have a higher affinity for water than do granular materials. In addition, for a given material type, the lower water content would be expected to corre-

TABLE 2 (*continued*)

Site	Depth(m)	Station 1		Station 1S		Station 4/5	
	(m)	qc(MPa)	w(%)	qc(MPa)	w(%)	qc(MPa)	w(%)
7	0.8	7.1	11.0	14.1	10.2	13.6	9.0
	1.2	3.7	16.1	1.3	10.3	7.2	8.9
	1.8	1.8	16.1	1.0	18.3	1.9	16.9
	2.4	2.0	18.4	1.0	22.5	1.2	20.3
	3.0	1.3	25.8	1.1	26.8	2.3	24.5
	3.7	1.6	26.7	1.1	28.6	2.8	24.5
	4.3	2.2	26.0	1.8	28.6	7.4	22.2
	4.9	3.4	17.1	6.1	11.8	10.8	5.7
	5.5	7.9	11.5	5.6	11.8	N/A	5.7
	6.1	9.1	15.0	N/A	19.0	N/A	12.1
8	0.8	6.4	8.9	7.1	7.1	9.6	10.6
	1.2	6.0	10.6	1.5	13.9	2.3	17.5
	1.8	6.4	18.0	N/A	14.0	6.2	21.4
	2.4	N/A	12.8	N/A	14.5	7.1	16.0
9	1.0	5.3	10.3	1.7	8.4	N/A	3.3
	1.5	29.1	19.3	1.3	21.0	2.1	20.2
	2.1	N/A	N/A	21.8	21.0	2.4	21.0
10	0.8	27.6	17.8	13.8	8.8	28.5	17.3
	1.2	2.4	19.2	1.7	26.7	2.2	25.6
	1.8	N/A	N/A	19.6	24.3	2.5	24.6
	2.4	N/A	N/A	N/A	24.2	8.7	27.6
	3.0	N/A	N/A	N/A	24.2	11.1	20.4
	3.7	N/A	N/A	N/A	16.3	17.3	20.4
11*	0.2	45.9	1.2	0.6	3.3	N/A	1.9
	0.5	45.4	1.9	21.8	5.7	42.5	2.8
	0.8	N/A	2.5	7.3	10.1	16.1	4.2
	1.1	N/A	5.3	11.8	8.5	34.1	8.2
	1.4	25.8	6.8	N/A	8.9	N/A	7.6
	1.7	13.8	6.8	N/A	8.9	N/A	9.7
12	0.6	35.5	4.2	5.4	7.4	26.9	4.3
	1.2	11.4	6.8	25.8	5.5	14.8	7.1
	1.8	19.5	6.9	16.2	6.3	16.3	9.2
	2.4	N/A	4.6	N/A	4.9	22.7	5.5
	3.0	24.9	3.8	N/A	4.9	5.1	4.8
	3.7	7.1	3.8	N/A	2.6	2.3	9.2
	4.3	11.7	3.8	N/A	2.6	7.2	9.2
	4.9	18.9	2.6	N/A	2.5	11.1	6.3
	5.5	4.6	4.2	N/A	2.7	12.5	5.0
	6.1	10.2	4.1	N/A	2.7	12.5	4.1
	6.7	9.8	3.7	N/A	3.0	15.5	3.0
	7.3	21.7	3.7	N/A	4.0	14.4	3.0
13	0.3	14.3	7.5	1.6	12.4	23.0	6.9
	0.6	2.8	9.0	9.9	17.2	10.8	6.6
	1.0	14.4	8.4	24.0	12.2	22.2	6.6

NOTES: N/A - Not Available

* - Data under Station 4/5 applies to Station 5. Without * the data applies to Station 4.

sat'd - saturated, no water content samples taken

(continued on next page)

spond to higher cone resistance because soil suction (negative pore-water pressure) increases with decreasing water content. It was observed during the hole logging operation that, in many cases, the high cone-penetration values corresponded to materials that appeared cemented. Soil cementation arises both from soil suction and from cementing agents such dried clay and calcium carbonate.

In general, whether the change in water content is due to a difference in material type or variations in soil suction for the same material type, the expected trend would be to observe increasing cone resistance with decreasing water content. The role of soil suction can be evaluated only by studying the effect of water content on cone resistance for a given material type.

TABLE 2 (*continued*)

Site	Depth(m)	Station 1		Station 1S		Station 4/5	
	(m)	qc(MPa)	w(%)	qc(MPa)	w(%)	qc(MPa)	w(%)
14	0.3	15.5	7.2	11.3	9.3	22.6	5.0
	0.6	10.6	15.7	5.6	17.4	8.6	11.5
	1.0	5.2	17.4	4.1	19.9	14.4	16.3
	1.2	35.0	19.0	18.5	19.9	8.3	15.2
	1.5	N/A	18.5	12.3	17.6	9.1	22.8
	1.8	N/A	9.5	N/A	16.6	15.1	14.6
	2.1	N/A	9.4	N/A	11.7	26.0	10.9
15	0.3	3.9	5.8	4.1	6.0	2.4	5.3
	0.6	1.4	6.2	1.1	5.5	8.7	5.3
	1.0	3.8	5.4	2.4	5.5	3.0	5.1
	1.2	2.5	5.4	4.7	5.5	5.0	3.6
	1.5	3.7	5.4	4.1	3.8	6.3	12.4
	1.8	5.2	5.4	4.7	8.9	4.9	9.3
	2.1	28.7	6.7	15.2	4.3	12.0	4.7
	2.4	23.3	4.4	18.4	8.1	33.1	4.7
	2.7	N/A	8.2	N/A	9.2	32.8	6.8
16	0.6	10.9	5.9	6.2	5.9	20.5	6.4
	1.2	1.4	5.6	2.1	5.1	2.0	4.5
	1.8	2.4	8.7	4.6	6.5	2.3	8.9
	2.4	12.5	6.9	5.4	5.8	12.2	10.7
	3.0	N/A	6.9	38.2	6.8	20.5	10.3
17*	0.6	2.8	18.8	45.3	13.0	9.7	3.1
	1.2	5.1	18.6	14.9	13.2	11.7	13.9
	1.8	5.6	30.5	10.7	15.3	2.4	15.2
	2.4	2.9	21.5	N/A	22.0	1.3	22.9
	3.0	1.7	17.9	N/A	21.2	1.1	23.0
	3.7	10.9	N/A	N/A	N/A	0.7	22.6
	4.3	9.9	N/A	N/A	N/A	1.0	22.6
18	0.3	34.5	3.5	16.3	4.6	N/A	4.5
	0.6	N/A	4.6	32.5	5.4	N/A	4.6
	1.0	N/A	7.0	N/A	6.0	N/A	5.1
	1.2	N/A	7.4	N/A	6.9	N/A	6.7
	1.5	N/A	6.8	N/A	11.1	N/A	9.3
	1.8	11.7	7.5	N/A	9.0	N/A	10.7
	2.1	15.0	9.5	N/A	8.0	N/A	10.0
	2.4	11.4	13.8	N/A	5.9	N/A	10.5
	2.8	21.7	9.5	N/A	5.4	N/A	7.3
19	0.3	31.4	9.9	6.3	13.0	18.6	8.8
	0.6	19.1	13.1	1.8	22.5	4.7	9.2
	1.0	5.9	24.4	1.2	29.2	28.3	16.5
	1.2	2.8	30.2	0.7	28.7	N/A	21.2
	1.5	6.5	24.6	16.8	29.4	N/A	20.0
	1.8	1.0	25.4	N/A	N/A	N/A	23.5
	2.1	34.5	N/A	N/A	N/A	N/A	N/A

NOTES: N/A - Not Available

* - Data under Station 4/5 applies to Station 5. Without * the data applies to Station 4.

sat'd - saturated, no water content samples taken

In an attempt to eliminate some of the sources of data scatter in the cone-resistance/water-content correlations, the sites having subgrade materials consisting primarily of silt or silty sand were studied alone. The gradation of the materials has an effect on the variation in q_c that is not completely accounted for by the variation in water content. Therefore, inclusion of the primarily clayey and gravelly sites in the predominantly silty soil data base would add to the scatter. The average cone resistance and the average water content for each of the silty sites were computed. A plot of average q_c versus average water content for the silt and silty sand subgrades is shown in Figure 4. Although averaging the values for each site, and including only the silty soils, tends to decrease some of the scatter in the data, significant scatter still exists in the data given in Figure 4. Variations in gradation within the predominantly silty soils still exist, no doubt, and cause some variation in water content. In addition, some of the scatter in the data results from the presence of rock or gravel fragments. When rock fragments are encountered, this can lead to inconsistently high cone resistance values for the reported water content. Presence of rock or gravel fragments also leads to more apparent variability in subgrade materials than might actually be exhibited in situ. The appropriate dimensions for averaging for pavement applications are typically much greater than the dimensions of the CPT cone or the pebbles and rock that sometimes yield erratically high CPT values.

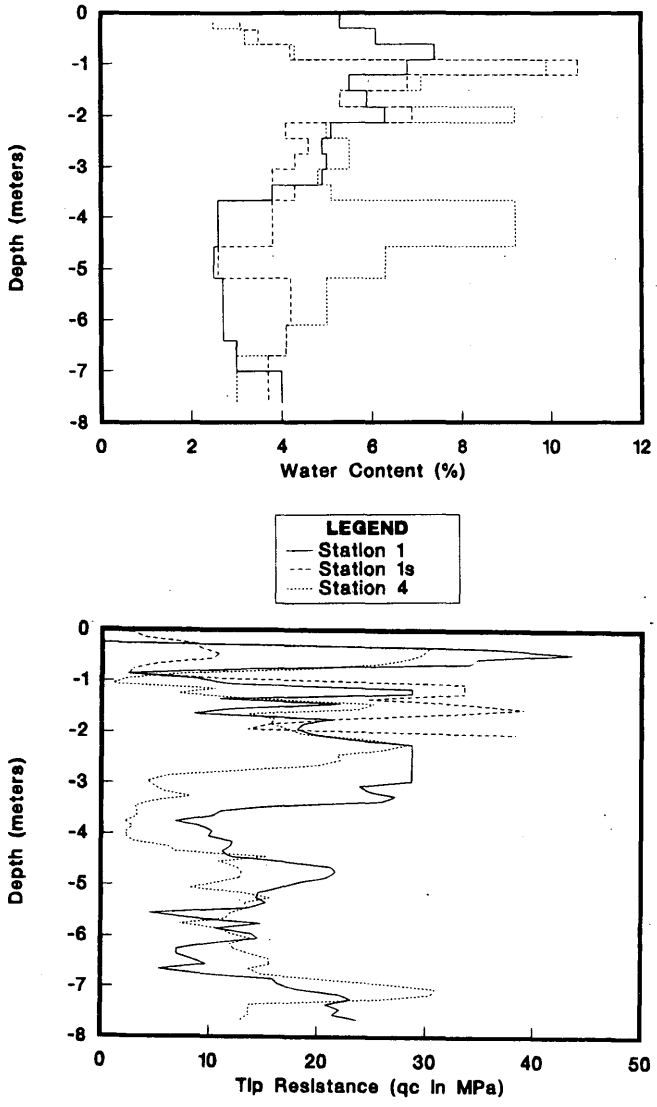

FIGURE 1 Cone tip resistance and water content profiles for Site 12.

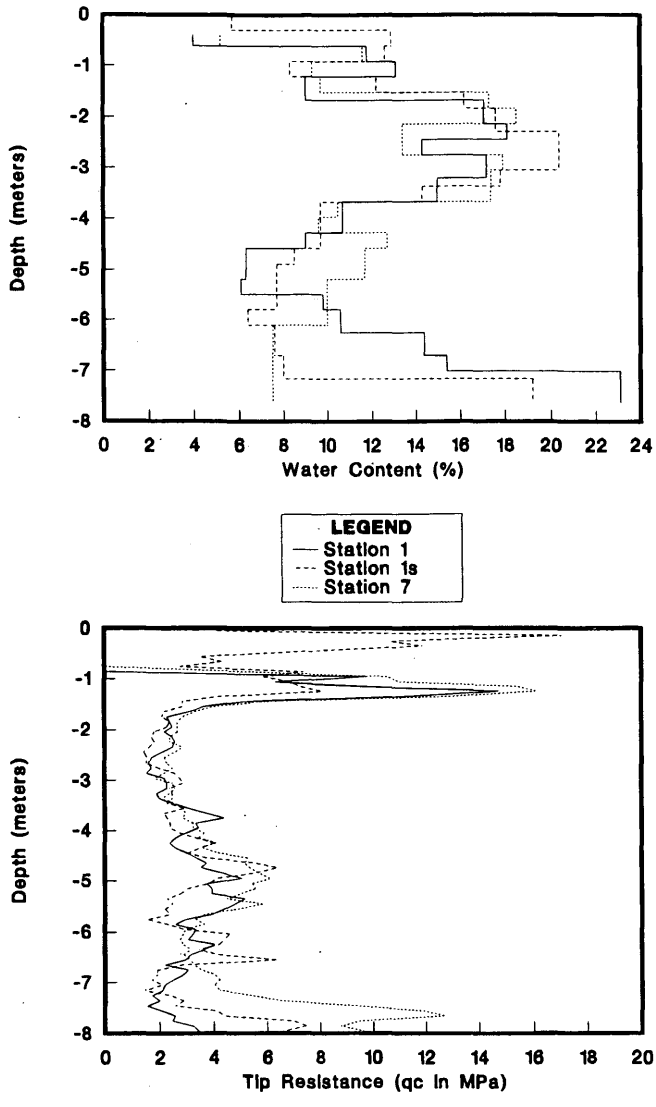

FIGURE 2 Cone tip resistance and water content profiles for Site 3.

ROLE OF SOIL SUCTION

The relationship between soil shear strength and soil suction has been well established (*6*). For a given soil gradation and density, the higher the soil suction, the higher the effective stress, and therefore the greater the soil shear strength and cone tip resistance. For a given soil type and density, the soil suction can be correlated directly to water content and degree of saturation (*7*). The increase in shear strength associated with decreasing water content is apparent from the direct shear data obtained for a silty soil, shown in Figure 5 (*8*).

Because soil suction is not dependent on density, a relationship between soil suction and soil water content is often established for a given material type. A soil-water characteristic curve, showing the relationship between water content and soil suction for a typical silty sand, appears in Figure 6. A typical curve, such as that depicted in Figure 6, can be used to obtain qualitatively correct suction data for the silty soils in this study. By using the soil–water characteristic curve shown in Figure 6 an approximate relationship between average cone tip resistance and soil suction, shown in Figure 7, was established for the sites with silty subgrade materials. Although there is significant scatter (most likely resulting from vertical nonhomogeneities), a clear trend of increasing cone resistance with increasing suction exists.

EFFECTS ON PAVEMENT DESIGN

The cone penetrometer data demonstrate the potential for a high level of variation in subgrade material properties. This observation affects pavement and overlay design because the subgrade materials play a significant role in the pavement surface deflections exhibited during pavement loading and during NDT tests, such as the falling weight deflectometer tests. Pavement surface deflections are of primary consideration in the design of new pavements and overlays for existing pavements.

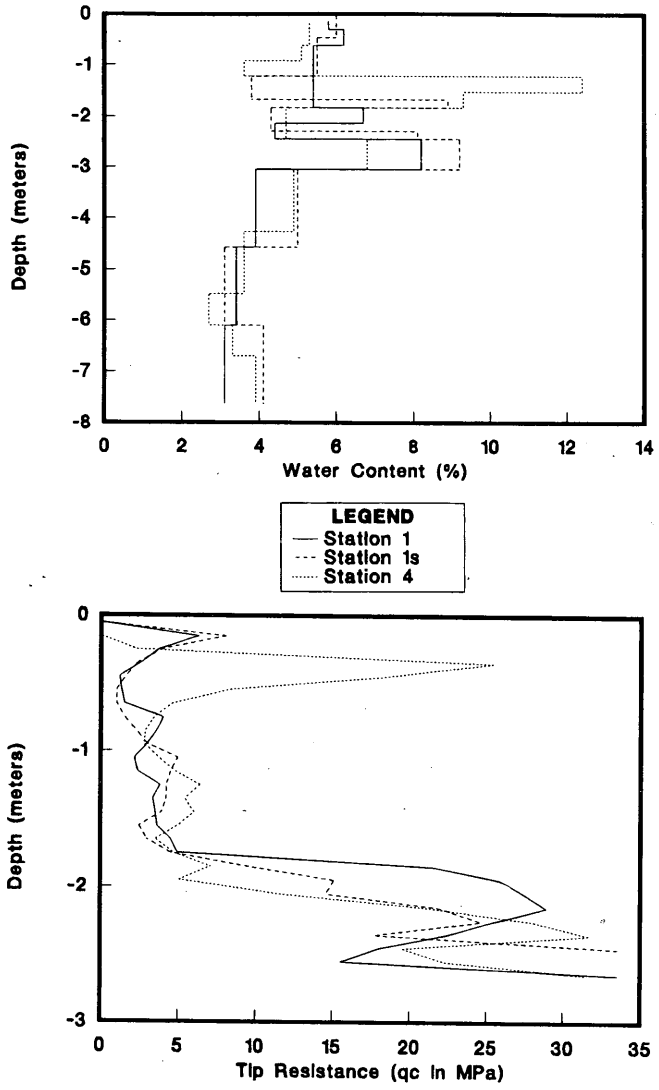

FIGURE 3 Cone tip resistance and water content for Site 15.

If the modulus of the subgrade was constant all the way down to firm (or bedrock) material, then NDT deflection basins should be consistent at a given site. Even if the subgrade were highly layered in the vertical direction, provided that there was little or no lateral variation at the site, the deflection basin should be repeatable over short distances because the deflection basin provides a weighted average or "lumped" indicator of the subgrade modulus. Thus, for laterally uniform subgrade, variations in deflection basins from the falling weight deflectometer test would not be expected to be significant over distances as small as a few feet. However, the NDT deflection basins at the test sites considered in this study did, in fact, show significant variation over distances of approximately 3 m. Data from falling weight deflectometer (FWD) tests indicate pavement and subgrade nonhomogeneities, as shown in Figure 7. A statistical analysis of the variability of NDT deflection basins was previously reported for the same sites considered in this paper (*3*). In general, the NDT deflection basins at the 18 test sites were found to vary significantly over fairly short distances. Although there are certainly material property differences in the pavement surface and subbase materials, especially when poor construction quality control is implemented, these differences are unlikely to occur over very short distances. In addition, variations in material properties of the engineered surfaces and subbase materials are very small in comparison to variations in subgrade materials. Therefore, it is probable that the variations in the deflections, especially at the outer sensors, are caused by natural vertical and lateral variations in subgrade material properties. The outer sensor (geophone) has been shown to have a very strong correlation to the subgrade modulus (*9*). The subgrade materials to a significant depth (i.e., 8 to 10 m) below the pavement surface can also be shown to contribute to the outer sensor deflection measurements.

Given the significant influence of subgrade materials on the surface deflections and the tremendous variabilities detected for the subgrade materials from cone penetrometer, water-content, and boring log data, it appears plausible the variations in subgrade are predominantly responsible for much of the variability in NDT deflection basins. Therefore, any pavement overlay design procedure that is based on the deflection basin data or moduli backcalculated from these deflection basins would be sensitive to subgrade material property and water-content variations.

A great deal of subgrade material variation should be expected over short spans of highway. Even with good quality control of the construction methods, variations in deflection basins from NDT should be anticipated. The subgrade material variability is usually out of the control of the design engineer, because the materials are not engineered. Therefore, the design engineer must be aware of the potential of significant variability in subgrade response over short distances and its potential effect on the design selected. Because of the relationship among soil water content, soil suction, and soil shear strength, seasonal and spatial variability in water content must also be taken into consideration. Test intervals and length of design sections are best selected on the basis of statistical characterization and on the basis of local experience with subgrade variability.

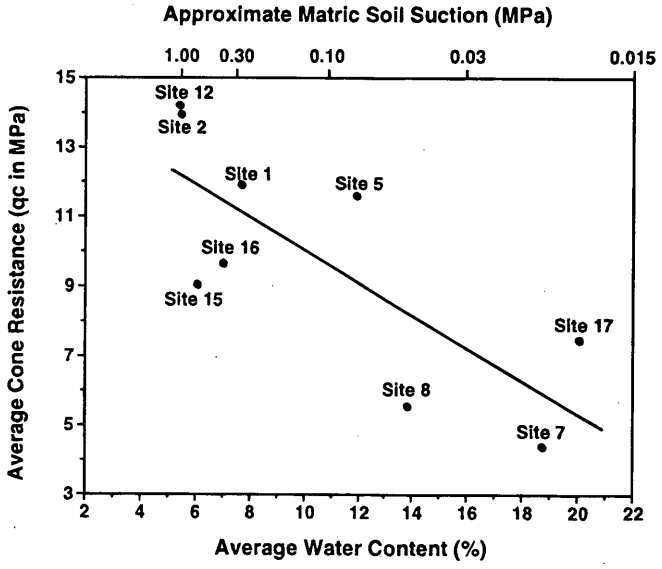

FIGURE 4 Average cone resistance and water content for sandy silts and silty soil profiles.

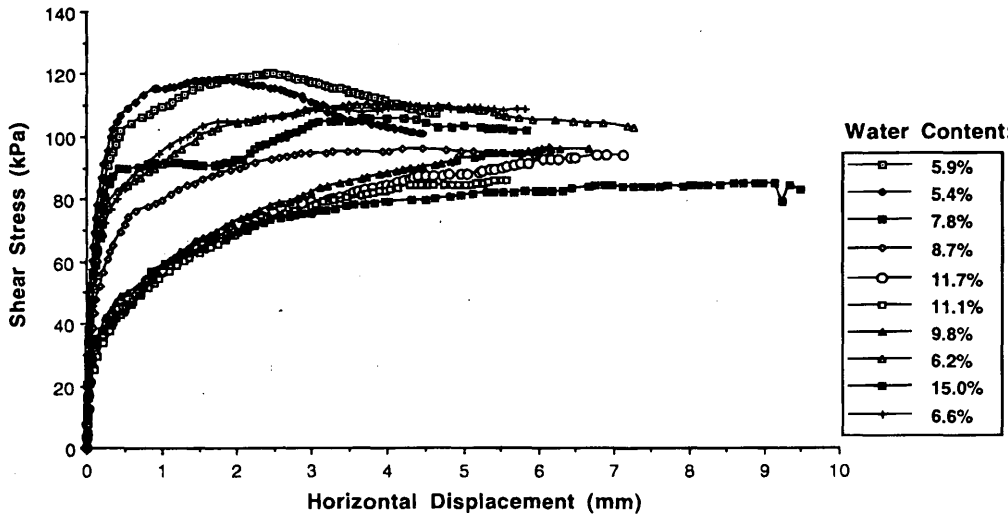

FIGURE 5 Direct shear test results for silt at various water contents.

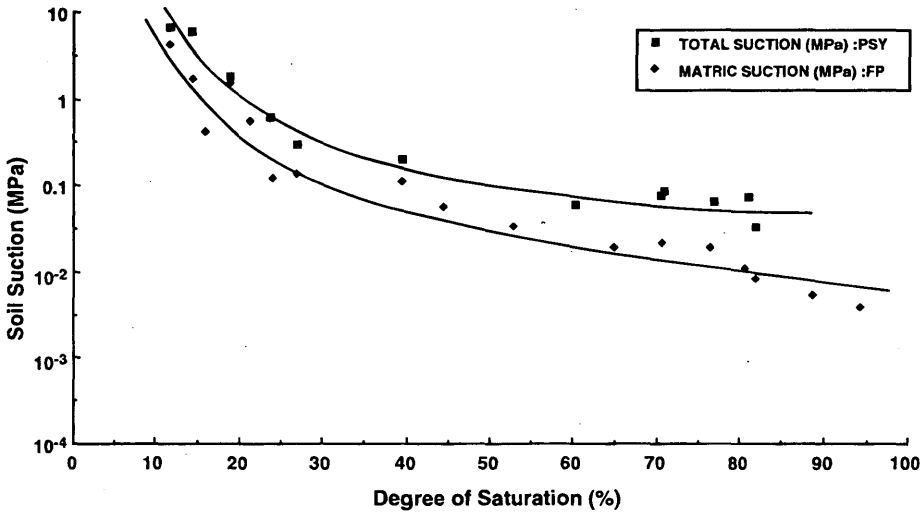

FIGURE 6 Typical soil suction versus degree of saturation for silt.

CONCLUSIONS AND RECOMMENDATIONS

Because of the considerable length of highway involved in new roadway or overlay construction and because of the huge volume of material that must be characterized, an assessment of the degree and effect of natural subgrade variations is of considerable importance. The decisions regarding the frequency of sampling and boring, NDT testing, and length of design section clearly should be related to the degree of nonhomogeneity at any given site. Cone penetrometer data from 18 sites in Arizona demonstrated the potential of many subgrade materials to exhibit significant variability both vertically and horizontally over distances of a few meters or less. Large variations in subgrade water content were also observed over short spans of highway. Water-content variations could be indicative of material type changes, negative pore-water pressure differences, or both. In any case, the lower the soil water content and the higher the soil suction, in general, the greater will be the cone resistance and subgrade stiffness.

The deep CPT and borings were useful as research tools to quantify the subgrade property variations and identify their sources. However, the CPT and borings are not practical for routine design applications. NDT with an FWD or similar apparatus is much more practical and useful for characterization of pavement structure properties for routine design.

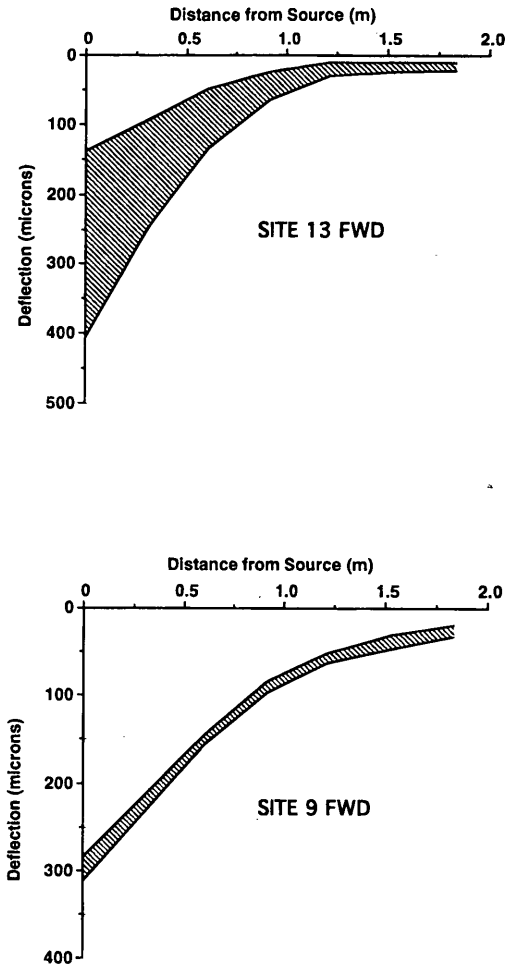

FIGURE 7 Deflection basins for: *top,* relatively high variability site and *bottom,* relatively low variability site (*3*).

ACKNOWLEDGMENT

The research presented in this paper was sponsored, in part, by the Arizona Department of Transportation through the Arizona Transportation Research Center.

REFERENCES

1. Way, G. *Environmental Factor Determination from In-Place Temperature and Moisture Measurements under Arizona Pavements.* Report FHWA/AZ-80/157, Arizona Department of Transportation, Phoenix, 1980.
2. Houston, S., and R. Perera. Impact of natural site variability on nondestructive test deflection basins, *Journal of Transportation Engineering,* ASCE, Vol. 117, No. 5, 1991, 550–565.
3. Mamlouk, M., W. Houston, S. Houston, and J. Zaniewski. *Rational Characterization of Pavement Structures Using Deflection Analysis.* Report FHWA/AZ-88/254. Arizona Department of Transportation, Phoenix, 1988.
4. Douglas, B., A. Strutynsky, L. Mahar, and J. Weaver. (1985). *Soil Strength Determination from Cone Penetrometer Tests.* Civil Engineering in the Arctic Offshore, ASCE, Arctic, San Francisco, Calif. March 1985.
5. Villet, W., and J. Mitchell. Cone Resistance, Relative Density, and Friction Angle. *Proc., ASCE Meeting on Cone Penetrometer Testing and Experience,* St. Louis, Mo., 1981.
6. Fredlund, D., and H. Rahardjo. *Unsaturated Soil Mechanics.* John Wiley and Sons, Inc., New York, 1993.
7. Houston, S., W. Houston, and A. Wagner. Filter Paper Technique for Soil Suction Determination. *ASTM Geotechnical Testing Journal,* Vol. 17, No. 2, 1994, pp. 185–194.
8. Wang, C. *Relationship Between Soil Suction and Soil Shear Strength.* MS thesis, Department of Civil Engineering, Arizona State University, Tempe, 1994.
9. Zaniewski, J., W. Hudson, S. Seeds, and L. Moser. *Pavement Performance Model Development.* FHWA/RD-84/104. Vol. 2, Office of Engineering Highway Operations and Research Development, McLean, Va. 1984.

Publication of this paper sponsored by Committee on Environmental Factors Except Frost.

PART 2

Nonearth Materials' Thermal Effects on Pavements

Case Study of Insulated Pavement in Jackman, Maine

MAUREEN A. KESTLER AND RICHARD L. BERG

Traditionally, detrimental effects of frost action are reduced by thick fills or by excavation and removal of large quantities of frost-susceptible material and replacement with a thick layer of non–frost-susceptible material. However, incorporating an insulating layer within the pavement structure can often provide a cost-effective alternative for protecting the subgrade from frost penetration. In 1986 the runway, taxiway, and parking apron at Newton Field, a small airport in Jackman, Maine, were reconstructed using a layer of extruded polystyrene insulation 51 mm (2 in.) thick as part of the pavement structure. Because test results from the first winter of observation showed substantial frost penetration beneath the runway insulation, four additional test sections of various combinations of insulation and sand subbase thickness were constructed adjacent to the parking apron in 1987. The insulated test sections, which were constructed under tighter controls, on a firm working platform, and in a slightly drier location than the runway, experienced very little frost penetration into the subgrade. The good performance of the insulated test sections as well as runway observations, methods used to investigate insulation integrity, and theories considered to explain the relatively poor performance of some sections of the insulated runway pavement are discussed.

Newton Field, which includes an 18- × 884-m (60- × 2900-ft) insulated runway, taxiway, apron, and four adjacent insulated pavement test sections, is in the town of Jackman, Maine (45°38′N, 70°15′W). The runway at Newton Field was reconstructed in 1986 to replace an old, smaller runway that exhibited severe differential frost heaving and excessive cracking. Jackman has an average annual air temperature of 3°C (38°F) and a design air freezing index of approximately 1428°C-days (2570°F-days). The runway elevation is approximately 358 m (1175 ft) above mean sea level; the 100-year flood level of nearby Moose River is approximately 357 m (1170 ft). Figure 1 shows an aerial view of Newton Field and the town of Jackman.

DESIGN AND CONSTRUCTION OF TEST SITES

According to U.S. Army Corps of Engineers and Maine Department of Environmental Protection criteria, the entire airfield is classified as a wetlands zone. Deep frost penetration and highly frost-susceptible materials in the immediate vicinity are reported (*1*).

Traditionally, detrimental effects of frost action are reduced by thick fills or by excavation and removal of large quantities of frost-susceptible material and replacement with a thick layer of non–frost-susceptible material. However, incorporating an insulating layer within the pavement structure can often provide a cost-effective alternative for protecting the subgrade from frost penetration.

Civil and Geotechnical Engineering Research Branch, U.S. Army Cold Regions Research and Engineering Laboratory, 72 Lyme Road, Hanover, N.H. 03755.

Runway construction contracts for insulated and noninsulated pavements were sent out for bid. The insulated-pavement alternative was selected because the bid was less than 4 percent higher than the bid for a conventional pavement.

Construction began during the summer of 1986. The entire area of the 18- × 884-m (60- × 2900-ft) runway, the 9- × 75-m (30- × 245-ft) taxiway, and the 38- × 91-m (125- × 300-ft) parking apron was underlaid by a layer of extruded polystyrene insulation panels 51 mm (2 in.) thick. A total of one-half million board feet of insulation was used. A typical insulated pavement cross section is shown in Figure 2*a*. A geotextile separated a sand leveling course of varying thickness [25 mm (1 in.) minimum specified] from the underlying wet silty subgrade.

The final design was for total frost protection of the subgrade. Minimum compressive strength of the insulation was 276 kPa (40 psi), and the design load was for a 134-kN (30,000-lb) single-wheel load. The high water table at the site presented challenges to both design and construction personnel.

Also in 1986, the first 46 m (150 ft) of nearby Nichols Road were reconstructed to a cross section similar to that of the noninsulated conventional pavement specified for the runway at Newton Field. Figure 2*b* shows the typical cross section.

Because test results from the first winter of observation (1986–1987) showed substantial frost penetration beneath the insulation on the runway, four test sections consisting of various combinations of insulation and sand subbase thickness were constructed adjacent to the aircraft parking apron in July 1987. The test section site was wet but not quite so swampy as much of the runway site. Figure 2*c* shows a longitudinal section of the test sections. Test section 1 most closely approximates the design used for the insulated runway. In contrast to placement of single-thickness insulation panels in the runway, test section insulation panels were placed in multiple layers with joints staggered. The original soil profile was the same as that of the runway.

INSTRUMENTATION

Instrument installation in 1986 and 1987 is discussed in detail in works by Kestler and Berg (*2,3*) and by Allen (*4*). Initial instrumentation included thermocouples and thermistors to monitor subsurface temperatures above, within, and beneath the insulation; tensiometers to measure soil moisture; and electrical resistivity gauges to indicate frozen/nonfrozen conditions beneath the insulating layer. The water table was monitored by water wells, frost heave was measured by conducting periodic pavement surface elevation surveys with an engineer's level and rod, and pavement stiffness was measured nondestructively with the U.S. Army Cold Regions Research and Engineering Laboratory's (CRREL) falling weight

FIGURE 1 Newton Field, Jackman, Maine (photographed by S. Coleman of Dave Walker Cards).

deflectometer. During later years of observation linear-motion potentiometers were installed across selected transverse cracks to monitor diurnal and seasonal asphalt concrete (AC) expansion and contraction and to determine AC shrinkage associated with aging. In addition, vibrating-wire piezometers and pressure transducers were installed in water wells (located on a line perpendicular to the lateral edge drain) to define changes in phreatic surface throughout the year.

DESIGN METHODS

For a design air-freezing index of 1428°C-days (2570°F-days), the Army and Air Force (*5*) require an insulation thickness of approximately 76 mm (3 in.). Several other charts and rule-of-thumb design methods yield a desired insulation thickness of approximately 64 mm (2.5 in.). Each method ensures designs that prevent frost penetration into the subgrade. During the winters of observation at the test sections the 0°C (32°F) isotherm penetrated through the bottom of the insulation 51 mm (2 in.) thick in Test Section 1 but not into the subgrade. From these data it appears that the test section field results conformed well to design thicknesses. During a design winter, frost is expected to penetrate the 51-mm (2-in.) insulation but not the 76-mm (3-in.) insulation. Although the winters in Jackman during the observation period ranged from average to colder than average, the design freezing index was never attained.

The test sections, which were constructed under tighter controls, on a firm working platform, and in a slightly drier location than the runway's, performed quite well and as expected. In comparison, some areas of the insulated runway did not perform particularly well. The following sections briefly discuss the good performance of the insulated test sections but concentrate on runway observations, methods used to investigate insulation integrity, and theories considered to explain the relatively poor performance of some insulated runway pavement sections.

FROST PENETRATION

Although the insulated test sections experienced little frost penetration into the subgrade, the runway experienced appreciable frost penetration into the subgrade where our instruments were located. Figure 3 shows a general trend of increasing temperatures with increasing depth beneath the surface of the pavement for noninsulated Nichols Road. Figure 4 shows the same trend but also demonstrates the efficiency of the insulating layer in the test sections. Figure 5, however, shows a distinct temperature discontinuity immediately beneath the insulating layer in the runway. A probable explanation of the temperature discontinuity and resulting frost penetration follows.

Two vertical thermocouple assemblies, one located in and above the insulation and the second located entirely below the insulation, are separated horizontally by approximately 1.5 m (5 ft). It is believed that the temperature discontinuity between thermocouple assemblies is caused either by damage to the insulation or by horizontal separation of the insulation panels. The problem probably occurred during construction. Evidence of this problem was encountered during construction in areas 9 to 5 m (30 to 50 ft) square near Stations 4+50 and 8+00. At both locations trucks, bulldozers, and other construction traffic caused a large subgrade flow that in turn raised the insulation. Under direction of the resident engineer, insulation was removed in the problem areas; subgrade was removed to the desired depth; and the geotextile, insulation, and base course were all replaced.

INSULATION DISCONTINUITIES

In July 1987, a 3- × 9-m (10- × 31-ft) section of pavement near station 30+00 was removed because of excessive local settlement. Figure 6 shows the overlapping and damaged insulation that was removed and replaced.

During the years following removal of the pavement section at Station 30+00 a variety of nondestructive methods were used to confirm the suspicion that damaged or separated panels, or both, were not limited to Station 30+00. Methods included infrared photography, ground-penetrating radar, and hand excavation of the base course alongside the runway.

The infrared camera showed considerable variation in surface temperatures. However, it could not identify insulation discontinuities.

Ground-penetrating radar provided more information than did infrared photography. Investigations yielded profiles such as those shown in Figure 7 (*6*). Assuming a uniform water content between the AC and the insulation, approximate depths from AC to insulation panels can be determined from these radar records. The uppermost set of dark bands represents the antenna direct coupling. The next series of bands represents the interface between insulation panels and the subbase (i.e., the bottom of the insulation). The third, less distinct set is caused by multiple reflection of the radar pulse between the various layers. Depths to insulation panels appear to range from 127 mm (5 in.) to 610 mm (24 in.) beneath the runway pavement surface. Although individual panels 610 mm (2 ft) wide can be identified in Figure 7 (bottom), the resolution of the ground-penetrating radar was not sufficient to permit estimation of gap sizes between individual panels. It should be noted that, in contrast to the nonuniform depth of insulation panels beneath the runway, the depth of insulation panels beneath the test sections was uniform. As stated previously, the primary differences between the test sections and the runway were that the test section site was not so wet as the runway site and that the test sections were constructed under tighter controls. The test sections also had a deeper subbase than the runway.

Hand excavation of trenches and random holes alongside the runway yielded the most definitive evidence of damaged and separated

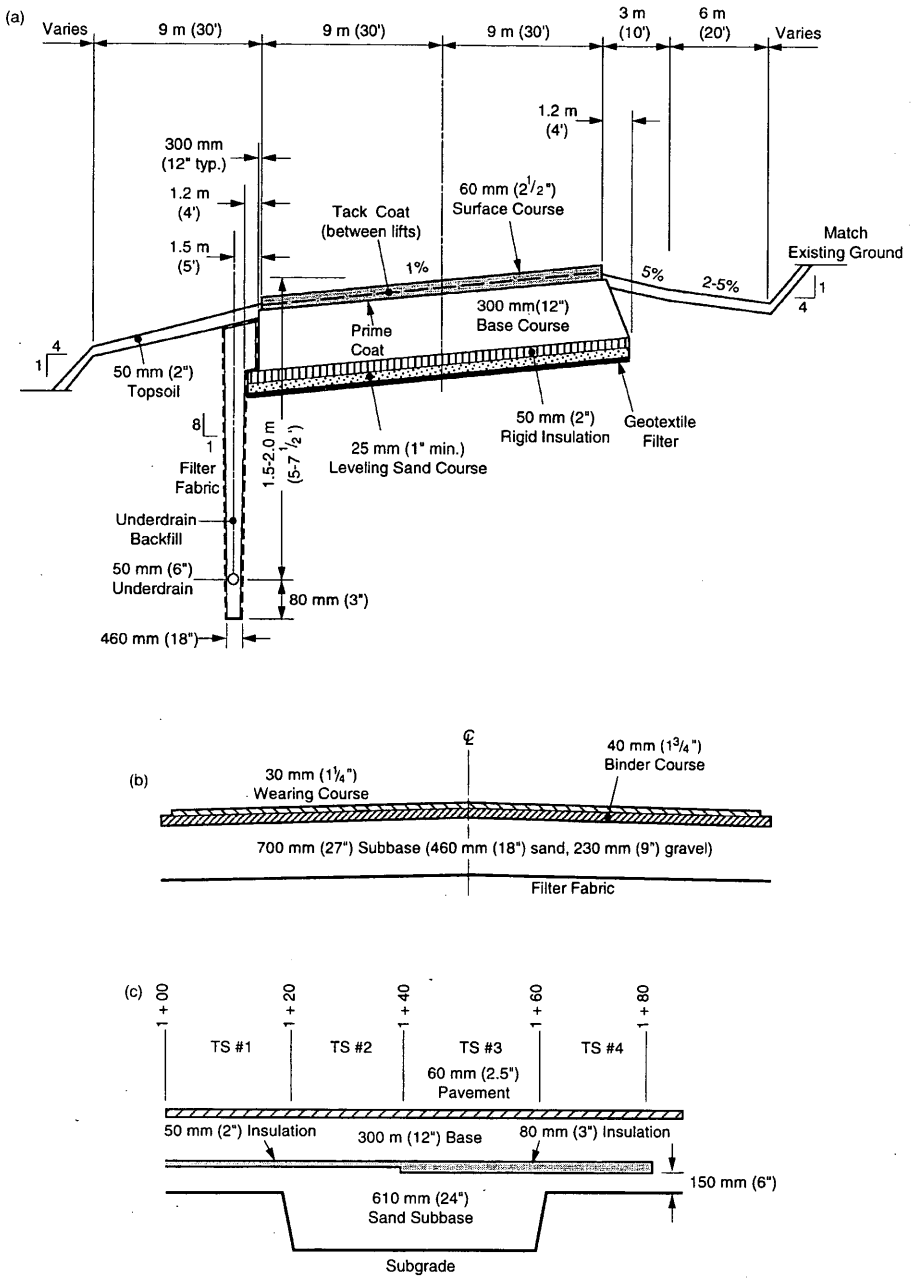

FIGURE 2 Typical cross section of (*a*) Newton Field runway and (*b*) Nichols Road and (*c*) longitudinal section of insulated test sections.

panels. A 64-mm (2.5-in.) gap was uncovered in the second 610- × 1520-mm (2- × 5-ft) trench alongside the runway at Station 7+75 in 1988. Further excavation yielded several gaps of approximately 51 mm (2 in.). During summer 1991 small holes alongside the runway at or near the ends of transverse cracks were excavated down to the insulation. Figure 8 shows cracked insulation at Station 22+80, which was representative of most test holes. It appears that cracking that occurred during periods of freezing conditions propagated down through the insulating layer and broke the insulation panels. The figure also shows a gap between insulation panels, which was typical.

FROST HEAVE

Maximum vertical displacement was similar each winter throughout the 4 years of observation. The maximum frost heave in test sections 1 to 4 and the conventional pavement at Nichols Road was approximately 25 mm (1 in.). Maximum frost heave along most of the runway was slightly greater than that observed at the test sections. However, the two ends of the runway exhibited 76 mm (3 in.) and 102 mm (4 in.) of frost heave, with localized areas of differential heaving. Areas of substantial frost heave correspond to areas that were excavated to a lesser depth during construction. In addition,

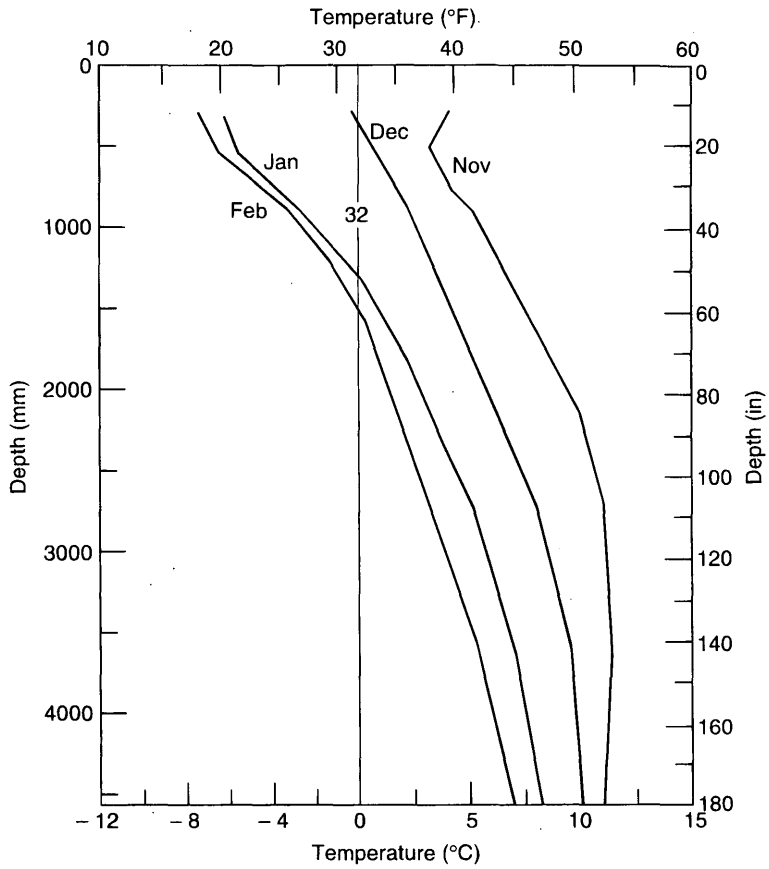

FIGURE 3 Nichols Road temperature profiles, winter 1987–1988.

both ends of the runway were particularly spongy during construction. Maximum differential movement within a length of 1.5 m (5 ft.) was approximately 152 mm (6 in.). Because of its absence from the test sections, differential frost heave on the runway was used as an indicator of damage to the underlying insulation. As discussed earlier, gaps in the insulating layer beneath the runway probably occurred during construction. The resulting nonuniform frost penetration into the subgrade undoubtedly caused most of the differential frost heaving. Differential frost heaving may, in turn, contribute to further cracking of insulation panels, thus perpetuating the cycle.

CRACKS

General

By far the most serious distress exhibited by the 8-year-old pavement is cracking. Crack types include small longitudinal cracks that typically occur in localized groups and individual transverse cracks ranging in width from hairline to several inches. The severity of the transverse cracks has been a cause for concern. Generally, (a) one or two more develop each winter, (b) no one year has been more conducive to crack production than another, and (c) they continue to increase in size.

In December 1992 several cracks were measured, of which the maximum width was approximately 127 mm (5 in.). By June 1994 the maximum width had increased to 229 mm (9 in.). Figure 9 shows one of the more severe cracks. Cracks have been sealed with a rubberized crack sealer several times. Nevertheless, the AC is exhibiting signs of secondary cracking and some crack settlement. One possible reason for this is that the base course may have eroded from beneath some of the larger cracks. During several heavy rains, granular material was observed in motion atop the AC at unsealed cracks, where the sealer has been removed by snowplows.

Of concern is the ever-increasing width of the cracks. It is recognized that insulated pavements experience greater temperature fluctuations than do conventional pavements because of the reduced effective thermal mass of insulated pavements. Greater temperature extremes cause the insulated pavement to undergo slightly greater thermal expansion and contraction than would a conventional pavement. Increased thermal stresses caused by these lower temperatures are discussed in the section entitled Laboratory AC Testing.

Pavement temperatures were recorded approximately biweekly during the 1986–1987 through 1990–1991 winters. Average base course temperatures in the insulated pavements were generally a few degrees lower than in the conventional pavement at Nichols Road throughout the freezing season, a few degrees higher during the summer season (but sometimes lower), and sometimes higher in fall and spring. Figure 10 shows base course temperatures just

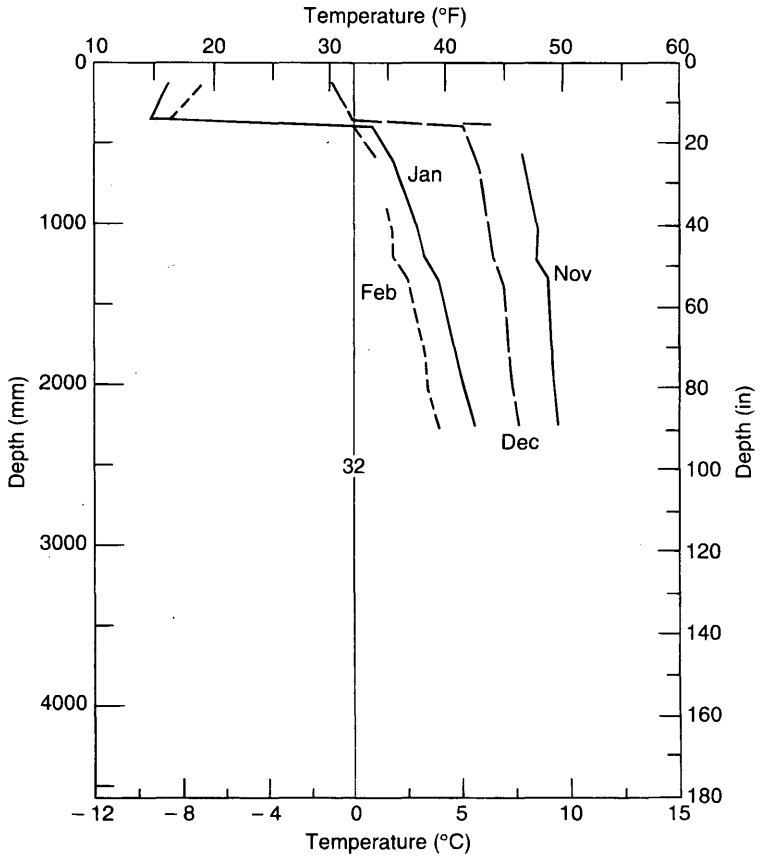

FIGURE 4 Test section temperature profiles, winter 1987–1988.

above the insulating layer in Test Section 1 and at a comparable depth in Nichols Road during the 1988–1989 observation season. Even if the lower temperatures contributed to additional cracking, they should not be responsible for the 229-mm (9-in.) crack observed during June 1994.

It is suspected that abnormally wide cracks are initiated by something other than the insulation but may be made worse by the insulation. During construction the asphalt mixture was hauled several hours from the asphalt plant to the project site. It is quite possible that the asphalt was overheated at the plant or placed at the site at a temperature below that desired. This could accelerate oxidation, making the AC brittle and susceptible to shrinkage and fracture (*7*).

Linear Motion Potentiometers

To differentiate diurnal thermal contraction and expansion, seasonal thermal contraction and expansion, and shrinkage of AC caused by aging, linear-motion potentiometers (LMPs) were installed across a transverse crack at Stations 16+15 and 18+00 (Figure 11). Figure 12 shows diurnal crack movement at Station 16+15 and corresponding temperatures recorded by temperature sensors embedded in the AC. Neither LMP functioned continuously for an entire year, so shrinkage because of asphalt aging could not be determined by this means. It is, however, believed that an LMP picked up a cracking event. Figure 12 shows appreciable damping in diurnal crack width variation starting February 3, 1991. During the first visit following February 3 a new crack between Station 16+15 and what had been the next closest crack was observed Clearly, the reduced slab length on one side of the monitored crack would cause some or all of the observed LMP attenuation.

Manual Measurements

The runway asphalt has shrunken considerably during the monitoring period, which began almost 6 years after the runway was built. A manual method was also used to measure this shrinkage. Nails were installed in the AC at 30-m (100-ft) intervals and on either side of each transverse crack. Distances between nails were measured with a 30-m (100-ft) steel surveyor's chain pulled taut with 67 N (15 lb) of tension. Temperature corrections were applied to the measurements of the AC and the steel chain. Total slab shrinkage from June 1992 to June 1994 was nearly 127 mm (5 in.). It should be noted that this method underestimates total runway shrinkage because new cracks occurred between old cracks during the monitoring period. Also, total runway length (from the center of the first AC slab to the center of the last) remained constant. This serves as a check of manual measurement accuracy, and reductions in slab

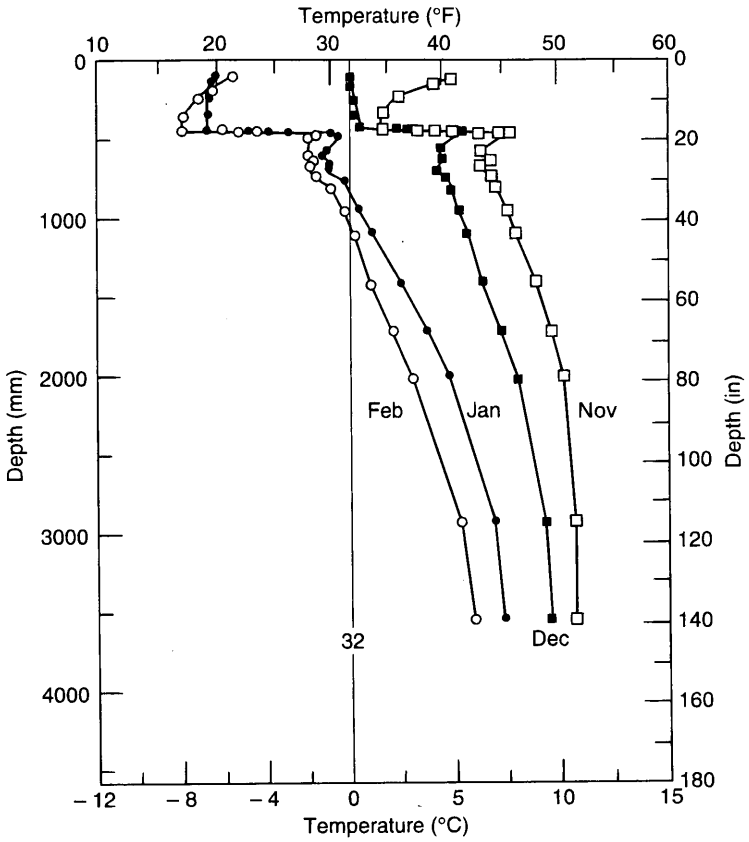

FIGURE 5 Newton Field temperature profiles, Station 4+50, winter 1987–1988.

lengths attributed to shrinkage far exceed manual measuring tolerances. Additional crack width is probably the result of secondary cracking and spalling.

Laboratory AC Testing

Laboratory tests to determine both a coefficient of thermal contraction and the temperature necessary for thermal cracking under an applied load were conducted on AC samples obtained from the Newton Field runway in 1992.

The coefficient of thermal contraction was determined to be approximately 20×10^{-6} mm/mm/°C (11×10^{-6} in./in./°F), which is typical. In contrast, thermal stress test results were not typical. Results help support the belief that excessive cracking could be as attributable to the asphalt as to the insulation. An AC sample 254 mm (10 in.) long was subjected to decreasing temperatures in accordance with the procedure discussed elsewhere (*8*). The sample broke at −20°C (−4°F), which is well outside the expected range of −25° to −30°C (−13° to −22°F) for this type of AC.

Again, it is possible that overheating for the lengthy plant-to-site haul could have caused a loss of higher-end volatiles, which effectively altered the AC to a higher-grade AC that is more susceptible to low-temperature cracking. Compounding the situation, temperatures experienced by the insulated pavement were lower than those for a conventional pavement.

FIGURE 6 Damaged and overlapping insulation panels, Station 30+00, Newton Field runway.

NONDESTRUCTIVE TESTING

Falling weight deflectometer tests were conducted periodically to assess stiffness of the conventional and insulated pavements. Back-calculated moduli [using WESDEF (*9*) and MODCOMP (*10*)] and deflection basin areas were used as indicators of pavement stiffness.

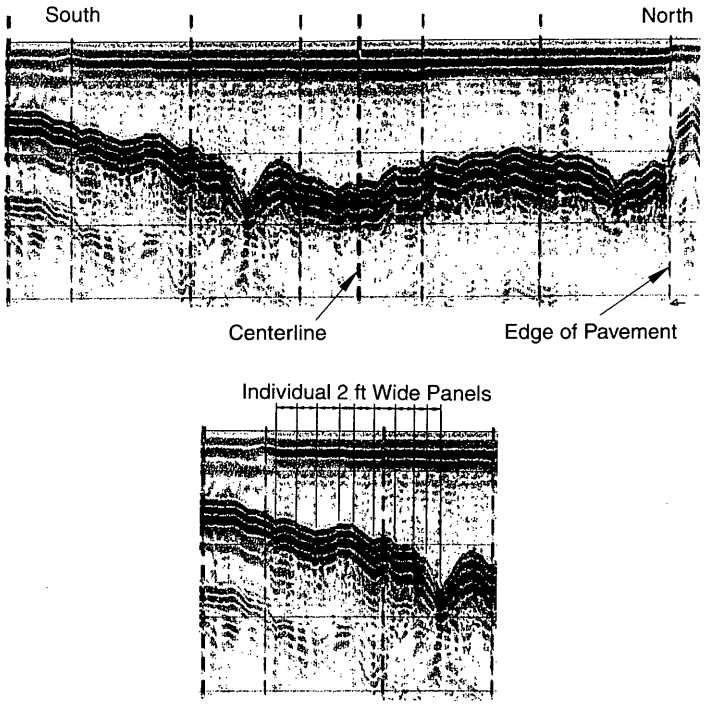

FIGURE 7 Ground-penetrating radar profile, *top,* and enlargement of south end of profile showing insulation panels 610 mm (2 ft) wide, *bottom.*

FIGURE 8 Insulation panels alongside runway, showing crack and gap between panels.

At temperatures above freezing, typical modulus values for all the insulated pavements were appreciably lower than those for non-insulated Nichols Road. This was probably because of the near-surface water table at Newton Field compounded by the low modulus of extruded polystyrene.

Although conventional pavements typically experience appreciable strength loss during spring thaw and recover with time, the strength of the insulated test sections remained relatively constant through spring and summer, with fluctuations caused primarily by AC temperatures. If insulation prevents frost from penetrating into the subgrade, the subgrade never undergoes thaw weakening. However, the high water table again complicates the issue because it may cause the subgrade to remain weak during what would otherwise be a recovery period.

FIGURE 9 Transverse runway crack.

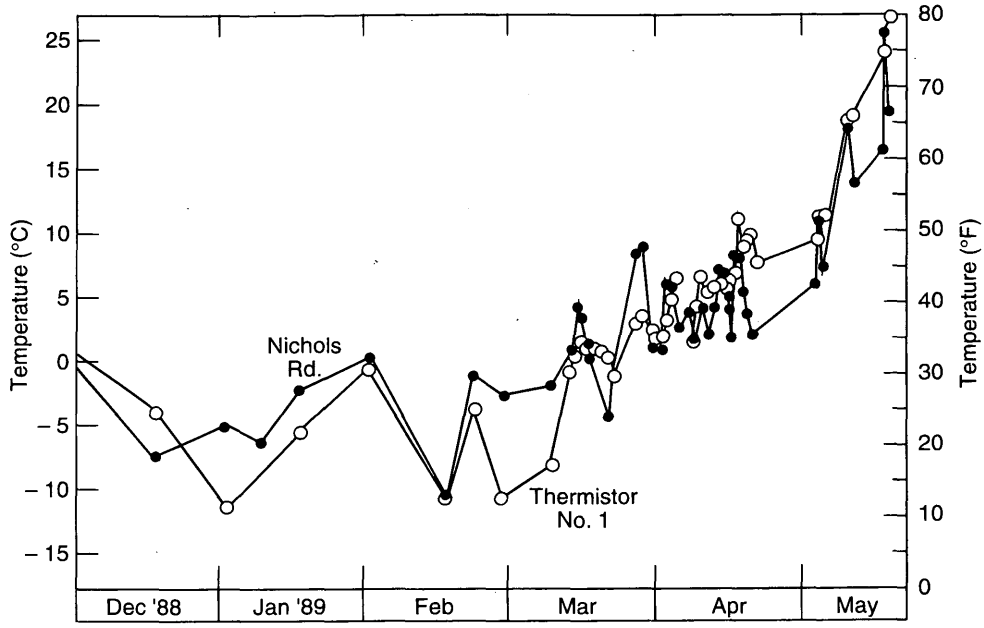

FIGURE 10 Base course temperatures for insulated and noninsulated pavements.

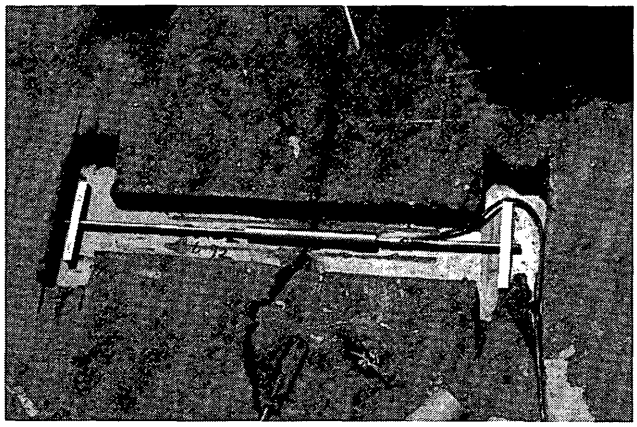

FIGURE 11 Linear-motion potentiometer installed across crack.

The two ends of the runway were noticeably weaker than the middle and test sections. Furthermore, they exhibit more variation in pavement strength during spring thaw. These two nondestructive testing observations agree with the previously discussed runway performance observations. The ends of the runway were particularly wet during construction. All other factors being equal, this typically indicates a weaker pavement. In addition, the middle of the runway was undercut deeper and, as a consequence, has a thicker subbase than do the ends. Finally, as discussed earlier, the ends of the runway exhibit substantial absolute and differential frost heave, possibly because of insulation damage and discontinuities. This heaving indicates frost penetration into the subgrade (observed), which in turn implies subgrade weakening during spring thaw.

SURFACE ICING

The Army and Air Force (5) require insulation to be placed at a minimum depth of 457 mm (18 in.) beneath the pavement surface to minimize surface icing. Differential icing is not an uncommon phenomenon at transitions between insulated and noninsulated pavements. However, there are no such transitions in the AC surfaced pavements at Newton Field. (Paved insulated test sections transition into a noninsulated gravel road.) The range in depth to the insulating layer could promote differential icing on the runway surface under certain environmental conditions. Visual observations were limited to those made by CRREL personnel, the town snowplow operator, and local pilots. Although surface icing was observed by CRREL personnel on several occasions, differential surface icing was not observed. Surface temperature sensors showed that the insulated pavement was generally colder than the noninsulated pavement throughout the freezing season.

CONCLUSIONS

The four insulated pavement test sections performed well. Frost penetration into the subgrade beneath insulation panels 51 mm (2 in.) and 76 mm (3 in.) thick was minimal, and frost heave was similar to that of a conventional (control section) pavement at Nichols Road. Field results for the insulated pavement test sections conformed well to those predicted by the design thickness.

Why did the insulated runway pavement perform so poorly when the insulated pavement test sections (one of which was nearly identical in design to the runway) performed so well? A variety of investigative methods was used to confirm suspicions that frost penetration and localized frost heave could be at least partially attributed to

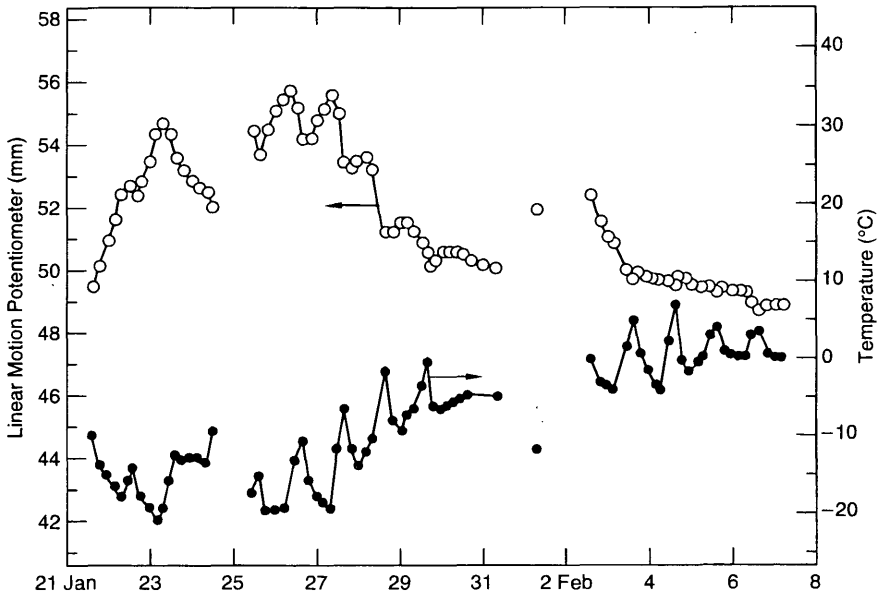

FIGURE 12 Linear-motion potentiometer data.

insulation irregularities at the ends of the runway: (a) hand-excavated trenches and holes alongside the runway revealed cracked insulation panels and gaps of up to 64 mm (2.5 in.) between panels, (b) mechanical excavation during runway repair exposed damaged and overlapping insulation panels, (c) infrared photography showed irregularities in pavement surface temperatures, and (d) ground-penetrating radar investigations revealed that the depth to the insulation/subbase interface ranged from 127 to 610 mm (5 to 24 in.).

The insulated pavements did not exhibit the strength of noninsulated pavements. In contrast, however, the insulated pavement test sections did not exhibit significant strength loss because frost never penetrated into the subgrade and, as a consequence, the subgrade did not undergo thaw weakening. The ends of the runway, however, did exhibit thaw weakening. This is probably because damaged insulation and insulation discontinuities allowed deeper subgrade frost penetration, as was shown by frost heaving.

As indicated by differences in performance between the ends of the runway and the center, the thickness of the granular subbase appears to be a critical component contributing to pavement performance. The granular base, particularly in wet areas, provides a firm working platform for panel placement and subsequent construction.

The runway pavement exhibits several severe transverse cracks up to 229 mm (9 in.) wide. Periodic measurements of the asphalt slabs between adjacent cracks show excessive asphalt shrinkage with aging. In addition, thermal stress tests showed that the asphalt was susceptible to thermal cracking at a considerably higher temperature than is typical for asphalt mixtures of that grade. It is suspected that cracking is primarily the fault of the AC but is perhaps compounded by the insulation. Because insulated pavements undergo greater temperature fluctuations than do noninsulated pavements, it is possible that the slightly lower temperatures could induce cracking. However, no other instances of extensive cracking in thermally insulated pavements were found in the literature.

ACKNOWLEDGMENTS

The authors express their appreciation to FAA; Marcia Van Camp of Jackman, Maine; Fred Boyce of Bangor, Maine; Dave Walker Cards of Dixfield, Maine; and Dale Bull, Dick Guyer, Chris Berini, Jack Bayer, Wendy Allen, Kris Rezendes, Rosa Affleck, the editing staff, and many others at CRREL who assisted with various aspects of instrumentation installation, testing, and paper preparation.

REFERENCES

1. Prue, F., and M. Morgan. *Soils Investigation for Moose River Project F-033-2(1).* Internal report. Maine Department of Transportation, 1970.
2. Kestler, M., and R. Berg. *Use of Insulation for Frost Prevention at Jackman Airport, Maine: 1986–1987 Winter.* CRREL Report 91-1. U.S. Army Cold Regions Research and Engineering Laboratory, Hanover, N.H., 1991.
3. Kestler, M., and R. Berg. *Performance of insulation pavements at Newton Field, Jackman, Maine.* CRREL Report 92-9. U.S. Army Cold Regions Research and Engineering Laboratory, Hanover, N.H., 1992.
4. Allen, W. L. Observations of the Thermal Regime Surrounding a Longitudinal Edge Drain in a Deep Frost Area. *Proc., Cold Regions Specialty Conference,* Hanover, N. H., Feb. 1991, p. 164.
5. *Pavement Design for Seasonal Frost Conditions.* Ch. 6, U.S. Departments of the Army and Air Force. TM-518-2/AFM 88-6, Jan. 1985.
6. Martinson, C. R. *Radar Profiling of Newton Airfield in Jackman, Maine.* Special report 89-4. U.S. Army Cold Regions Research and Engineering Laboratory, 1989.
7. Santosa, W., N. Garrick, and J. Stephens. The Effect of Air Voids on Laboratory Aging of Asphalt Mixtures. Presented at 71st Meeting of the Transportation Research Board., Washington, D.C., 1992.
8. Janoo, V. C., T. S. Vinson, R. Haas, and J. Bayer Jr. Test Methods To Characterize Low Temperature Cracking. *Proc., 4th Workshop on Paving in Cold Areas,* Sapporo, Hokkaido, Japan, Sept. 4–6, 1994.
9. Alexander, D. WESDEF. U.S. Army Corps of Engineers, Waterways Experiment Station, Vicksburg, Miss., 1988.
10. Irwin, L. MODCOMP. Cornell University, Local Roads Program, Ithaca, N.Y., 1986.

Publication of this paper sponsored by Committee on Frost Action.

Long-Term Evaluations of Insulated Roads and Airfields in Alaska

DAVID C. ESCH

The use of expanded plastic foam insulations in Alaska to reduce freezing and thawing of soils beneath road and airfield embankments began in 1968 with the installation of polystyrene and polyurethane foam products for frost-heave control. This was followed in 1969 by the first insulated roadway section over permafrost in North America, at Chitina, and by the first insulated airfield runway, at Kotzebue. Since then, many roadway sections, totaling more than 45 lane-km, have been insulated by the Alaska Department of Transportation, as have four additional airports. Materials used have been primarily extruded-expanded polystyrene foam, with one installation of foamed-in-place polyurethane and three of molded polystyrene beadboard. Evaluations of the long-term performance of these installations have included periodic sampling and testing of the insulations. On the basis of these observations, foamed-in-place polyurethane insulation was rejected for subgrade insulation uses, whereas extruded polystyrene was preferred based on its superior performance and longevity. Molded polystyrene beadboard has given acceptable performance, but it must be installed at a thickness 30 to 50 percent greater than that of the extruded polystyrenes to provide comparable thermal performance. Comparisons are given between insulated and noninsulated embankment behavior on permafrost and between measured and calculated late summer thaw depths. The modified Berggren calculation method, which provided reasonable 1-year thaw estimates, was used for the comparisons.

The Alaska Department of Highways constructed its first experimental installation of expanded plastic foams for frost-heave control in 1967 at a site 18 km south of Anchorage. This was followed in 1969 by construction of both the first insulated roadway section over permafrost in North America, at a site near Chitina, and the first insulated airfield runway, at Kotzebue (*1*). Since that time, many additional roadway sections on permafrost have been insulated by the Alaska Department of Transportation, along with six airport runways. Applications of insulation for frost-heave control have been numerous, particularly in the Anchorage–Wasilla area where various glacial deposits can result in severe differential frost heaving. Insulation layers are also frequently used beneath roadway crossings of buried water and sewer lines and subdrain systems. Materials used for subgrade insulations have been primarily extruded-expanded polystyrene foam (Styrofoam HI-35, HI-40, or HI-60 and UCI Foamular 400), with several installation of polyurethane foam and six of molded polystyrene beadboard. Note that for these products the final number designation indicates compressive strength in pounds per square inch (psi) for Styrofoam and in psi × 10 for Foamular (1 psi = 6.89 kPa). Brand names are mentioned herein only to indicate the actual products installed and evaluated. The manufacturing processes for foamed insulation products of the molded and extruded types may differ among manufacturers. It is not known whether the competing products with similar compressive strengths and dry densities will be similar to those evaluated in this study. Current AASHTO specifications for polystyrene foam insulations do not require conductivity testing and lack procedures for evaluating the long-term resistance of these materials to moisture absorption.

To evaluate the long-term thermal performance of these installations, extensive air and ground temperature monitoring instrumentation, consisting of thermocouples, thermistors, and chart recorders were installed at six sites (*2*). Temperatures have been monitored monthly or semiannually at the different sites, the longest period being 25 years at the Chitina permafrost site. In September of 1984 and 1994 insulation samples were taken from selected road and airfield sites and tested for thermal conductivity and moisture absorption to analyze their long-term performance. At the airfield insulation sites, soil moisture contents and thaw depths were also measured. Thaw depth calculations were then made by the modified Berggren calculation method to compare predicted and actual thaw depths.

Roadway and airfield insulation sites constructed by the Alaska Department of Highways and the Alaska Department of Transportation to control frost heaving or permafrost thaw settlements are listed in Tables 1 and 2.

GENERAL SITE PERFORMANCE OBSERVATIONS

Frost Heave Sites

The first sites insulated in 1967 for frost-heave control were monitored for 3 years, and their performance was documented (*3*). The basic conclusions of this study were that the foamed-in-place polyurethane insulation used was not adequately resistant to water absorption, even when coated top and bottom with a thick layer of hot asphalt. In fact the polyurethane absorbed as much as 70 percent water by volume in some test applications. Therefore, this type of insulation was not allowed in future roadway insulation applications. The extruded polystyrene, however, performed very well and was recommended for future frost-heave control applications. For these instrumented sites, the modified Berggren calculation method predicted freeze depths beneath the insulation with reasonable accuracy, with a tendency to overpredict these depths slightly for thick insulation layers. This study also demonstrated that the full extent of the frost-heave problem area must be known before the length of the insulation section is designed, to avoid creating heave bumps at the ends of the insulation. On the basis of data from these sites a composite thermal design approach is recommended, with specified thicknesses of non–frost-susceptible gravels or sands placed above and below the insulation layer. By allowing freezing to penetrate into gravel fill placed beneath the insulation, the most economical

Alaska Department of Transportation and Public Facilities, 3132 Channel Drive, Juneau, Alaska 99810.

TABLE 1 Anchorage Area and Parks Highway Frost-Heave Control Sites

Year Built	Site or Route	Specific Location	Insulation Type	Thickness cm	Cover Depth cm	Length Lanes km
1968	Seward Hwy	Potter	FIP Urethane	5	46	0.058
1968	Seward Hwy	Potter	Styrofoam HI	7.5	46	0.068
1970	Parks Hwy	MP 75.0	Styrofoam HI	10	46	0.089
1970	Parks Hwy	MP 84.2	Styrofoam HI	10	46	0.156
1971	New Seward	Tudor-East	Styrofoam HI	7.5	61	1.464
1971	Talketna Spur	MP 9.3	Styrofoam HI	7.5	46	0.274
1971	Parks Hwy	MP 117.0	Styrofoam HI	10	46	1.249
1975	Minnesota Drive	15 ST. Jct.	Styrofoam HI	10	68	0.122
1975	New Seward	Tudor-East	Styrofoam SM	7.5	61	2.109
1978	Parks Hwy	MP 36.7	Styrofoam HI	10	152	0.177
1981	Minnesota Dr.	At Dimond	Sty. Beadboard	10	61	1.224
1983	Northern Lights	Goose Lake	Styrofoam, HI	10	112	1.341
1984	Minnesota Ext.	At Dimond	Sty. Beadboard	10	91	3.767
1985	A-Street	@ 23 St.	Styrofoam HI	10	119	0.488
1985	A-Street	@ 15 St.	Styrofoam HI	10	119	0.853
1984	Parks Hwy	Panguingue	Styrofoam HI	10	61	0.061
1986	Parks Hwy	MP 293-297	Foamular 400	5&10	107	4.266

design can be achieved. A depth of cover of at least 45 cm of gravel and pavement above the insulation is recommended to provide tolerable wheel load stresses on the insulation.

The problem of differential frost formation on the road surface in insulated areas is lessened by increased depth of cover over the insulation. As shown by Table 1, the depth of cover over frost-heave insulation has varied from 45 cm to 1.2 m. Surface frost forms more quickly on bridge decks and above insulated areas than on normal road structures. The resulting decreases in traction have been treated by installation of Plus-Ride process rubber-modified asphalt pavement surfacing above the insulated areas at the A-Street, New Seward at Tudor, and Canyon Creek sites. The benefits of this pavement type have been investigated and reported elsewhere (*4*).

Permafrost Sites

The Chitina insulated road site, constructed in 1969 over relatively warm (−1°C) permafrost, has performed reasonably well, with almost total annual refreezing of the summer thaw zones beneath the roadway and a long-term subroadway permafrost temperature of −0.1°C to −0.3°C. However, the gravel sideslopes of the embankment, which are insulated by snow in winter and exposed to direct sunlight in summer, have caused progressively deeper annual thawing; the increases in thaw depth average approximately 8 cm per year into the permafrost beneath the slopes. This has resulted in progressive slope sloughing and cracking in the shoulder areas (*5*). By comparison, the adjacent uninsulated roadway areas have continued to settle annually at a rate of 3 to 6 cm per year. The surface of this experimental roadway section was left as gravel for the first 2 years. It was then topped with a cold-road–mixed pavement in 1971 to evaluate the effects of the darker asphalt surfacing on thaw into the underlying permafrost. It was returned to gravel surfacing between 1975 and 1987 and finally paved with hot-mixed asphalt in 1988. Settlements of the embankment continued throughout these periods, and measured settlements of the outer edges of the travel lanes are reported in Figure 1. These measurements demonstrate the relatively improved performance of the insulated sections but the lack of overall stability even after 20 years. Sideslope thawing movements have been similar in insulated and uninsulated areas, and some settlements caused by stress-related creep of the warm permafrost foundation soils continue to be noted in all areas of this roadway.

Cross-section plots of one side of this road embankment after 20 years of monitoring of settlements and thaw depths are shown in Figures 1–4, which include data for the four different embankment types at the Chitina site. These figures demonstrate the continually deepening thaw zones that result from the warming influence of the road embankment.

The performance of most other insulated permafrost roadway sites has been similar to that at Chitina. Embankments do not reach full annual refreezing of soils beneath the insulated roadway areas and progressively faster and deeper annual thawing and related movements of the sideslope areas. The insulated road sections

TABLE 2 Permafrost Highway Insulation Sites in Alaska

Year Built	Site or Route	Specific Location	Insulation Brand & Type	Thickness cm	Cover Depth cm	Length Lanes km
Insulated Roadways on Permafrost for Thaw Control:						
1969	Chitina N.	MP 27	Styrofoam HI	10	152	0.113
1973	Parks Hwy	MP 231.8	Styrofoam HI	10	137	0.274
1974	Parks Hwy	Alder Ck. S.	Styrofoam HI	10	137	0.201
1974	Parks Hwy	Alder Ck. N.	Styrofoam Hl	10	305	0.116
1979	Farmer's Loop	Fairhill Rd.	Insulfoam BB	10	122	0.124
1985	Canyon Creek	Rich. MP 299	Styrofoam HI	7.6	84	1.708
1986	Edgerton Hwy	MP 1.3-7.0	Styrofoam HI	5	107	3.349
1989	Alaska Hwy	Dot Lake	Insulfoam 2 BB	10	102	1.708
1990	Alaska Hwy	MP 1285-1303	Styrofoam HI	10	102	14.39
1991	Rich. Hwy	MP 80.2	Styrofoam HI	10	91	0.111
1991	Davis Road	Fairbanks	UCI Foamular	10	102	1.010
1993	Tok Cutoff	MP 59	Insulfoam 2 BB	10	473	1.915
1994	Alaska Hwy	Mp 1380 N.	Insulfoam 2 BB	10	102	2.027
Insulated Airfield Runways on Permafrost:						
1969	Kotzebue Airport		Styrofoam HI-35	10	107	.580
1981	Buckland Airport		Styrofoam HI-35	15	91	.732
1981	Deering Airport		Styrofoam HI-35	5	76	.824
1985	Nunapitchuk Airport		Styrofoam HI-60	15	76	.839
1985	Deadhorse Taxiway B		Styrofoam HI-60	10	142	.110
1988	Golovin Airport		Styrofoam HI-40	10	91	.701
1990	Selawik Airport		Styrofoam HI-40	10	91	1.333

typically are in climates with mean annual air temperatures of −3°C to −5°C, where the permafrost is best described as discontinuous. All roadway sections monitored have continued to exhibit annually increasing settlements over time and are still deforming after as long as 25 years. The use of insulation has typically reduced settlements to half of those of the uninsulated adjacent road segments. By comparison, airfield insulation sites typically are in areas with lower air temperatures, and full annual refreezing of the seasonal thaw zones is more common. For these sites the insulated embankment performance has been better than that of the roadways, primarily because of the colder local climates.

Cover depths used over permafrost insulation layers tend to be greater than for frost-heave control, primarily because of construction traffic considerations. Permafrost insulation has generally been designed based on borings and installed during embankment construction. The heavy construction equipment used requires care to avoid crushing. By contrast, frost-heave insulation sections have nearly always been designed as corrective measures for heaves on existing roads, where minimizing the depth of excavation is of major concern. As such they have proved very successful.

FIELD SAMPLING AND INSULATION TESTING PROGRAMS

Insulation sampling and testing to measure moisture absorption and compression under field conditions has been done at various times and locations to verify the field performance of the buried insulation layers. Results are discussed below by insulation type.

Polyurethane Foams

The most extensive testing of polyurethane road insulation samples was in September 1972 at an Arco Chemical road test site near Prudhoe Bay. At that location urethane foam board samples taken from beneath a permafrost area roadway after 2 years of exposure on a wet tundra foundation demonstrated moisture contents as high as 30 percent by volume or 1000 percent by weight of the dry foam. Unfortunately, data from this polyurethane field test and sampling program were never published because of the unexpectedly poor insulation performance. This investigation was followed in March 1979 by a

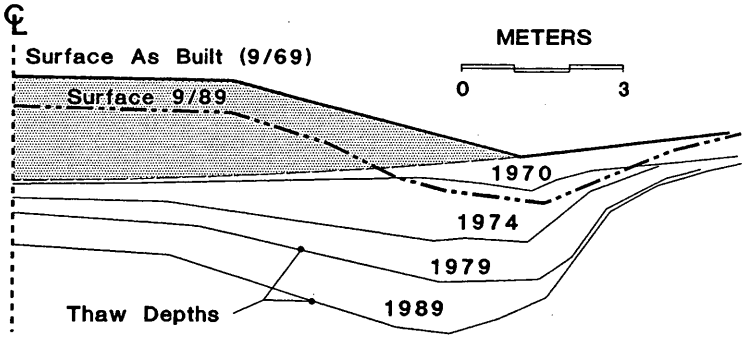

FIGURE 1 Cross section of normal noninsulated embankment over vegetation and brush layers (maximum thaw depths after 1, 5, 10, and 20 years and settlements after 20 years).

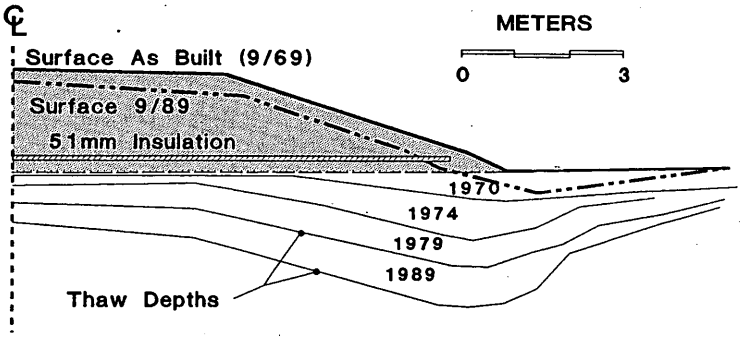

FIGURE 2 Embankment constructed as in Figure 1 except for addition of 51-mm insulation layer at 0.4 m above original ground surface (maximum thaw depths and 20-year surface settlements).

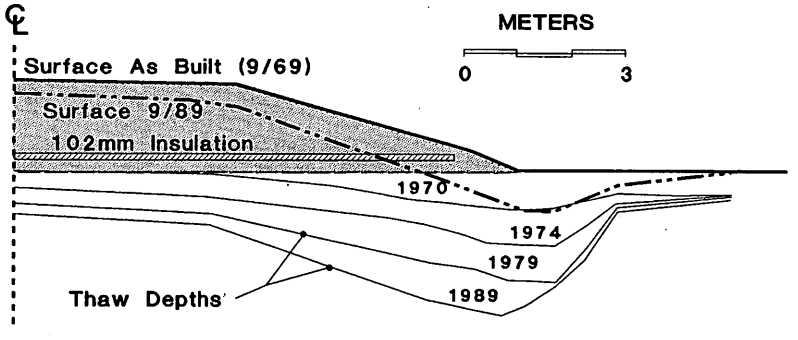

FIGURE 3 Embankment constructed with 102-mm insulation layer at 0.4 m above original ground surface (maximum thaw depths and 20-year surface settlements).

foamed-in-place urethane insulation sampling program at the Potter frost-heave insulation test site located near Anchorage (*3*).

At Potter several samples were obtained from the wheelpath areas after 12 years of insulation exposure to traffic and environment. In addition, two samples were obtained from an extension of the urethane insulated area placed in 1974. Six representative samples of the 1967 insulation were tested for absorbed moisture and had total moisture contents, calculated as percent water by volume, ranging from 31 to 72.0 percent.

Thickness measurements were made in many locations that were believed to be within the original (1968) 5-cm insulation area, and an average thickness of approximately 2.3 cm was noted. No foam

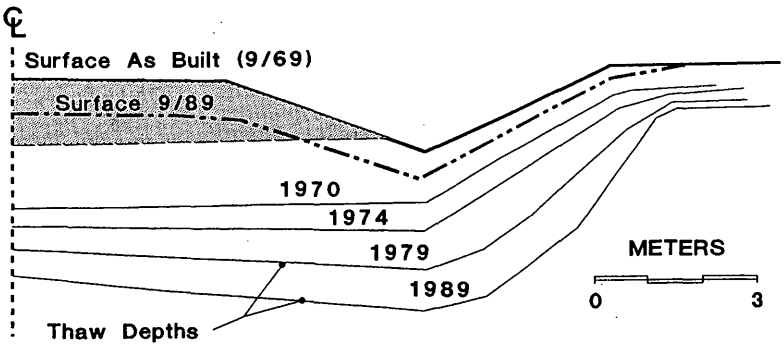

FIGURE 4 Embankment constructed in cut section where all surface vegetation is removed (maximum thaw depths and 20-year settlements).

thicker than 3 cm could be found. Exact thickness comparisons are not possible because of the somewhat random thickness obtained from in-place foaming of urethanes, but measurements at the time of placement indicated an average thickness very close to 2.5 cm. Many areas of thickness as low as 12 mm were noted, and foam in these areas was generally nearly saturated. This foamed-in-place urethane had an average compressive strength of 217 kPa when placed in 1967. All data indicate that this foam insulation failed by moisture absorption and compression under field service. By contrast to the generally compressed and relatively wet state of the 1968 urethane foam, the samples from the 1974 extension appeared to be in excellent condition, offering hope that polyurethane foams may perform reasonably well under direct soil burial conditions. Two samples of this insulation had dry densities of 32 and 34 kg/m, absorbed water contents of 1.3 and 1.0 percent by volume, and average compressive strengths of 194 and 181 kPa at 5 percent strain. The strength and moisture properties of this product appeared satisfactory for acceptable performance in direct burial. Unfortunately, this entire test site was excavated in 1979, so the long-term performance of this material could not be followed. The reasons could not be determined for the good performance of this foam compared with the failures of the two urethanes previously mentioned.

Polystyrene Foams

Field samples of in-service polystyrene subgrade insulations were taken in September 1984 from various road and airfield sites in Alaska. Repeat sampling was again done in 1994 at three roadway sites. Samples were typically taken from hand-dug test pits located at the edge of the asphalt pavement or near the toe of the embankment slope. All samples were sealed in zip-lock bags and subsequently tested for moisture absorption and wet thermal conductivity by the thermistor bead technique detailed in a work by Atkins (*6*) in the 1984 sampling program and by the more accepted "guarded-hot-plate" method in 1994.

In the thermistor method a single thermistor bead, approximately 1.0 mm in diameter, is inserted into the insulation board, and a controlled electrical current is applied to cause resistance heating of the thermistor. Periodic readings are taken of temperature rise versus time, from which the thermal conductivity can be calculated. Multiple readings at various depths within a foam sample are used to produce a profile of conductivity versus depth, from which an average value is calculated. Results are consistent and agree well with the more precise laboratory guarded-hot-plate method.

Two of the study sites, the Fairbanks-area Fairhill Access Road, constructed in 1979, and Anchorage's Minnesota Extension—Phase I, constructed in 1981, contain white molded polystyrene with a compressive strength greater than 200 kPa. This product is molded into boards of the desired thickness in a two-step process starting with the preexpansion of foam beads and is commonly called a polystyrene beadboard. The remaining sites all were insulated with polystyrene insulation of the type foamed and formed in a single extrusion process in the desired thicknesses and is termed extruded polystyrene. Results of all testing of the recovered insulation samples are included in Table 3, and averages for each site are plotted on Figure 5 to show relationships between moisture absorbed and thermal conductivity measured on wet insulations. Initial test results on new, dry polystyrene foam products at 22°C average approximately 0.029 and 0.032 W/m°C for the extruded (type E) and molded beadboard (type BB) insulation products.

As shown in Figure 5, the relationships between moisture content and thermal conductivity for extruded and molded foam boards were found to be in excellent agreement with other reported data from laboratory tests at higher moisture contents (*7,8*). All samples were within 5 percent of the original nominal thickness, indicating that compression and creep with time has not been a problem. The extruded Styrofoam insulation board, sampled in 1984 from six sites with a maximum age of 15 years and averaging 9.5 years of service, had an average moisture content of 1.16 percent by volume. Thermal conductivities (k factors, or k) of these samples averaged 0.032 W/m°C at 22°F. Maximums were a moisture of 2.4 percent and a k of 0.036. By comparison the molded beadboard samples, from sites 3 and 5 years old, had an average moisture of 2.9 percent and an average k of 0.043. Maximum values for the beadboard were 8.7 percent moisture and a k of 0.60. When analyzed by a standard statistical approach, the long-term minimum k factors expected at the 95 percent confidence level are 0.037 for extruded polystyrene foam and 0.055 for high-strength molded polystyrene beadboard. This results in a thickness ratio for equivalent performance of 1.5 cm of molded polystyrene foam to 1.0 cm of extruded polystyrene foam. If this ratio is based on average instead of minimum insulation values, a thickness ratio of 1.36 to 1 is indicated; however, a ratio this low would be unfair to extruded foams, which are more consistent and better able to resist moisture gains and R-value losses with time in service.

TABLE 3 Polystyrene Insulation Test Results at 22°C

Site	Layer	Thickness (cm)	Dry Foam Density (kg/m3)	Insulation Type	Water by Volume (%)	K avg. (W/m C)	Year Placed
1984 Samples and Test Data:							
Kotzebue	Top	5	38.2	E	2.38	.031	1969
Kotzebue	Bottom	5	34.2	E	0.89	.028	1969
Buckland	Top	7.5	36.2	E	0.41	.029	1981
Buckland	Bottom	7.5	33.6	E	0.23	.030	1981
Deering	Single	5	34.6	E	1.37	.029	1981
Chitina	Top	5	40.9	E	0.71	.034	1969
Chitina	Bottom	5	42.1	E	0.88	.037	1969
Chitina	Single	5	42.1	E	1.54	.031	1969
Bonanza Creek	Single	5	35.8	E	1.48	.036	1974
Bonanza Creek	Single	5	45.3	E	2.38	.036	1974
Fairhill	Single	10	39.0	BB	1.18	.040	1979
Fairhill	Top	5	34.7	E	0.50	.032	1979
Fairhill	Bottom	5	36.3	E	0.20	.031	1979
Fairhill	Single	10	47.7	B	1.48	.042	1979
Minnesota Dr.	Top	5	39.4	BB	5.88	.052	1981
Minnesota Dr.	Bottom	5	43.4	BB	2.90	.038	1981
Geneva Woods	Single	7.5	---	E	0.64	---	1970
Geneva Woods	Single	7.5	---	E	0.53	---	1970
1994 Samples and Test Data:							
Chitina	Top	5	43.8	E	1.36	.034	1969
Chitina	Bottom	5	43.0	E	1.72	.035	1969
Fairhill	Single	10	39.2	BB	5.15	.046	1979
Bonanza Creek	Single	5	47.4	E	3.10	.038	1974

Type E = Extruded Expanded Foam Type BB = Molded and Cut Beadboard Foam

THAW DEPTHS: INSULATED AIRFIELDS ON PERMAFROST

Observations of the thaw depths were made between September 4 and 6, 1984, at the three insulated airfields investigated in this study, and soil moisture contents were measured at intervals of depth to permit comparisons between thaw depth calculation methods and actual field values.

Thaw depth calculations were made for each of these runways, using the actual measured soil and insulation properties, the modified Berggren calculation method as programmed elsewhere (*9*), the recorded Kotzebue air thawing index of +820°C-days, and surface *n* factors (ratios of surface to air thawing indexes) of 1.70 for Kotzebue (paved) and 1.30 for the other (unpaved) sites. These calculations overpredicted the thaw depths by 6 to 15 cm, as shown in Table 4, indicating that this calculation method is slightly conservative for designing insulation layers on cold ($T < -1$°C) permafrost.

SUMMARY

Since 1967 the Alaska Department of Transportation has insulated more than 20 lane-kilometers of roadways and 2,970 m of airfield runway to control frost heaving and permafrost thawing. Insulation materials used have included foamed-in-place polyurethanes, molded polystyrene beadboard, and extruded-expanded polystyrene foam boards. Polyurethane foams have varied greatly in field performance, with high moisture absorption and compression failure noted at two of three sample locations. For this reason polyurethane foams are not now accepted by the Alaska Department of Transportation for use beneath roads or airfields. On the basis of observations from field sampling of the insulations after various exposure periods, the superiority of extruded-expanded polystyrene foam is evident after as much as 25 years in service. In fact, all the extruded samples taken in 1994 were removed from locations below the water table and had been immersed for periods as long as 10 years, yet they showed excellent resistance to moisture absorption.

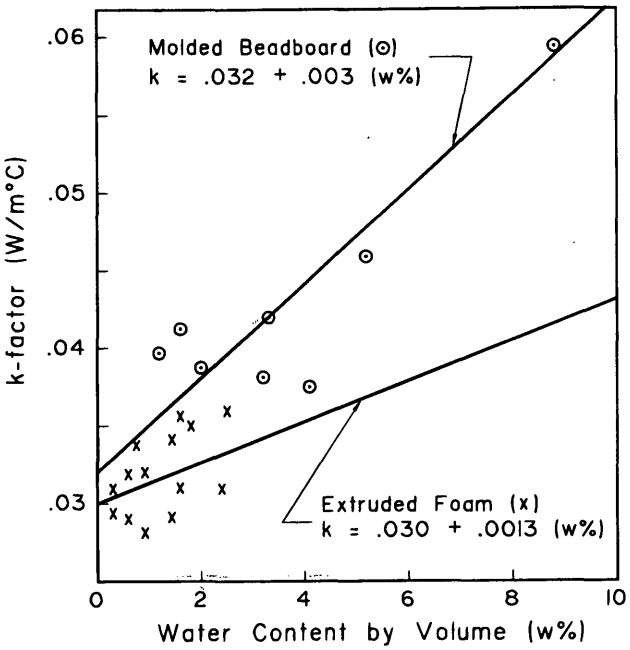

FIGURE 5 Moisture contents and thermal conductivities at 22°C of in-service polystyrene insulation samples from roads and airfields in Alaska.

Molded polystyrene beadboard products, evaluated after 3 to 15 years of service, were somewhat less resistant to moisture absorption in the subroadway environment, although they had not been similarly immersed. To provide equivalent long-term thermal performance under soil burial conditions, beadboard insulation thicknesses should be 30 to 50 percent greater than extruded foam thicknesses. It should be noted that the insulation sampling locations used were not located beneath the pavement or in areas exposed to cyclic pressures from wheel loadings. Information from Norway suggests that in some instances moisture-content increases in insulations may be greater beneath paved surfaces than beneath unpaved shoulders and that moisture levels in insulations may vary seasonally to some extent. Data on moisture contents in polystyrene roof insulations show that, when temperatures are high, temperature differences between the top and the bottom of an insulation layer are very high and moisture is present, the moisture gain over time is greatly increased. When insulation layers are buried in soil at depths great enough to avoid cyclic tire pressure effects and high temperature gradients across the insulation layer, moisture pickup will be very slow, even if the insulation layer is submerged.

On the basis of the data obtained over the course of this study, the functional design life of extruded foams installed beneath roads and airfields is projected to be much greater than 25 years. Increases in thermal conductivity of insulations as the result of moisture absorption after 15 to 25 years of field exposure averaged only 10 to 22 percent for extruded polystyrenes and 34 to 44 percent for molded polystyrene beadboard products.

TABLE 4 Measured and Predicted (Based on Modified Berggren Calculation Method) Total Thaw Depths for Insulated Airfields on Permafrost

			Insulation		Thaw Depths	
Site	Thawing Index	Surface	Depth	Thickness	Measured	Predicted
	(C-Days)	n-Factor	(m)	(cm)	(m)	(m)
Kotzebue	820	1.70	1.07	10	1.43	1.50
Buckland	820	1.30	1.01	15	1.16	1.31
Deering	820	1.30	0.70	5	0.85	0.98

REFERENCES

1. Esch, D. C., and J. J. Rhode. Kotzebue Airport Runway, Insulation over Permafrost. *Proc., 2nd International Symposium on Cold Regions Engineering,* University of Alaska, Fairbanks, 1977, pp. 44–61.
2. Hulsey, J. L. *Permafrost Database, Final Report.* Research Report SPR-UAF-92-10. Alaska Department of Transportation and Public Facilities, Juneau, 1994.
3. Esch, D.C. *Subgrade Insulation for Frost Heave Control.* Research Report. Alaska Department of Transportation and Public Facilities, Juneau, 1971.
4. Esch, D.C. Construction and Benefits of Rubber-Modified Asphalt Pavements. In *Transportation Research Record 860,* TRB, National Research Council, Washington, D.C., 1982, pp. 5–13.
5. Esch, D.C. 20 Year Performance History of First Insulated Roadway on Permafrost in Alaska. *Proc., Permafrost—6th International Conference,* Beijing, China, 1993, pp. 164–74.
6. Atkins, R. T. *In-Situ Thermal Conductivity Measurements.* Report FHWA-AK-RD-84-06. Alaska Department of Transportation and Public Facilities, Juneau, 1983.
7. Dechow, F. J., and K. A. Epstein. *Laboratory and Field Investigations of Moisture Absorption and Its Effect on Thermal Performance of Various Insulations.* STP 660, 1982, ASTM, pp. 234–260.
8. McFadden, T. Effects of Moisture on Extruded Polystyrene Insulation. *Proc., ASCE Cold Regions Specialty Conference,* Anchorage, Alaska, 1986.
9. Braley, W. A. *A Personal Computer Solution to the Modified Berggren Equation.* Report AK-RD-85-19. Alaska Department of Transportation and Public Facilities, Juneau, 1984.

The contents of this report reflect the views of the author, who is responsible for the facts and the accuracy of the data presented herein. The contents do not necessarily reflect the official view or policies of the Alaska Department of Transportation and Public Facilities or of FHWA, which provided the funding.

Publication of this paper sponsored by Committee on Frost Action.

Use of Alternative Materials in Pavement Frost Protection: Material Characteristics and Performance Modeling

GUY DORÉ, JEAN MARIE KONRAD, MARIUS ROY, AND NELSON RIOUX

With freezing indexes ranging from 1,200°C to over 2,000°C day and frost penetration reaching 3 mm under pavement surface, frost action has always been a major concern for pavement engineers in Québec, Canada. The province's ministry of transportation has thus undertaken a study on frost action in pavements with two main objectives. The first is to revisit the whole approach of pavement design in severe frost conditions and develop a rational pavement design method to mitigate efficiently the effects of frost action. The second objective is to evaluate alternative techniques that might protect pavement against the detrimental effects of frost action. To gather the data needed to evaluate the performance of different pavement designs in support of those objectives, a specific pavement monitoring program was developed. The modeling and the laboratory work carried out to define the characteristics of the main test site constructed during summer 1994 are described. Mechanical and thermal simulations using ELSYM 5 and a finite element model developed at Laval University have led to an optimal pavement structure for the test site. The benefit of thermal insulation was weighed against the detrimental effect of incorporating a soft layer within the pavement structure to determine the best combination of thickness and depth for the insulation layer. Alternative insulation materials were identified and characterized through a comprehensive laboratory testing program. Based on criteria such as local availability, mechanical and thermal performance, cost, and environmental considerations, three promising materials were selected for the field testing. Saw dust, tire chips, and plastic crumbs were tested and compared with conventional insulated (expanded and extruded polystyrene) and uninsulated pavements.

Frost action on pavements has always been a major concern for engineers in the province of Québec. Recent surveys show that between 10 and 20 percent of the 30 000-km provincial network exhibit distresses associated with frost action. Moreover, the rate of degradation on these affected pavements in terms of change in roughness with time (]IRI/year) is, on average, twice that of non-affected pavements. Based on these numbers, efforts to correct the frost problem in the provincial network can be estimated at more than $100 million (Canadian), excluding additional construction costs to build frost-resistant pavements, user costs, and indirect costs such as those related to the decline in transportation productivity during the period when spring load restrictions are in place.

It is generally believed that more can be done to better understand and control pavement performance in severe frost conditions. Existing methods, typically based on empirical models if not simply on rules of thumb, cannot support performance prediction and are not sensitive to specific site conditions. Moreover, it is believed that methods that take only thaw weakening into consideration cannot properly address frost problem in Québec's severe climatic context.

The Québec ministry of transportation has undertaken a major study with the following two objectives:

- Revisit the whole approach to pavement design in frost conditions and develop a rational method that specifically deals with freezing and thawing of pavement structures; and
- Review and assess the performance of all mitigation methods with a special emphasis on the evaluation of alternative insulation materials such as plastic, rubber, and wood residues.

A work plan was prepared, illustrated in Figure 1, which presents the concept of the proposed design approach (white boxes) and the research required to achieve the objectives (grey boxes).

The project is planned over a 4-year period. Until now, most of the efforts have been directed toward the preparation of the main test site. The work done includes site selection, mechanical and thermal simulation, design of pavement structures, laboratory characterization of alternative insulation materials, and the development of an instrumentation plan.

TEST SITE SELECTION

To achieve the maximum benefit from the large investment required for pavement monitoring, test sites must be rigorously selected and designed. Guidelines for site selection were based on the international state of knowledge on pavement monitoring and the experience of the Strategic Highway Research Program (SHRP).

The selected site, in St. Martyrs Canadiens, 50 km south of Victoriaville, involved the rehabilitation of a provincial road affected by frost action. Moderately aggressive climatic and traffic conditions characterized the site, where one control section and four sections insulated with different materials were built and instrumented.

The design of the test sections was based on mechanistic modeling and on a specific program of laboratory testing on potential insulation materials.

MODELING OF ST. MARTYRS CANADIENS TEST SITE

The two main objectives of the test site were to provide high quality, real-time information on pavement response and performance in frost conditions, and assess the performance of alternative frost protection

G. Doré and N. Rioux, Québec Ministry of Transportation, 200 Dorchester Sud, 3rd Floor, Québec, Qc., Canada G1K 7P4. J. M. Konrad and M. Roy, Civil Engineering Department, Laval University, Québec, Qc., Canada G1K 7P4.

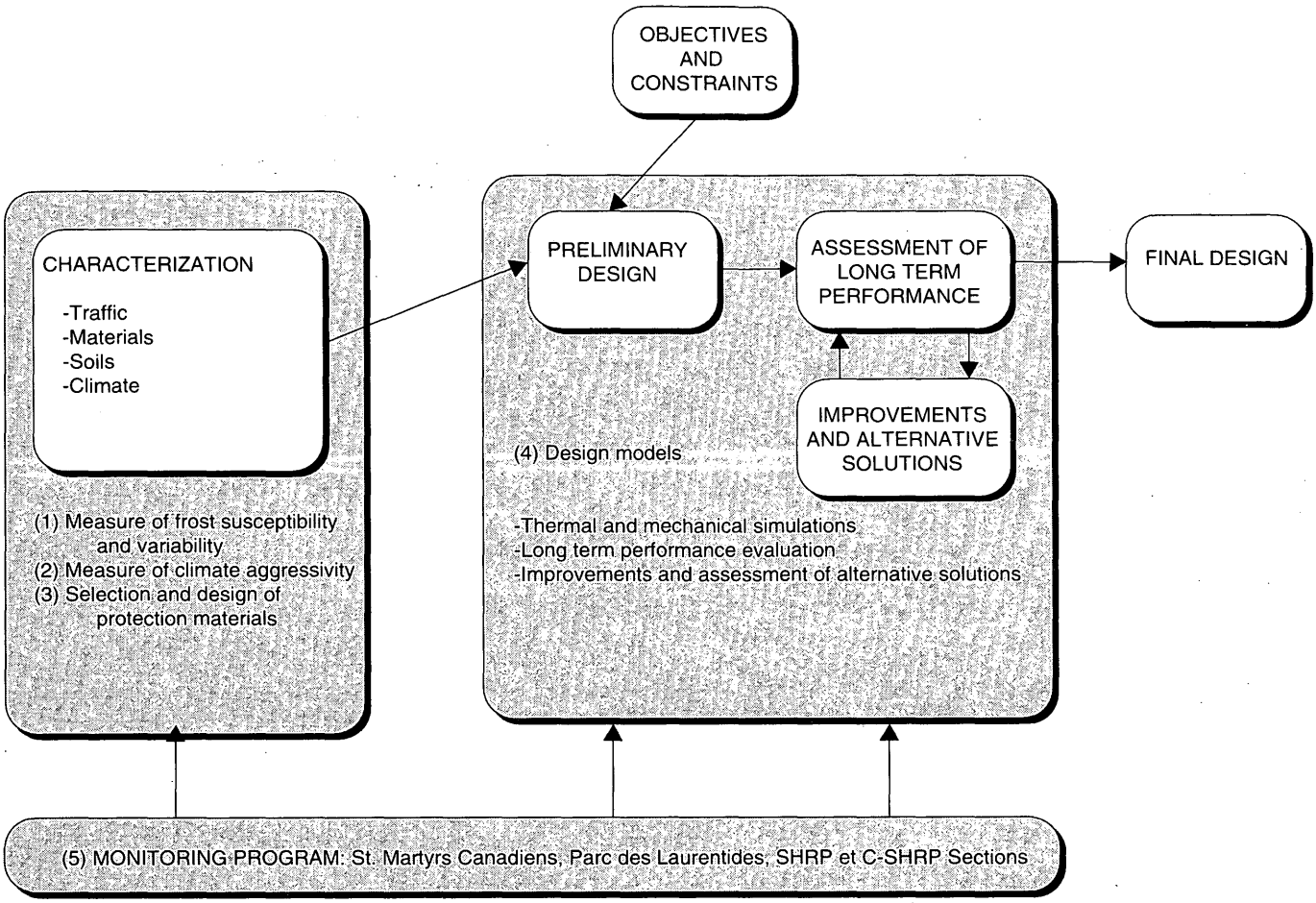

FIGURE 1 Pavement design in frost conditions: concept of proposed method and research required.

materials in pavements. Because the site was located on a provincial highway, it also was important to make sure that the test sections provided satisfactory service at a reasonable cost to travelers. The structural design of the test pavements was therefore critical.

It is expected that introducing a relatively soft insulation layer to the pavement system will improve its thermal performance. However, its mechanical performance will likely be significantly affected. Thus, a design approach was adopted that allowed the best possible compromise between the benefit due to the insulation and the associated structural loss. The 12 sections illustrated in Figure 2, characterized by different depths and thicknesses of the insulation layer, were analyzed using a mechanical and a thermal model. The results of the simulations were then combined in an attempt to assess the overall performance of the different pavement structures.

Three types of bulk insulation materials were initially considered in the study: wood residues, tire chips, and plastic crumbs.

Mechanical Simulation

The principle of mechanical simulation is to calculate stresses, strains, and displacements at critical locations in the pavement structure under a static load. These values are then used to estimate the life of the pavement structure using fatigue models. The simulation was done using ELSYM 5. Based on the linear elastic theory applied to multi layer systems, the system calculates the idealized response of the specified pavement structure at a given location under the specified load.

Performance modeling was needed for project preparation and had to be done before any specific laboratory and field information was available. The mechanical and thermal properties of the materials considered were thus extracted or estimated from available data in the literature. The characteristics used are presented in Table 1. Because no information was available on plastic crumbs at the time of the simulation, only the wood residues and the tire chips were used in the analysis.

The results of the mechanical simulation are shown in Figures 3 and 4. As expected, the total deflection of the pavement (Figure 3) and the strain at the bottom of the asphalt layer (Figure 4) grow with increasing thickness and decreasing depth of the insulation layer. These figures also illustrate the large difference in the response of the structures insulated with crumb rubber compared with the reference structures (no insulation) or the structures insulated with wood residues.

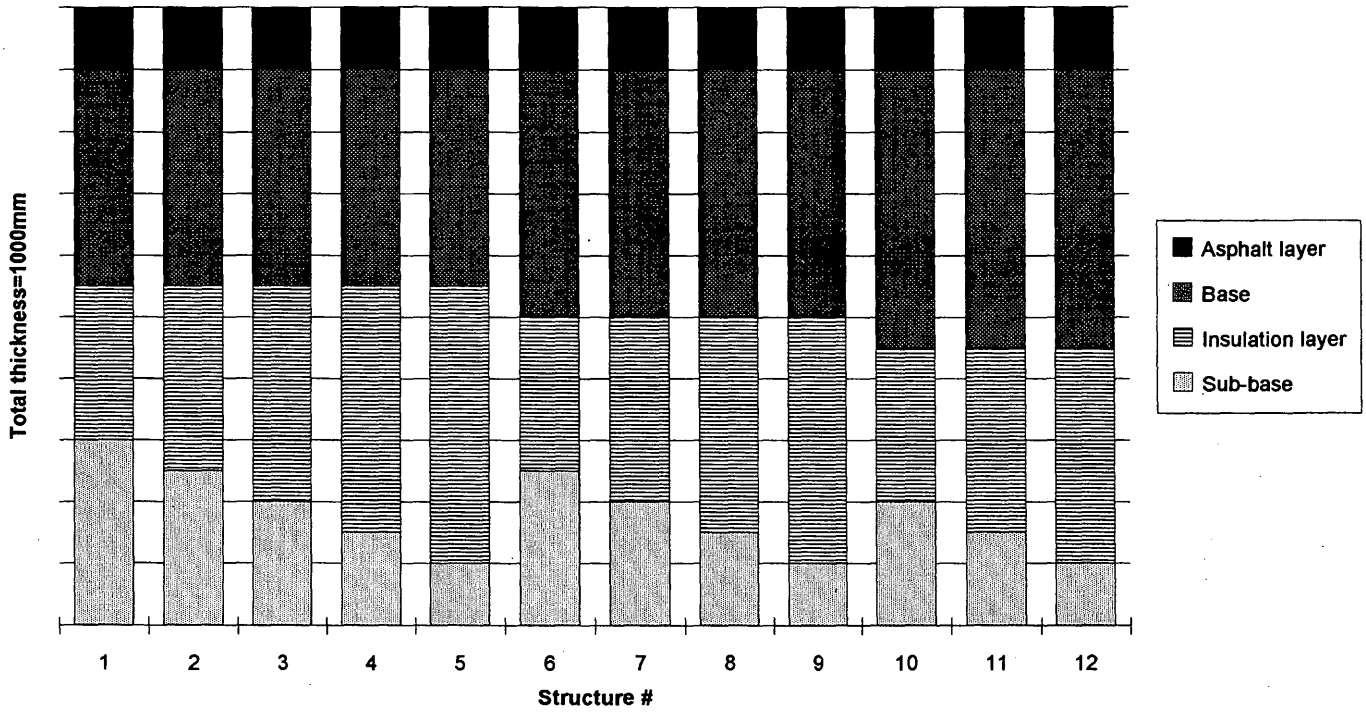

FIGURE 2 Pavement structures analyzed.

TABLE 1 Working Assumptions: Materials Characteristics, Highway 161, St. Martyrs Canadiens

	Asphalt layer	Base	Tire chips	Wood residues	Sub-base	Natural soil
	MB	GW-GC	CP	CB	SC	Cl
Thermal cond.k (W/m°C)	1.5 (a)	2.0 (a)	0.25 (1)	0.25 (1)(d)	2.3 (a)	1.5 (a)
Thermal cap. Cm (kJ/m^3°C)	2300 (a)	2700 (a)	600 (1)	440 (1)(a)	2800 (a)	3000 (a)
W (%)	***	6.0 (1)			15.0 (1)	25.0
Dry dens. (kg/m^3)	2500 (a)	2200 (a)	500 (b)	160 (f)	2000 (a)	1900 (a)
Initial temperat. cond.(°C)	4.5	4.5	4.5	4.5	4.5	4.5
Freezing index (°C.j)	1226	1226	1226	1226	1226	1226
Segregat. Potent. (mm^2/°C.h)	***	50 (1)	***	***	125 (1)	175 (1)
Plate Modulus M_E (Mpa)		300 (a)	1.55(1) (b)(c)	95 (1)(b)	60 (a)	15 (a)
Elastic Modulus E (Mpa)	3100 (g)	200 (b)(g)	1.1 (c)	70 (b)	83 (g)	48 (g)
Poisson coeff.	0.35	0.30	0.45 (b)	0.26 (b)	0.35	0.45

(a) Dysli [10]
(b) Newcomb/Drescher [11]
(c) Humphrey [12]
(d) Ladanyi [13]
(f) Johnson [14]
(g) MTQ [15]

(1) Estimated

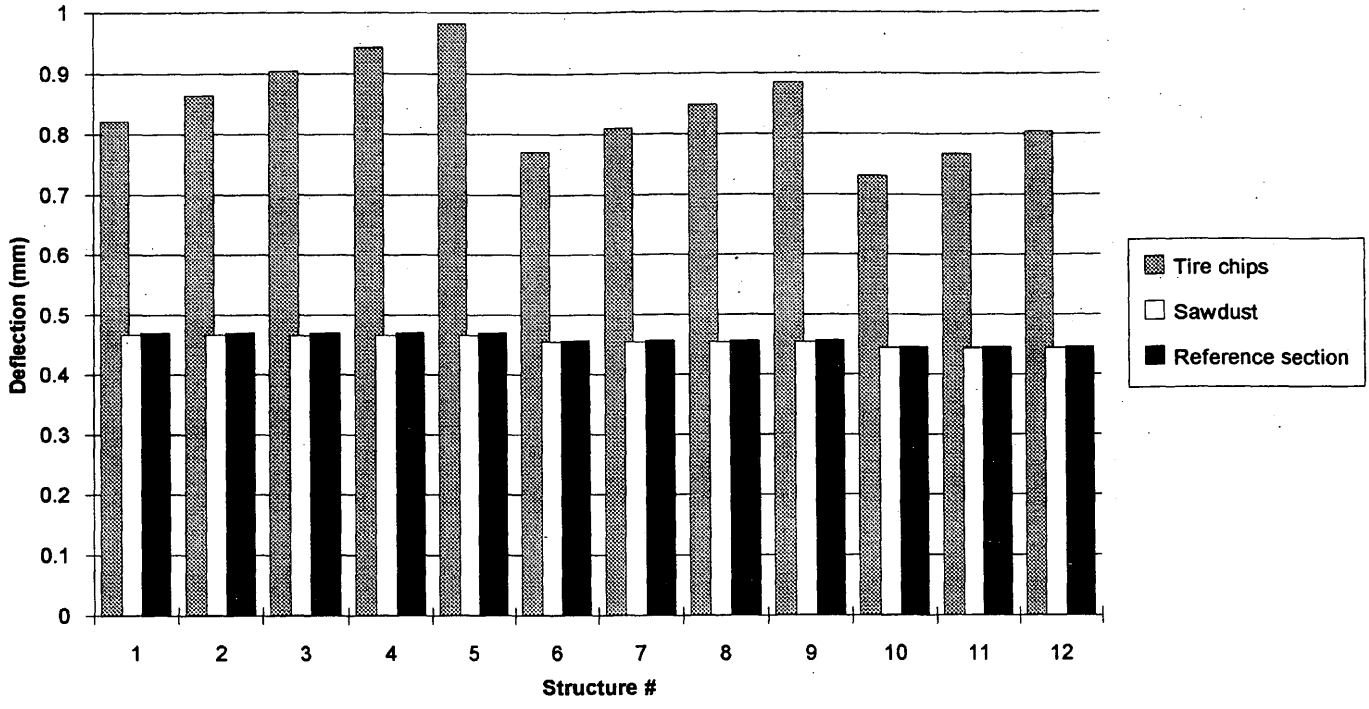

FIGURE 3 Calculated deflection at surface of pavement.

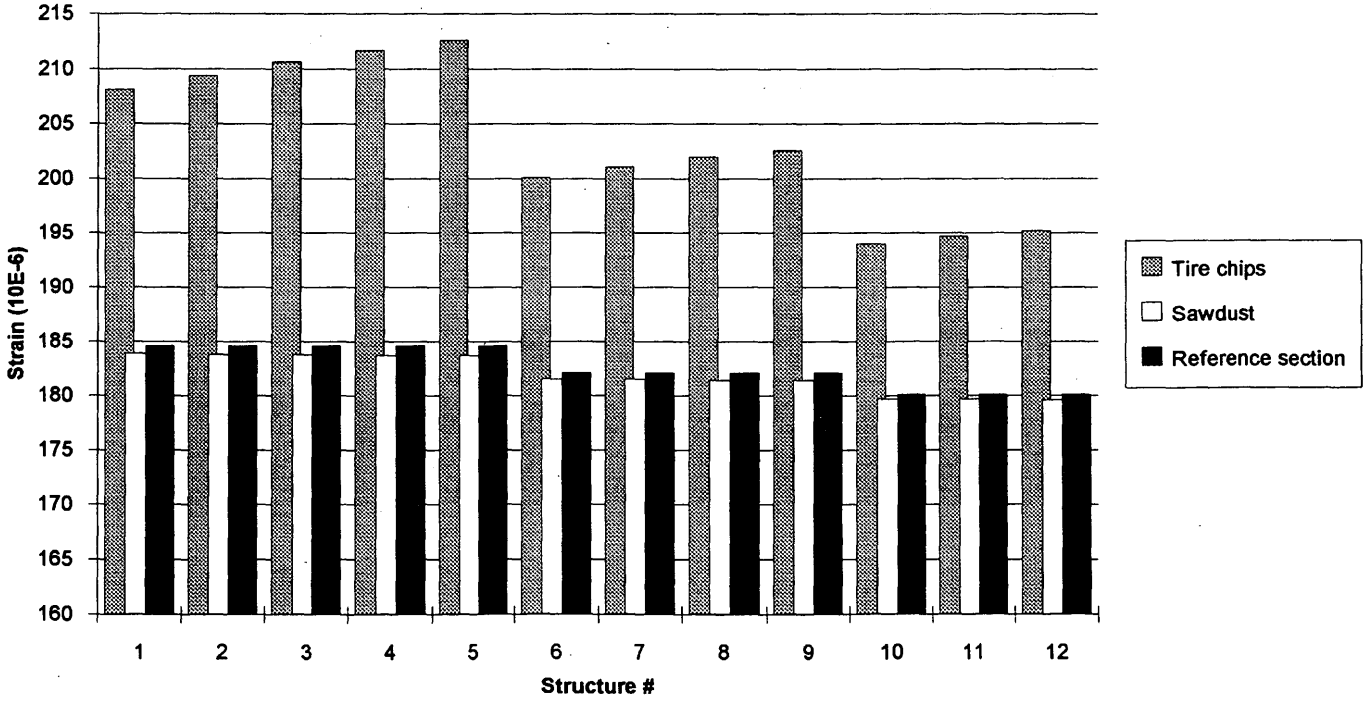

FIGURE 4 Calculated horizontal strain at base of asphalt layer.

Thermal Simulation

Thermal simulation was used to estimate vertical movements resulting from frost action beneath the pavement. The same 12 structures illustrated in Figure 2 and the same three bulk insulation materials were modeled using a numerical bi-dimensional model developed at Laval University (*1*). The model estimates heat and mass transfer as well as the resulting distribution of water and vertical movements of the pavement structure using the segregation potential concept developed elsewhere (*2,3*).

The use of wood residues is relatively well-documented in the literature (*4*). However, it is difficult to find relevant literature on the use of tire chips or plastic crumbs. In two recent experiments, tire chips were used as insulation material in a pavement structure (*5,6*). Although no specific measurement of thermal conductivity was done on the material, the experiments still provided useful information on the thermal behavior of tire chips.

Based on the literature search and on the judgment of frost experts from Laval University and the Canadian National Research Council, it was assumed for the first simulation iteration that all three materials had equivalent thermal conductivities as shown in Table 1.

The results of the thermal simulation for average winter conditions (FI = 1,226°C.d) are shown in Figures 5 and 6. Figure 5 shows that for all structures modeled, the insulation layer was sufficient to keep the freezing front within the pavement structure (1000 mm), thus reducing the expected total heave to less than 28 percent of the expected heave for the reference section.

Combined Performance

Given the working assumptions and the results of the simulations, it is generally observed that increasing thermal performance leads to decreases in mechanical performance, and unless each component is analyzed for its specific contribution to the overall performance of the pavement, the selection of the optimal pavement structure is very difficult.

Because they are the weakest of the three materials considered, the tire chips constitute a critical case and will be used in an attempt to combine the thermal and the mechanical performances to identify the optimal pavement structure for the test site. To make the analysis possible, it was necessary to assume that the serviceability loss associated with frost action was equal to the serviceability loss due to traffic. Based on the AASHTO model (*7*) (which predicts that the maximum serviceability loss ($\rfloor PSI$) due to frost action is between 1,5 and 2,0 and the total expected serviceability loss should be about 3,0), it appears that this assumption is realistic in the context of the St. Martyrs Canadiens test site.

The performance has been analyzed relatively to the reference section using fatigue and performance models. These models are empirical transfer functions linking mechanistic model outputs to observed pavement performance. To evaluate pavement performance as it relates to frost action, the AASHTO model (*7*) has been used. As Equation 1 shows, the model links the heaving rate to the Pavement Serviceability Index (PSI):

$$\rfloor PSI_{sg} = 0.01\, P_f\, \rfloor PSI_{\max}\, [1 - e^{-(0.02\phi t)}] \quad (1)$$

where

$\rfloor PSI_{sg}$ = loss of serviceability of pavement associated with frost action,
P_f = proportion of pavement surface subjected to frost action,
$\rfloor PSI_{\max}$ = maximum serviceability loss due to frost action,
ϕ = heaving rate, and
t = time.

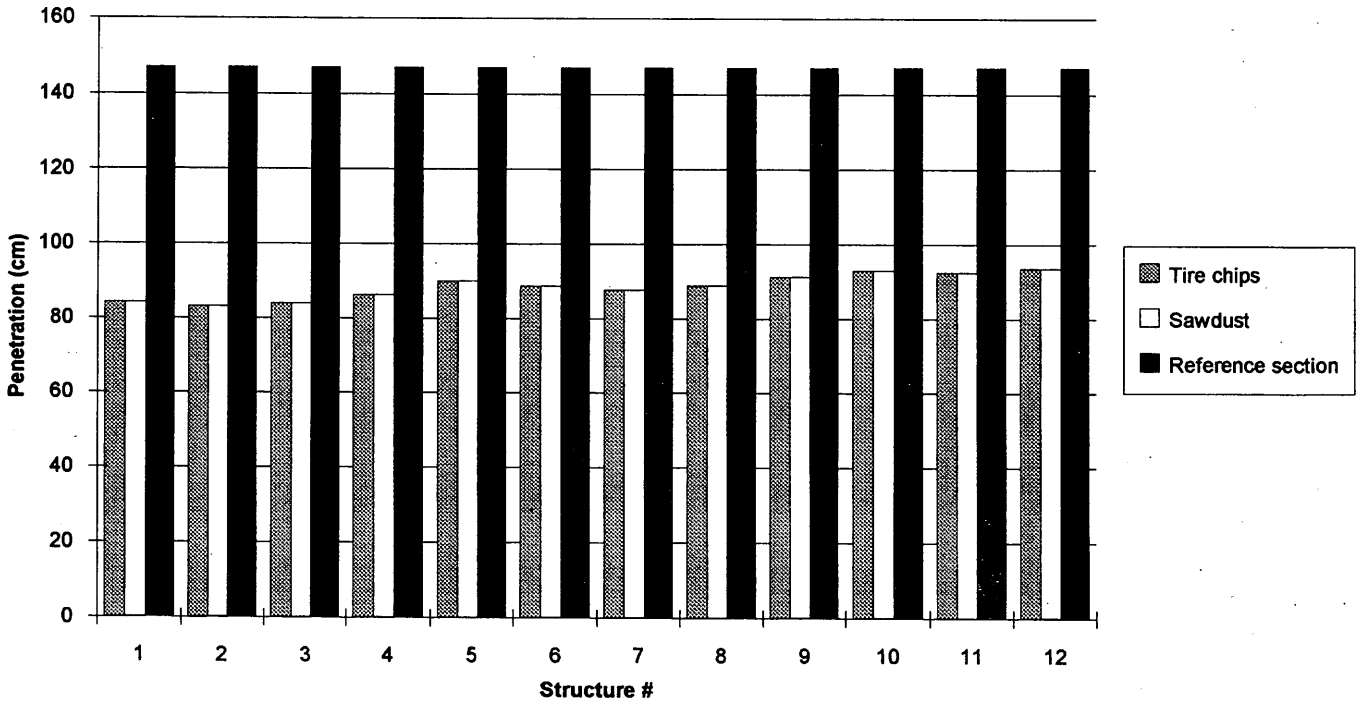

FIGURE 5 Calculated frost penetration (average winter, FI = 1,226°C.d).

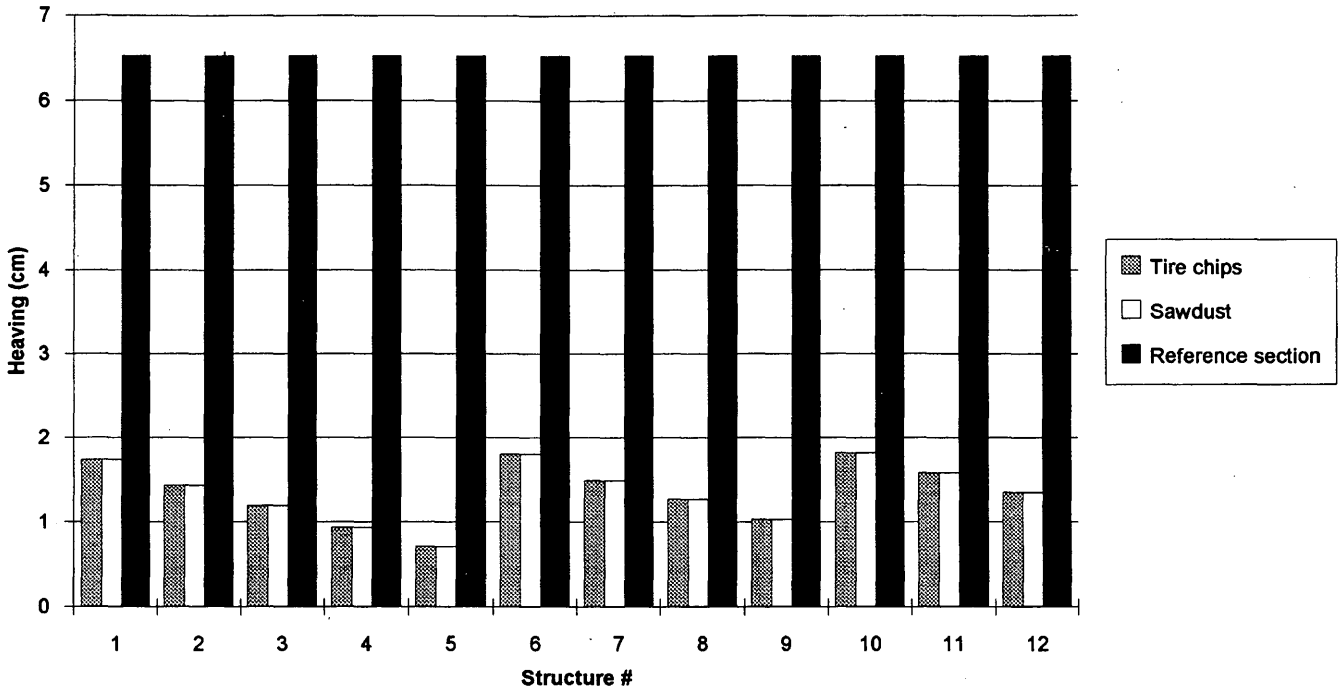

FIGURE 6 Calculated maximum heaving (average winter, FI = 1,226°C.d).

Pavement performance associated with traffic was evaluated using the following model reported elsewhere (*8*):

$$I = 0.5\,(E_t/X)^{4.27}N \tag{2}$$

where

I = cumulative damage to pavement,
E_t = strain at bottom of asphalt structure,
X = reference strain value, and
N = number of load cycles.

The relative performance (Pr) related to traffic (Pr_t) or frost action (pr_f) is defined as follows:

$$Pr = \frac{\text{performance of insulated structure}}{\text{performance of reference structure}} \tag{3}$$

The resulting combined performance is thus

$$P = (Pr_f - 1) + (Pr_t - 1) \tag{4}$$

The results of the analysis of the combined performance are given in Figure 7. The analysis shows that the combined performance improves as depth and thickness of the insulation layer increase. However, it is more sensitive to depth than thickness. Based on the working assumptions and considering the limitations of the method, it is believed that a properly designed pavement, including a layer of bulk insulation material, can significantly outperform a conventional pavement despite the low rigidity of the layer. Because it is expected that construction cost will increase with the thickness and depth of the insulation layer, and because there is not a major difference in the combined performance for Sections 8 to 12, Section 10 was selected as the optimal pavement structure for the test site.

LABORATORY TESTS

The three material types used in the simulation were selected on the basis of cost, local availability of materials, and potential benefit to the thermal performance of the pavement. However, there were major concerns about the mechanical performance of these materials. The calculated performance of modeled structures, based on material characteristics extracted from the literature or simply estimated, showed interesting potential for the insulation materials considered and led to the structural design of the test site. The next step was to validate and, if possible, improve material properties through an extensive laboratory program.

The materials tested included the following:

- Wood residues: sawdust, wood chips, and combinations of both;
- Recuperated rubber: tire chips, ground tires (powder), combinations of both, and combinations of chips with sawdust and sand; and
- Recuperated plastics: plastics from domestic recuperation and plastics from the recycling of electric wires.

To assess the best-performing materials within the three generic groups and properly characterize them, the following tests were performed on the 17 different combinations of materials described in Table 2: one-dimensional compression, shearing, California Bearing Ratio (CBR), permeability, and thermal conductivity.

Mechanical Properties

Except for a series of thermal conductivity tests conducted on dry materials, all tests were conducted on saturated materials under a

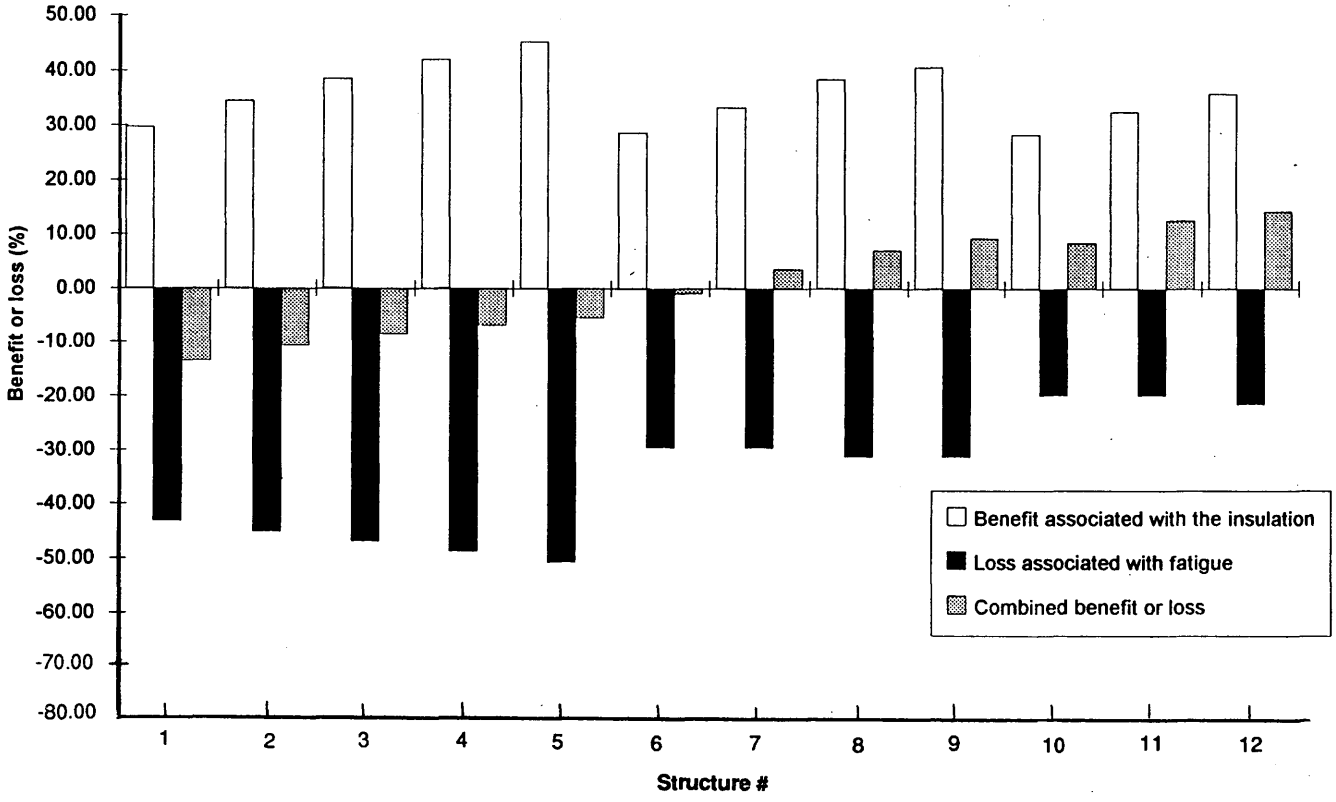

FIGURE 7 Anticipated combined performance.

TABLE 2 Materials Descriptions and Laboratory Tests Results

Material description	Maximum density (kg/m3)	Compression modulus (MPa)	Shear modulus (kPa)	CBR (%)	Hydraulic conductivity (cm/sec)	Dry thermal conductivity (W/mC)
Crushed stone (CS): 20-0mm	2250.00	150.00	23.10			
Sand (S): Poorly graded class A	1817.00	100.00	16.87	27.17		
Ground tire (GT): 1-4mm	698.00	0.82	3.00	0.56		0.32
Tire chips (TC): 20-40mm, steel and polyester not removed	667.00	1.02	2.70	0.55		0.38
Sawdust (SD): 1-4mm	201.00	6.67	13.59	2.60	0.0013	0.16
Wood Chips (WC): 20-40mm	234.00	6.81	15.46	3.07		
Plastics from domestic recuperation (RP): 8-12mm, polyethylene	506.00	5.83	9.06	0.36	0.0024	
Plastics from electric wire recycling (TP): 5-10mm, thermoplastic	492.00	3.82	7.71	0.67		0.28
Mixes (Volumetric proportions)						
GT(30)/TC(70)	807.00	1.22	3.75	0.79		
GT(50)/TC(50)	819.00	1.53	4.05	1.06	0.0013	0.34
GT(70)/TC(30)	765.00	1.55	3.81	0.89		
S(30)/TC(70)	1222.00	3.27	4.87	3.52		
S(50)/TC(50)	1519.00	28.36	15.08	9.93		
SD(50)/TC(50)	553.00	2.83	6.46	1.48		
SD(30)/WC(70)	315.00	6.92	14.79	3.20		
SD(50)/WC(50)	271.00	10.67	15.78	3.47		
SD(70)/WC(30)	348.00	6.54	13.20	3.61		

surcharge of 20 kPa. For the one-dimensional compression test, a tangent modulus at the beginning of the second loading cycle (first reloading) was used. The shear test was done using a large shear box (250 × 250 × 150 mm). In an attempt to better represent strain conditions in a pavement structure, a secant modulus at 1 mm displacement was used, although it does not allow for the full mobilization of the strength of the material.

The results of the mechanical tests for the best performing materials among each class are given in Table 2, and illustrated in Figures 8, 9, and 10. Figures 11 and 12 illustrate the effect of combining different proportions of ground tires and sand with tire chips.

The tests used to characterize mechanical properties of alternative insulation materials have obvious limitations. As static tests they do not represent the dynamic stress conditions experienced by the insulation materials in a pavement structure very well. It is believed that the simple compression test provides the best overall evaluation of the stress-strain characteristics of the materials. However, material properties can also be related to CBR values. In all cases within this study, the real benefit of mechanical tests is obtained when the results are analyzed relative to known materials (sand and crushed stone).

Thermal Properties

Two techniques were used to determine thermal conductivity. The first, based on the principle of a linear source of unsteady state heat, has been used by the National Research Council of Canada (*9*). The second approach was developed at Laval University and uses the steady state heat flow conditions at the interface of two materials to derive their relative thermal conductivity. If one of the materials is a calibrated material of known properties, thermal conductivity of the tested material is readily inferred.

The results of the thermal conductivity tests for dry, saturated unfrozen, and saturated frozen materials are given in Table 2 and illustrated in Figure 13.

The tests procedures used should yield reliable results. It should be noted, however, that these results were obtained for set conditions of saturation (dry and saturated), which are not necessarily representative of actual filed conditions.

Hydraulic Conductivity

Hydraulic conductivity of the three types of material selected for the test site was tested using the falling head procedure. In all cases, the tests showed that the materials had adequate draining capacity because of their use in pavements.

DISCUSSION OF RESULTS

As expected, all three types of materials showed weak mechanical properties, but promising thermal characteristics. Of all the tire mixes the material made of 50 percent tire chips and 50 percent ground tire performed best and showed properties comparable to the ones used in the mechanical simulation. However, the production of such a mix might not be economically feasible and, even if it were, the mechanical properties remain weak and would limit its use to low-volume roads. The possibility of using a tire chips-sand mix will be explored further.

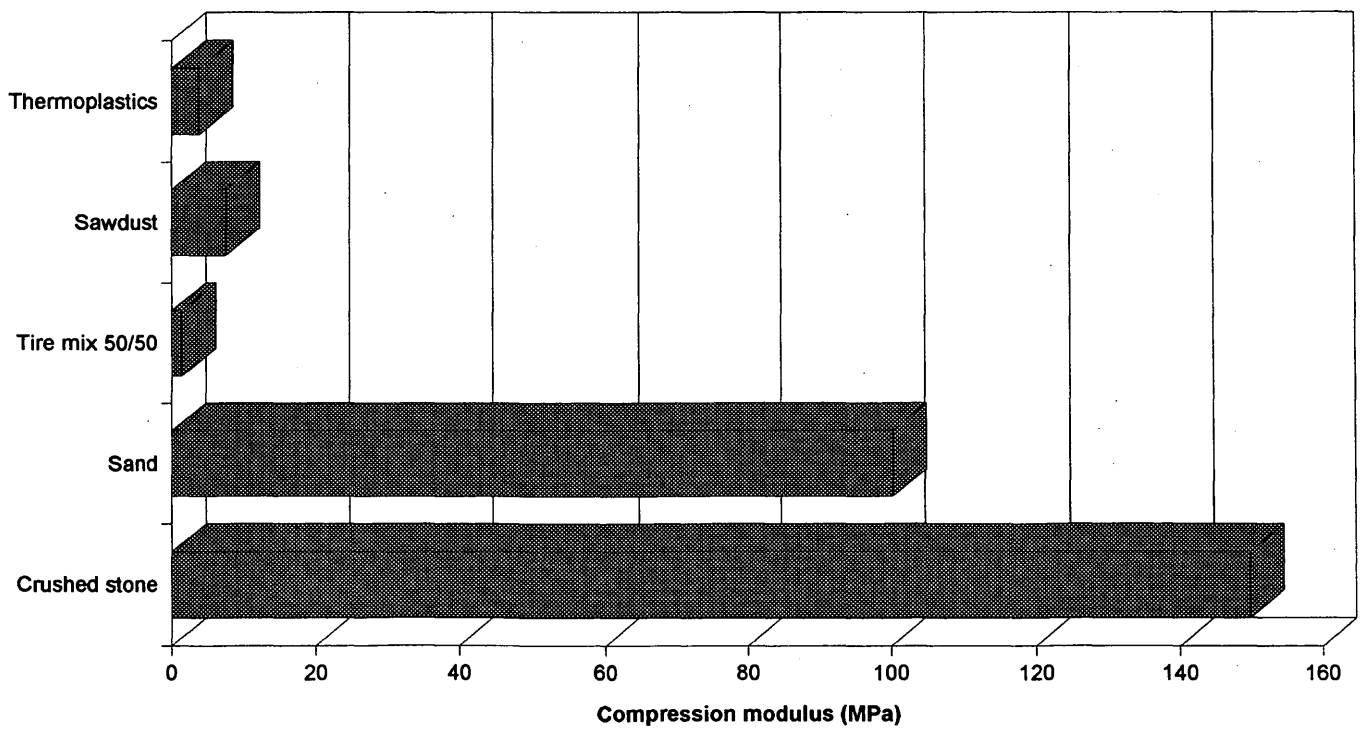

FIGURE 8 Results of simple compression tests on selected materials.

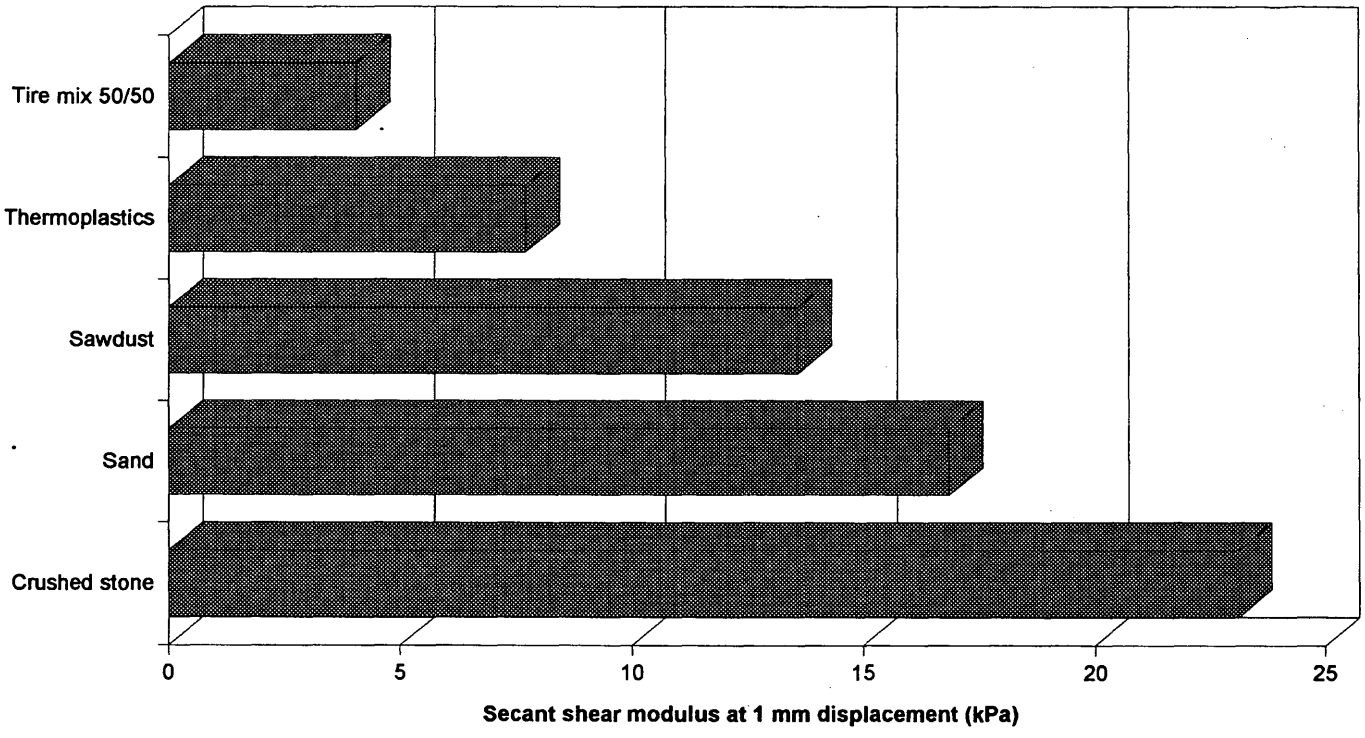

FIGURE 9 Results of shear resistance tests on selected materials.

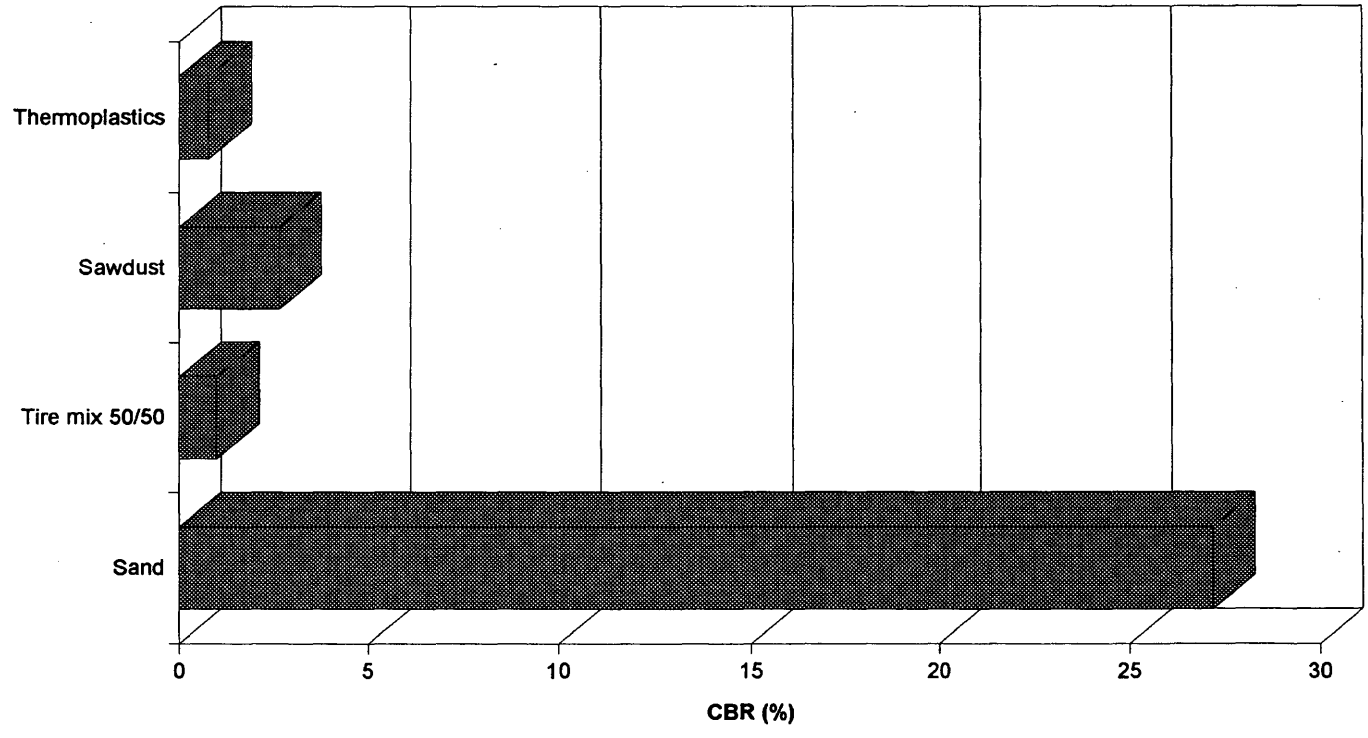

FIGURE 10 Results of CBR tests on selected materials.

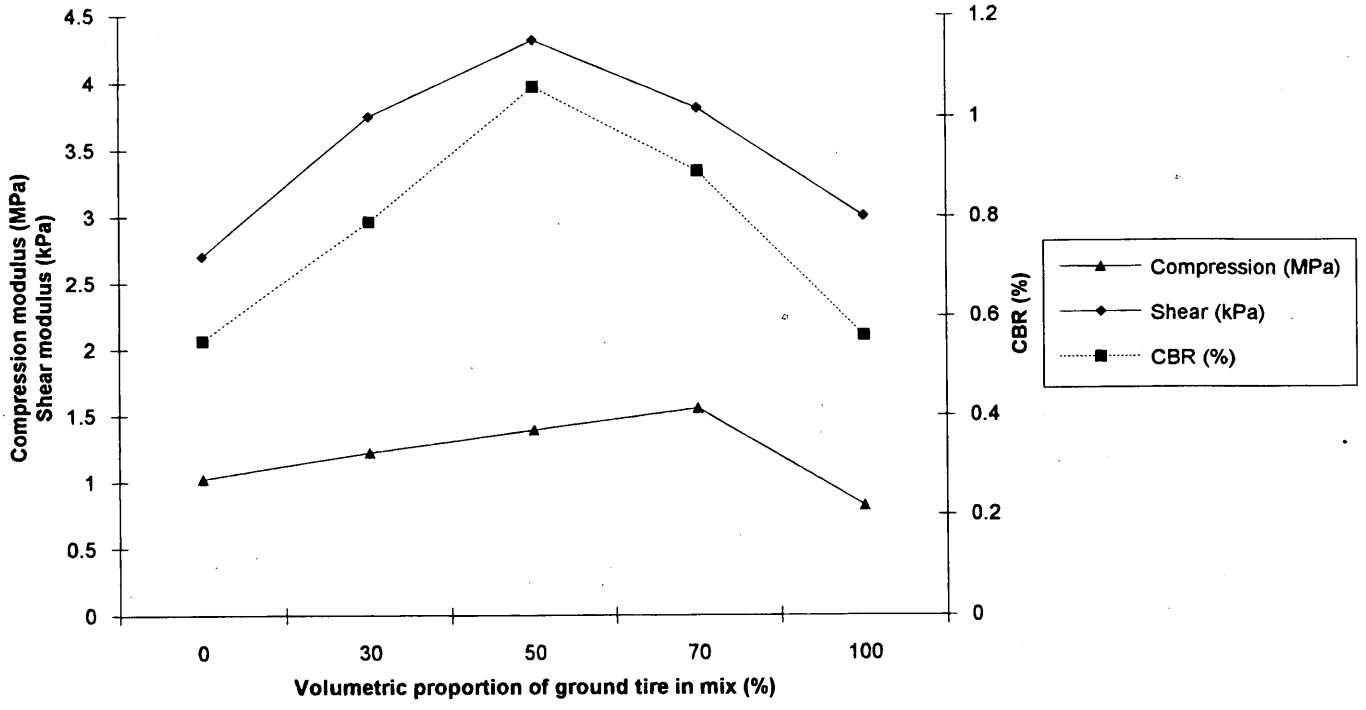

FIGURE 11 Mechanical properties for tire chips–ground tire mixes.

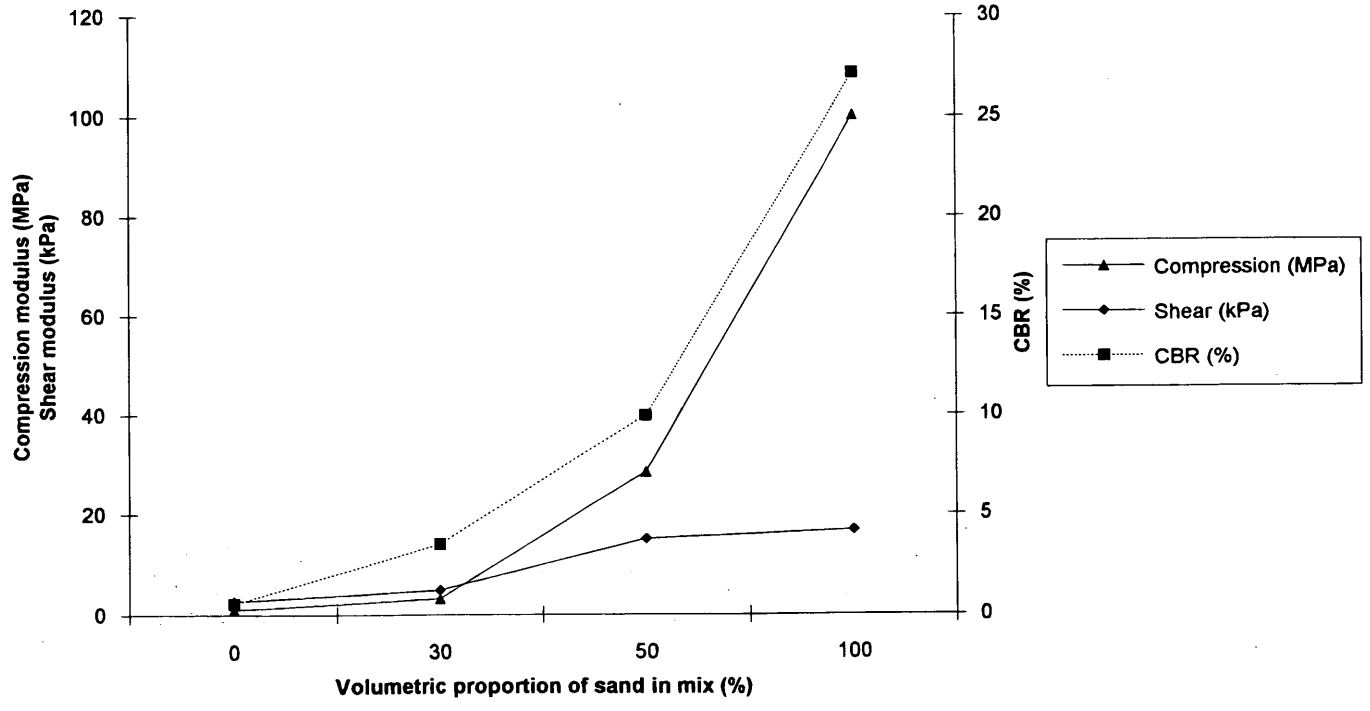

FIGURE 12 Mechanical properties for tire chips–sand mixes.

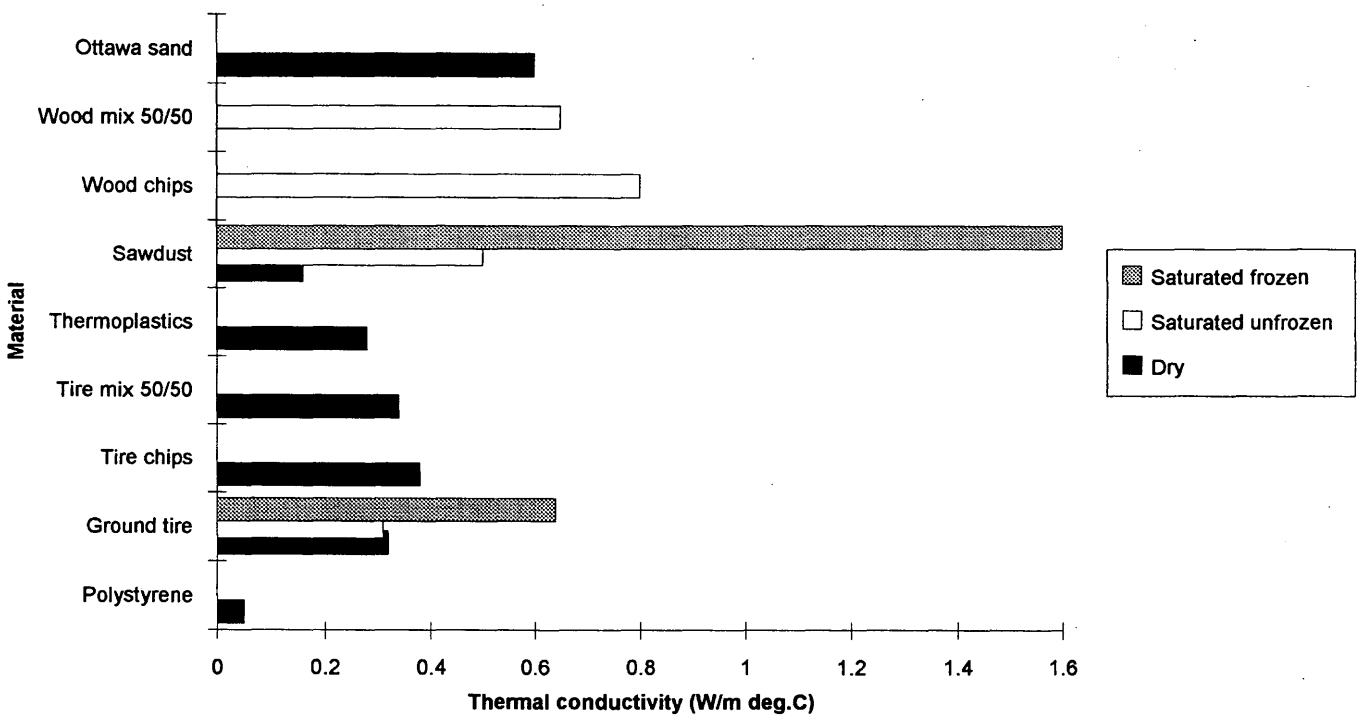

FIGURE 13 Results of thermal conductivity tests.

Among the wood residues, the sawdust showed the best combination of mechanical and thermal properties. The mechanical properties of the sawdust, however, were much lower than the ones used in the mechanical modeling but still much higher than the tire mix, which was used as the critical material for the optimization of the pavement design.

The thermal characteristics of sawdust are sensitive to moisture content and precautions should be taken at the design stage to prevent water from flowing into the layer through shoulders or cracked surface layers. The plastic recuperated from electric wires showed better potential performance than the one from domestic recuperation as well as a fairly good overall performance.

CONCLUSIONS

A major study on design and protection of pavements against frost action has been undertaken in the province of Québec. The study, designed to develop a rational design method and assess alternative frost protection materials, relies heavily on the long-term monitoring of eight pavement test sections to be constructed in 1994 and 1995. Most of the effort so far has been invested in the site preparation to allow for the longest monitoring period possible. Work done includes site selection, pavement design through mechanical and thermal modeling, material characterization, and preparation of the instrumentation plan.

Although the results reported in this paper were obtained at an early stage in the project, they provide useful information on the potential use of bulk insulation materials for frost mitigation in pavements. The following conclusions may be made based on this first phase of the research:

- The structural design of an insulated test section has been optimized using thermal (Laval model based on the segregation potential concept) and mechanical (ELSYM 5) simulations. By combining the expected mechanical performance with the expected thermal performance, it has been possible to determine that, if the pavement is properly designed, the expected loss in performance resulting from the addition of a soft layer is advantageously counterbalanced by the benefit associated with its insulating properties.
- Laboratory tests have significantly improved knowledge of the thermal, mechanical, and hydraulic characteristics of potential insulation materials, including recycled tires and plastics, as well as wood residues. Materials have been combined to maximize their performance. Pavement design must take into consideration the low rigidity and the fairly low thermal conductivity of these materials. Both aspects must be taken into account concurrently in the overall analysis of the performance.

The project will now focus on test site construction; instrumentation and monitoring; and model development. Relevant SHRP and C-SHRP long-term monitoring data will be incorporated in the study, and the C-SHRP BSTAT analysis package will be used in the development of the first-generation performance models.

REFERENCES

1. Konrad, J. M. Analyse Numérique des Chaussées Soumises à l'Action du Gel, du Dégel et du Trafic. *Colloque International Géotechnique et Informatique.* Paris, France, 1992.
2. Konrad, J. M., and N. R. Morgernstern. A Mechanistic Theory of Ice Formation in Fine-Grained Soils. *Canadian Geotechnical Journal,* Vol. 17, No. 4, 1980, pp. 473–486.

3. Konrad, J. M., and N. R. Morgernstern. Frost Heave Prediction of Chilled Pipelines Buried in Unfrozen Soils. *Canadian Geotechnical Journal,* Vol. 21, No. 1, 1984, pp. 100–115.
4. Gandhal, R. Bark as Road Building Material in Sweden. *Frost I Jord,* NR.5-, Dec. 1971.
5. Humphrey, D. N., and R. A. Eaton. Tire Chips as Insulation Beneath Gravel Surfaced Roads. *Frost in Geotechnical Engineering,* 1993.
6. Rioux, N. La Réutilisation des Pneux dans les Techniques de Protection contre le Gel. *Congrès de 1994 de la Fédération Routière Internationale,* 1994.
7. AASHTO. *Design of Pavement Structures.* Washington, D.C., 1985.
8. Ullidtz, P. *Pavement Analysis.* Elsevier, Amsterdam, the Netherlands, 1987.
9. Daigle, L. D., S. McDonald, L. E. Goodrich, and T. H. W. Baker. *Mesure de la Conductivité Thermique en Laboratoire de Différents Matériaux Recyclés* Saturés. Laboratoire d'infrastructures, Institut de recherche en construction, CNRC, Report H-7017.1, l'Université Laval, Canada, 1995.
10. Dysli, M. *Le Gel et son Action sur les Sols et les Fondations.* Complément au Traité de Génie Civil de l'École Polytechnique Fédérale de Lausanne, Switzerland, 1991.
11. Newcomb, D. E., and A. Drescher. Engineering Properties of Shredded Tires in Lightweight Fill Applications. Presented at the 73rd Annual Meeting of the Transportation Research Board, 1994.
12. Humphrey, D. N., T. C., Sandford, M. M., Cribbs, and W. P. Manion. Shear Strength and Compressibility of Tire Chips for Use as Retaining Wall Backfill. In *Transportation Research Record 1422,* TRB, National Research Council, Washington, D.C., 1993.
13. Ladanyi, B. *Guide sur la Conception et la Réhabilitation des Infrastructures de Transport en Régions Nordiques.* Ministry of Transportation, Québec, Canada, 1991.
14. Johnson, G. H. *Permafrost Engineering Design and Construction.* J. Wiley and Sons, 1981.
15. *Norme pour la Conception des Chaussées.* Ministry of Transportation, Québec, Canada, 1994.

Publication of this paper sponsored by Committee on Frost Action.